# STRENGTH AND DILATANCY OF ANISOTROPIC COHESIONLESS SOILS

by

Arshiya Abadkon

B.S., Civil Engineering, Azad Islamic University of Orumieh, 2003

M.S., Civil Engineering, Azad Islamic University of Mohabad, 2006

Submitted to the Institute for Graduate Studies in
Science and Engineering in partial fulfillment of
the requirements for the degree of
Doctor of Philosophy

Graduate Program in Civil Engineering

Boğaziçi University

2012

STRENGTH AND DILATANCY OF ANISOTROPIC COHESIONLESS SOILS

# ACKNOWLEDGEMENTS

I would like to express my sincere gratitude to my thesis supervisor Assist. Prof. Özer Çinicioğlu who has supported me throughout my study with his invaluable guidance, knowledge and patience. His enthusiastic encouragement and innovative ideas helped me a lot for the development of this thesis.

I would like to thank to the members of the thesis committee, Prof. Kutay Özaydin Prof. Feyza Çinicioğlu, Prof. Erol Güler, and Prof. Gökhan Baykal, for their precious suggestions.

I would like to thank to Turkish Scientific and Technical Researches Institute (TUBITAK) for supporting me financially during my Ph.D studies.

This research is supported by Turkish Scientific and Technological Research Council of Turkey (TUBİTAK), Project number: 110M595.

# ABSTRACT


## STRENGTH AND DILATANCY OF ANISOTROPIC COHESIONLESS SOILS

Peak friction angle and critical state friction angle are two key parameters representing the shear strength of cohesionless soils. Peak friction angle of sand is a function of critical state friction angle and dilatancy angle while the angle of dilatancy is a volumetric parameter. Researchers investigating this topic proposed different relationships between peak friction angle, dilatancy angle, and the critical state friction angle. The aim of this study is to investigate and quantify the influences of the critical state friction angle and the angle of dilatancy on the evaluation of the peak friction angle and to identify the variations of these relationships with the state of the cohesionless soil. The term "state of the soil" here defines the stress state and volumetric state of the cohesionless soil and quantified as the mean effective stress and relative density, respectively. For this purpose, a detailed experimental program with more than 80 $K_0$ CD triaxial tests has been conducted on reconstituted sands. Between these tests, several parameters were varied to understand their influences on the peak friction angle and dilatancy. These parameters are relative density, overconsolidation ratio, and effective vertical stress at the end of normal consolidation. Since the tests are $K_o$ tests, the influences of these parameters on the at rest lateral earth pressure coefficient are also examined. Obtained test results have been used for the construction of a new empirical equation that yields the dilatancy angle using mean effective stress ($p'$) and relative density ($D_R$) as input. The major advantage of the proposed equation is that it uses directly measureable and calculable parameters ($p'$ and $D_R$). Additionally, it is possible to enhance the quality and versatility of the constitutive models using the proposed equation instead of defining a constant dilatancy angle.Moreover, the equations proposed by other researchers for calculating the peak friction angle using the constant volume friction angle and dilatancy angle have been enhanced using the data obtained from the current testing program.

# ÖZET


## ANİZOTROPİK KOHEZYONSUZ ZEMİNLERİN MUKAVEMET VE GENLEŞİM ÖZELLİKLERİ

Maksimum sürtünme açısı ve kritik durum sürtünme açısı kohezyonsuz zeminlerin kesme mükavemetini temsileden iki ana parametredir. Dilatasyon açısı hacimsel bir parametere olmasına rağmen, kumun maksimum sürtünme açısı kritik durum sürtünme açısı ve dilatasyon açısının bir fonksiyonudur. Konuyu inceleyen araştırmacılar maksimum sürtünme açısı, kritik durum sürtünme açısı ve dilatasyon açısı arasında farklı ilişkiler önermişlerdir. Bu araştırmanın hedefi; kritik durum sürtünme açısı ve dilatasyon açısının maksimum sürtünme açısının ölçümünde ve değerlendirmesindeki etkisinin belirlenmesi ve bunlar arasındaki ilişkilerin değişimini kohezyonsuz zeminin durumuna göre tanımlanmasıdır. "Zeminin durumu" terimi basınç durumu ve hacimsel durumu tanımlamaktadır. Bu terim ortalama etkin basınç ve bağıl yoğunlukla ölçülmektedir. Bu amaçla, yeniden yapılandırılmış kumlar üzerinde 80 $K_0$ CD (konsolidasyonlu drenajlı) üç eksenli deneyden oluşan detaylı bir deneysel program gerçekleştirilmiştir. Deneyler sırasında maksimum sürtünme açısı ve dilatasyon açısına etkisini araştırmak amacıyla farklı parametrelerin değerleri değiştirilmişir. Bu parametreler bağıl yoğunluk, aşırı konsolidasyon oranı ve normal konsolidasyon sonundaki etkin dikey basınç değerleridir. Bu çalışmada $K_0$ deneyleri kullanıldığı için değişen parametrelerin $K_0$ üzerindeki etkileri de incelenebilmiştir. Deney sonuçlarından elde edilen değerler, dilatasyon açısını ortalama etkin basınç ve bağıl yoğunluk parametrelerine göre tanımlamak için yeni bir ampirik denklemde kullanılmıştır. Önerilen ilişkide en önemli avantaj; direk ölçülebilir ve hesaplanabilir parametreler kullanılmasıdır (p' ve $D_R$). Ayrıca sabit bir dilatasyon açısı kullanmak yerine önerilen denklemi kullanarak temel modellerinin kalitesi ve değişkenliğini iyileştirebilmek mümkünüdür. Buna ek olarak, literatürdeki araştırmacılar tarafından maksimum sürtünme açısını hesaplamak için kritik durum sürtünme açısı ve dilatasyon açısını kullanan denklemler bu çalışmada kullanılan deneysel programdan elde edilen sonuçlarla iyileştirilmiştir.

# TABLE OF CONTENTS

ACKNOWLEDGEMENTS ..... iii
ABSTRACT ..... iv
ÖZET ..... v
LIST OF FIGURES ..... viii
LIST OF TABLES ..... xvii
LIST OF SYMBOLS ..... xviii
LIST OF ACRONYMS/ABBREVIATIONS ..... xxii
1. INTRODUCTION ..... 1
2. LITERATURE REVIEW ..... 3
2.1. Previous Researches on Shear Strength and Dilatancy Properties of Soils ..... 3
2.1.1. An Introduction to Peak Friction Angle and Dilatancy Angle of Cohesionless Soils ..... 3
2.1.2. Taylor's Theory ..... 8
2.1.3. Rowe's Theory ..... 9
2.1.4. Bolton's Equation ..... 11
2.1.5. Schanz and Vermeer Equation ..... 14
2.1.6. Chakraborty-Salgado Equation ..... 16
2.1.7. Vaid and Sasitharan Equation ..... 20
2.1.8. Fukushima and Tatsuoka Research ..... 24
2.2. At Rest Lateral Earth Pressure Coefficient of Overconsolidated Cohesionless Soils ..... 25
2.2.1. Wroth (1973) Equation ..... 25
2.2.2. Meyerhof (1976) Equation ..... 26
2.2.3. Mayne-Kulhawy (1982) Equation ..... 26
2.2.4. Chau-ping Yang (1991) Equation ..... 28
2.2.5. Daramola (1980) Equation ..... 30
2.2.6. Hanna-Al-Romhein (2008) Study ..... 31
3. METHODOLOGY ..... 34
3.1. $K_0$ Triaxial Testing Program ..... 34
3.2. Testing Material ..... 37

3.2.1. Particle Shape Analysis of Sand Grains ……. 38
3.3. Sample Preparation ……. 42
3.4. Automatic Triaxial Testing Apparatus ...……. 44
3.5. Triaxial Testing Procedure ...……. 45
3.5.1. Initialisation Phase ……..…. 46
3.5.2. Saturation Phase ..……..……... 46
3.5.3. Consolidation Phase ..……...…… 46
3.5.4. Shearing Phase .……...…….…….……. 47
3.6. Triaxial Test Corrections .…….…….…… 48
3.6.1. Piston Area Correction .…….…… 48
3.6.2. Correction for the Rubber Membrane .…….....…… .. 50
3.6.3. Correction for Sample Area ..……...….. 51
3.7. Information about the Triaxial Tests .……..……..…… 54
4. EVALUATION OF TRIAXIAL TEST RESULTS ...……..... 64
4.1. Strength and Dilatancy of Sands ……...……. 64
4.1.1. Effects of Density and Mean Effective Stress on Dilatancy Angle.. 67
4.1.2. Effects of Density and Mean Effective Stress on Peak Friction Angle 77
4.2. At Rest Lateral Earth Pressure Coefficient of Overconsolidated Sands ……. 91
5. DISCUSSION ...……. 100
6. CONCLUSION ...……. 114
7. REFERENCES ..…….……..……. 116

# LIST OF FIGURES

Figure 2.1. Mohr circle at failure. ……..…… 3

Figure 2.2. Stress-strain curve of a sample reaching peak and critical state values. …. 4

Figure 2.3. Variation of vertical strain with shear strain for a dense sand. ….…….. 5

Figure 2.4. Dilation of dense sand in simple shear test. …….…...…… 5

Figure 2.5. Residual state of the soil during shearing. …..……...…. 6

Figure 2.6. Sliding block sliding over another in a flat plane. ..... 7

Figure 2.7. Analogy used in Taylor's energy assumption. …… 8

Figure 2.8. Assumed sliding mechanism for for Rowe's stress dilatancy relationship 10

Figure 2.9. Comparisson of Bolton's equation with Taylor and Rowe's theories. ..... 11

Figure 2.10. Variation of dilatancy angle with relative density index. ..... 13

Figure 2.11. Deviation of triaxial dilatancy from biaxial state. ……...…….. 14

Figure 2.12. Triaxial and plain-strain compression data points for Toyoura sand for determining $A_\Psi$. ……..……..…. 17

Figure 2.13. Variation of $\phi'_p - \phi'_c$ with $I_R$. …… 18

Figure 2.14. Variation of Q value with increasing effective confining stress for triaxial compression test. ……..…… 19

Figure 2.15. Schematic view of stress paths. …….…… 20

Figure 2.16. Relationship between peak friction angle and maximum rate of dilatancy $d\varepsilon_v / d\varepsilon_a$ in compression and extension tests. ……..…….…… 21

Figure 2.17. Relationship between peak friction angle and maximum dilatancy angle for compression and extension trixial tests. …….…….……. 23

Figure 2.18. Relationship between peak friction angle and $\sigma'_3$ for e=0.7 and 0.85. ….. 24

Figure 2.19. Volumetric strain values versus $\sigma'_3$. …….…… 24

Figure 2.20. Relationship between $K_0$ and OCR for cohesionless soils during Unloading. …….…….……..….. 27

Figure 2.21. Relationship between $\alpha$ and $\sin\phi'$ for clays and sands. ……..…..… 28

Figure 2.22. Variation of void ratio with effective vertical stress in $K_0$ triaxial test. ..... 29

Figure 2.23. Stress path during loading and unloading. …..……..……. 30

Figure 2.24. Variation of slope of unloading path with initial void ratio. ……..……. 31

Figure 2.25. View of the experimental setup. …….…… 32

Figure 2.26. Comparison between theoretical and experimental values of $K_0$. …..…… 33

Figure 3.1. Ottawa sand grain size distribution. ……...…….…….…… 37

Figure 3.2. Relative density test apparatus. …….……... 38

Figure 3.3. Particle shape determination chart. ….……..…. 40

Figure 3.4. Stereomicroscope. ..... 40

Figure 3.5. Samples of stereomicroscope photographs on shape determination chart. ... 41

Figure 3.6. Variation of the void ratio with raining height. ..…….…..…… 43

Figure 3.7. Air-pluviation set-up for sample preparation. …….…...…… 43

Figure.3.8. Automatic triaxial system. ……..……..…….... 44

Figure 3.9. Schematic of a flow trac unit. ……...…… 45

Figure 3.10. Piston area correction test. …….….. 49

Figure 3.11. Variation of uplift force with cell pressure. …….…….... 49

Figure 3.12. Tensile test. …….….…… 51

Figure 3.13. None area correction. ……..…….…….. 51

Figure 3.14. Uniform area correction. …..…….…… 52

Figure 3.15. Parabolic area correction. ..…….……... 52

Figure 3.16. Parabolic shape of the sample during shearing. …..….…… 53

Figure 3.17. Variation of effective vertical stress with the axial strain in a sample test. 57

Figure 3.18. Variation of deviatoric stress with the axial strain for a sample test. ……... 58

Figure 3.19. Variation of the mean effective stress with axial strain for a sample test. ... 58

Figure 3.20. Variation of radial strain with the effective vertical stress during the

consolidation stage of a sample test. ……..…..……. 59

Figure 3.21. Variation of the at rest earth pressure coefficient with effective vertical stress during the consolidation phase for a sample test. ..……...…….…… 60

Figure 3.22. Variation of the void ratio with vertical effective stress during the consolidation phase for a sample test. ……..…..….... 61

Figure 3.23. Variation of the dilatancy angle with axial strain for a sample test. …….. 61

Figure 3.24. Variation of volumetric strain with the axial strain during the shearing phase for a sample test. …….……..…. 62

Figure 3.25. Variation of at rest earth pressure coefficient with overconsolidation ratio during the unloading stage of consolidation phase. …….……..…… 63

Figure 4.1. Variation of the dilatancy angle with mean effective stress for $D_R$=0.30-0.35. …….…..…….. 68

Figure 4.2. Variation of the dilatancy angle with mean effective stress for $D_R$=0.40-0.45. …….……..…… 69

Figure 4.3. Variation of the dilatancy angle with mean effective stress for $D_R$=0.45-0.5. ..... 69

Figure 4.4. Variation of the dilatancy angle with mean effective stress for $D_R$=0.5-0.55. ..... 70

Figure 4.5. Variation of the dilatancy angle with mean effective stress for $D_R$=0.55-0.6. ..... 70

Figure 4.6. Variation of the dilatancy angle with mean effective stress for $D_R$=0.6-0.6. ..... 71

Figure 4.7. Variation of the dilatancy angle with mean effective stress for $D_R$=0.65-0.7. ..... 71

Figure 4.8. Variation of the dilatancy angle with mean effective stress for $D_R$=0.7-0.75. ..... 72

Figure 4.9. Variation of the dilatancy angle with mean effective stress for $D_R$=0.75-0.8. ..... 72

Figure 4.10. Variation of the dilatancy angle with mean effective stress for $D_R$=0.8-0.85. ..... 73

Figure 4.11. Variation of the dilatancy angle with mean effective stress for $D_R$=0.85-0.9. …… 74

Figure 4.12. Variation of the dilatancy angle with mean effective stress for $D_R$=0.9-0.95. …… 74

Figure 4.13. Variation of $\alpha_\psi$ parameter with relative density. ……..…… 75

Figure 4.14. Variation of $\beta_\psi$ parameter with relative density. …….……... 75

Figure 4.15. Variation of r with mean effective stress for $D_R$=0.45-0.5. ……..…… 78

Figure 4.16. Variation of r with mean effective stress for $D_R$=0.5-0.55. ……..… 79

Figure 4.17. Variation of r with mean effective stress for $D_R$=0.55-0.6. ……..…… 79

Figure 4.18. Variation of r with mean effective stress for $D_R$=0.6-0.65. ……. 80

Figure 4.19. Variation of r with mean effective stress for $D_R$=0.65-0.7. ……. 80

Figure 4.20. Variation of r with mean effective stress for $D_R$=0.7-0.75. ……. 81

Figure 4.21. Variation of r with mean effective stress for $D_R$=0.75-0.8. …….. 81

Figure 4.22. Variation of r with mean effective stress for $D_R$=0.8-0.85. …… 82

Figure 4.23. Variation of r with mean effective stress for $D_R$=0.85-0.9. …… 82

Figure 4.24. Variation of r with mean effective stress for $D_R$=0.9-0.95. …… 83

Figure 4.25. Variation of $\alpha_r$ with relative density. …… 84

Figure 4.26. Variation of $\beta_r$ with relative density. …… 85

Figure 4.27. Variation of peak friction angle with mean relative density value …… 87

Figure 4.28. Variation of peak friction angle with mean effective stress for $D_R$=0.6-0.65. …… 88

Figure 4.29. Variation of peak friction angle with mean effective stress for $D_R$=0.7-0.75. …… 89

Figure 4.30. Variation of peak friction angle with mean effective stress for $D_R$=0.75-0.8. …… 89

Figure 4.31. Variation of peak friction angle with mean effective stress for $D_R$=0.85-0.9. …… 90

Figure 4.32. Variation of peak friction angle with mean effective stress for $D_R$=0.9-0.95. …… 90

Figure 4.33. Comparisson of experimental results with Wroth equation. …… 92

Figure 4.34. Comparisson of experimental results with Meyerhof equation. …….. 93

Figure 4.35. Comparisson of experimental results with Mayne-Kulhawy equation. ….. 94

Figure 4.36. Variation of at rest earth pressre coefficient with peak friction angle. …… 96

Figure 4.37. Variation of $K_{0(OC)}$ with overconsolidation ratio. …… 97

Figure 4.38. Comparisson of experimental results with proposed empirical equation. ... 98

Figure 4.39. Comparisson of proposed equation with proposed empirical equations. … 99

Figure 5.1. Variation of the dilatancy angle with mean effective stress for $D_R$=0.26. ……..……..…… 103

Figure 5.2. Variation of the dilatancy angle with mean effective stress for $D_R$=0.56. ……..……..…… 103

Figure 5.3. Variation of the dilatancy angle with mean effective stress for $D_R$=0.70. ……..……..…… 104

Figure 5.4. Variation of $\alpha_\psi$ parameter with relative density for Vaid-Sasitharan study. 105

Figure 5.5. Variation of $\beta_\psi$ parameter with relative density for Vaid-Sasitharan study... 106

Figure 5.6. Variation of the r parameter with mean effective stress for $D_R$=0.26. ……. 107

Figure 5.7. Variation of r parameter with mean effective stress for $D_R$=0.56. ……...… 108

Figure 5.8. Variation of r parameter with mean effective stress for $D_R$=0.7. …….…… 108

Figure 5.9. Variation of $\alpha_r$ parameter with relative density. …….……...…… 109

Figure 5.10. Variation of $\beta_r$ parameter with relative density. ……..…….....….…….…….. 110

Figure 5.11. Variation of peak friction angle with mean effective stress for $D_R$=0.26. …….….. 111

Figure 5.12. Variation of peak friction angle with mean effective stress for $D_R$=0.56. 112

Figure 5.13. Variation of peak friction angle with mean effective stress for $D_R$=0.7. .. 112

# LIST OF TABLES

Table 3.1. Experimental program. …… 35

Table 3.2. Basic properties of the tested sand. .……. 38

Table 3.3. Sphericity and roundness of sand particles. ……..… 42

Table 4.1. Details of triaxial tests. …… 65

Table 4.2. Statistical comparison of experimental values with empirical formulas. …… 95

Table 5.1. Summary of the tests performed by Vaid-Sasitharan. ……... 102

# LIST OF SYMBOLS

| | |
|---|---|
| $A_c$ | Corrected area of the sample |
| $A_0$ | Initial area of the sample |
| A | Relative density parameter in Chau-Ping Yang equation |
| $A_\psi$ | Constant for relative density index in Bolton equation |
| $A_m$ | Area of the membrane |
| B | pore pressure parameter |
| $C_{comp}$ | Compression index of the soil |
| $C_s$ | Swell index of the soil |
| $C_u$ | Coefficient of uniformity |
| $C_c$ | Coefficient of curvature |
| D | Rate of horizontal strain change to vertical strain change |
| $D_c$ | Diameter of the sample after consolidation |
| $D_R$ | Relative density |
| $E_m$ | Young's modulus for the membrane material |
| $e_{min}$ | Minimum void ratio |
| $e_{max}$ | Maximum void ratio |
| e | Void ratio |
| $F_b$ | Buoyancy force |
| h | Sand raining height |
| $h_c$ | Height of sample after consolidation |
| $h_0$ | Initial height of the sample |

| | |
|---|---|
| $I_D$ | Density index |
| $I_R$ | Relative density index |
| $K$ | Coefficient representing the internal friction |
| $K_0$ | At rest earth pressure coefficient |
| $K_{0(OC)}$ | At rest earth pressure coefficient for overconsolidated soil |
| $K_{0(NC)}$ | At rest earth pressure coefficient for normally consolidated soil |
| L | Unstretched length of the membrane |
| $OCR$ | Overconsolidation ratio |
| $P'_A$ | Atmospheric pressure |
| $p'$ | Mean effective stress |
| Q | Constant value for Bolton relative density equation |
| $q$ | Deviatoric stress |
| R | Stress ratio |
| r | Constant parameter showing the amount of dilatancy contribution to shear strength property of soil |
| $t_{90}$ | Time corresponding to 90% primary consolidation |
| $t_m$ | Membrane thickness |
| $V_c$ | Volume of the sample after consolidation phase |
| $W_s$ | Width of circumferential strip |
| $a_\psi$ | Slope of the line showing the variation of $\alpha_\psi$ with relative density |
| $\alpha$ | Angle of shearing in sawtooth plane |
| $\alpha_r$ | Slope of the line correlating r parameter with $p'$ and $\beta_r$ |

$\alpha_{\psi}$ Slope of line correlating dilatancy angle with mean effective stress and relative density

β Angle of sliding on sawtooth plane

$\beta_{\psi}$ Zero intercept of the line showing the variation of dilatancy angle with p'

$\beta_{r}$ Zero intercept of the line correlating r parameter with $p'$

$b_{\psi}$ Zero intercept of the line correlating $\alpha_{\psi}$ with relative density

$\beta_{\psi}$ Zero intercept of the line correlating dilatancy angle with mean effective stress and relative density

$d\varepsilon_{v}$ Volumetric strain change

$d\varepsilon_{q}$ Deviatoric strain change

$d\varepsilon_{a}$ Axial strain change

$d\varepsilon_{r}$ Radial strain change

$\Delta u$ Pore pressurechange of the specimen

$\Delta\sigma_{3}$ Cell pressure change

$\Delta V_{s}$ Volume change of the sample during the shearing

$\Delta L$ Change in length of the membrane

$\Delta h$ Change in height of the specimen

$\dot{\varepsilon}_{1}$ Strain rate in verticals direction

$\dot{\varepsilon}_{2}$ Strain rate in horizontal direction

$\dot{\varepsilon}_{3}$ Strain rate in horizontal direction

$\dot{\varepsilon}_{v}$ Volumetric strain rate

$\dot{\varepsilon}$ Shearing strain rate for triaxial test

$\phi'$ Friction angle of the soil

$\phi'_{peak}$ Peak friction angle

$\lambda$ Ratio of the effective horizontal stress change to effective vertical stress change

$m_{\psi}$ Slope of the line correlating $\beta_{\psi}$ with relative density

$n_{\psi}$ Zero intercept of the line correlating $\beta_{\psi}$ with relative density

$\mu$ Poisson ratio

$\dot{\gamma}$ Shear strain rate

$\phi'_{cv}$ Critical state friction angle

$\phi_{\mu}$ Fundamental angle of friction for grain to grain contact

$\sigma'_{1f}$ Effective vertical stress at failure

$\sigma'_{3f}$ Effective horizontal stress at failure

$\sigma'_{c}$ Effective confining pressure

$\sigma'_{h}$ Effective horizontal stress

$\sigma'_{v}$ Effective vertical stress

$\sigma'_{n}$ Effective normal stress

$\psi_{\phi'}$ Strength dilatancy

$\psi$ Dilatancy angle

$\tau$ Shear stress

$\dot{W}$ Rate of input work

# LIST OF ACRONYMS/ABBREVIATIONS

ASTM American society for testing and materials

CD Consolidated drained

# 1. INTRODUCTION

Measurement, estimation or calculation of the shear strength of soils is central to the design of all structures that are resting in soils, on soils, and made up of soils. In the case of cohesionless soils, the crucial parameter of shear strength is dependent on soil friction angle. However friction angle as a soil parameter takes different values depending on the compactness and deformation state of the soil. These different friction angles are referred to as peak friction angle, critical state friction angle, and residual friction angle. Peak friction angle is the friction angle that corresponds to the maximum friction angle that can be measured for the considered soil sample at its current state. Critical state friction angle is the friction angle that corresponds to the frictional resistance of the soil during constant volume shearing. This friction angle is also the residual friction angle for soils dominantly composed of rotund particles. However for clay-like soils with platy particles, residual friction angle is reached after critical state friction angle when the plate-like particles are aligned parallel to each other in the direction of shearing to form slicken-sided surfaces. Accordingly, it is the aim of this investigation to identify the parameters that influence the evolution of different forms of the friction angle for cohesionless soils. As an outcome of an extensive literature review, it is has been observed that specialists in this field of study consider dilatant behavior to be the reason for the rise of the friction angle above the value it has during constant volume shearing. However, unlike the critical state friction angle, dilatancy angle does not have a constant value. Dilatancy angle varies with relative density and confining pressure. Unfortunately, the variation of dilatancy angle with relative density and confining pressure has not been quantified previously. Moreover, a soil dependent portion of dilatancy angle causes a rise in the friction angle. Therefore, it is the goal of this study to quantify the variation of dilatancy angle with confining pressure and relative density, and to investigate its impact on the peak friction angle for anisotropic cohesionless soils.

For this purpose, a triaxial testing program has been prepared to identify the influences of relative density, stress history, and confinement on the frictional properties of reconstituted cohesionless soils. The tests were conducted under $K_o$ conditions to reflect

the state of the soil in the field. This also enabled the researchers to investigate the theory of lateral earth pressure for at rest states.

In the theory of lateral earth pressure for at rest states, it is proposed that $K_o$ is a function of peak friction angle. However, it is known that through dilatant behavior peak friction angle is a function of both the confinement and density. Therefore in this study, a new empirical equation that allows the calculation of $K_o$ using confinement and density is proposed.

# 2. LİTERATURE REVIEW

Shear strength properties and at rest earth pressure coefficients of sands have been investigated in this research. Therefore a brief literature review has been presented for both titles.

## 2.1. Previous Researches on Shear Strength and Dilatancy Properties of Soils

### 2.1.1 An Introduction to Peak Friction Angle and Dilatancy Angle of Cohesionless Soils

Peak friction angle is the maximum friction angle of the soil corresponding to the maximum shear strength of the soil. Peak friction angle can be obtained from Mohr stress circle at failure condition as:

$$\sin\phi' = \frac{\sigma'_{1f} - \sigma'_{3f}}{\sigma'_{1f} + \sigma'_{3f}} \tag{2.1}$$

where $\phi'$ is friction angle, $\sigma'_{1f}$ and $\sigma'_{3f}$ are major and minor principal stresses at failure.

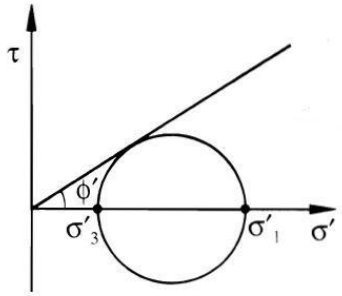


Figure 2.1. Mohr circle at failure

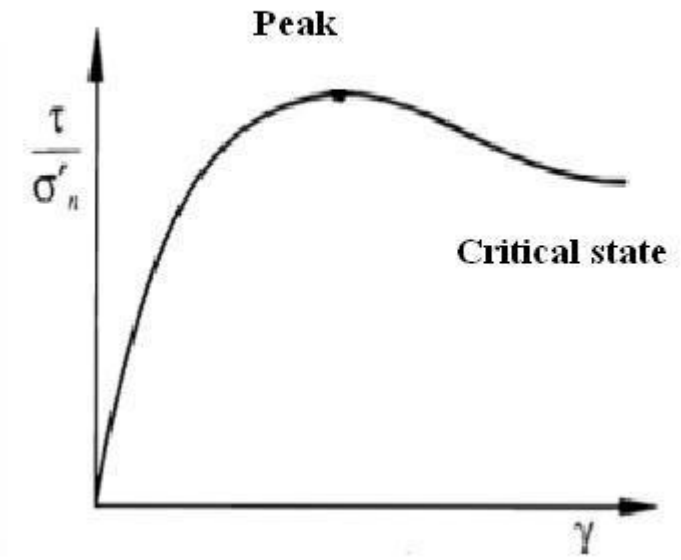


Figure 2.2. Stress-strain curve of a sample reaching peak and critical state values

Critical state friction angle is the friction angle of the soil shearing at a constant volume. The soil is said to have reached the critical state when shear stress remains constant but shear strain increasing. The critical state friction angle is denoted by $\phi'_{cv}$. Critical state friction angle of the soil is a fundamental soil parameter and considered to depend only on the mineralogy of the sand grains. Therefore critical state friction angle is constant for a given sand.

Compacted granular material tends to expand in volume as it is sheared. This occurs because grains do not have any freedom to move around one another but when they are stressed a motion occurs between neighboring grains and they start to slide over each other. In soil mechanics the term dilatancy is used to define the volumetric increase of dense sand during shearing and rate of dilation can be obtained by the gradient $\frac{d\varepsilon_v}{d\varepsilon_q}$

where $d\varepsilon_v$ represents the volumetric strain change of the soil and $d\varepsilon_q$ corresponds to shear strain change. Dilatancy angle can be defined in terms of principal strain rates for triaxial tests:

$$\sin\psi = \frac{-(\dot{\varepsilon}_1 + \dot{\varepsilon}_2 + \dot{\varepsilon}_3)}{\dot{\varepsilon}_1 - \dot{\varepsilon}_3} \tag{2.2}$$

where $\psi$ is the angle of dilatancy, $\dot{\varepsilon}_1$ is the strain rate in vertical direction, $\dot{\varepsilon}_2$ and $\dot{\varepsilon}_3$ are strain rates in horizontal directions. However for plain-strain conditions where $\dot{\varepsilon}_2 = 0$ Equation 2.2 can be written as:

$$\sin\psi = \frac{-(\dot{\varepsilon}_1 + \dot{\varepsilon}_3)}{\dot{\varepsilon}_1 - \dot{\varepsilon}_3} \tag{2.3}$$

The angle of dilation is positive when the soil expands therefore the term minus comes at the beginning of the Equation 2.2 and 2.3 from the convention that compressive stresses and strains should be taken positive in soil mechanics.

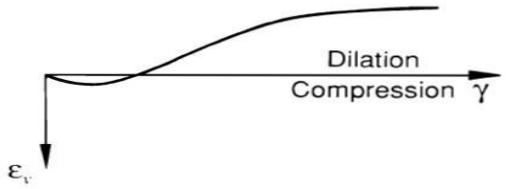


Figure 2.3. Variation of vertical strain with shear strain for a dense sand

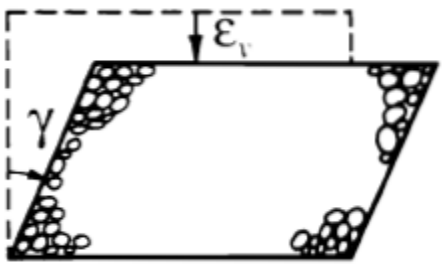


Figure 2.4. Dilation of dense sand in simple shear test

In case of loose sands there in no significant particle interlocking therefore principal stress difference increases gradually to its ultimate value without a peak. Therefore loose

sands do not show any dilative behavior and the angle of friction at failure equals the critical state friction angle of the soil.

If the shearing is continued to very large shear strains, the shear strength drops below the critical state shear strength. This strength is called the residual shear strength and the friction angle corresponding to this strength is the residual friction angle of the soil.

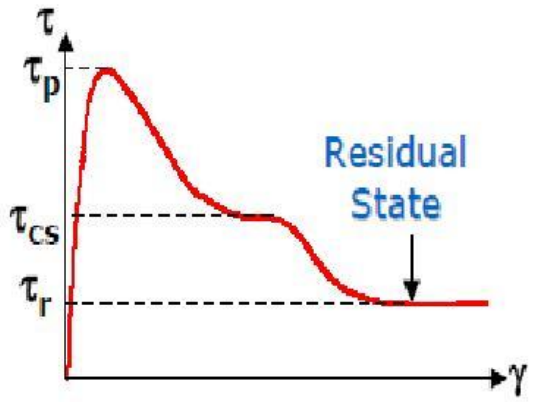


Figure 2.5. Residual state of the soil during shearing

Based on definitions above it can be concluded that the excess shear strength value over the critical state friction value ($\phi'_{peak} - \phi'_{cv}$) is related to dilatant behavior of sand and peak friction angle is a function of dilatancy angle as it does not change with critical state friction angle. To explain this relationship in a better way a simple model named sawtooth model is used.

The simplest way to understand the relationship between the angles of friction and dilatancy is the use of sawtooth model. As observed in Figure 2.6 if a frictional block slides over another on a flat plane with an angle of friction on the plane $\phi'_{cv}$ the ratio of the shear to normal stress can be obtained as:

$$\frac{\tau}{\sigma'_n} = \tan \phi'_{cv} \tag{2.4}$$

where $\tau$ and $\sigma'_n$ are shear and normal stresses. Using critical state friction angle indicates that in this condition shearing takes place at constant volume without any dilation.

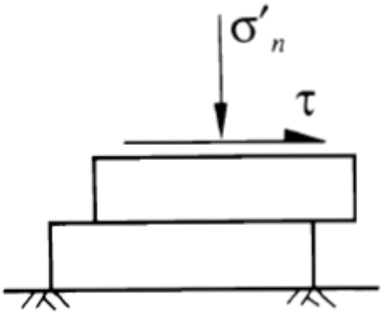


Figure 2.6. Sliding block sliding over another in a flat plane

If sliding occurs on a rough plane like a sawtooth with the teeth at an angle $\psi$ to the horizontal and with the same angle of friction $\phi'_{cv}$ as above acting on the teeth of the saw, then the relationship between the observed shear and normal stress can be obtained easily. This ratio can be defined as $\tan\phi'$ where $\phi'$ is the observed angle of friction. Therefore Equation 2.4 can be written:

$$\frac{\tau}{\sigma'_n} = \tan\phi' = \tan(\phi'_{cv} + \psi) \tag{2.5}$$

Therefore peak friction angle can be written:

$$\phi' = \phi'_{cv} + \psi \tag{2.6}$$

According to Equation 2.6 peak friction angle equals the sum of the critical state friction and dilatancy angles. There are some other theories explaining the relationship between peak friction and dilatancy angles which are discussed below.

### 2.1.2. Taylor's Theory

One of the first theories proposed for describing the relationship between dilatancy and friction angles is Taylor's theory. His theory included the dissipation of work in a frictional soil. It means that all frictional relationships can be assumed in terms of energy dissipation rather than directly in terms of forces. He used the rate of work for a sliding block on a smooth plane which is shown in figure 2.7 and derived the following equations:

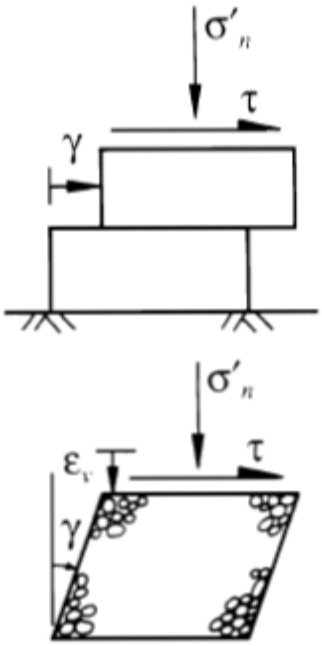


Figure 2.7. Analogy used in Taylor's energy assumption (Taylor, 1948)

$$\dot{W} = \tau\dot{\gamma} \tag{2.7}$$

where $\dot{W}$ is the rate of input work and $\gamma$ is the shear strain rate. Since this work is dissipated internally in a way which is proportional to the normal stress $\sigma_n'$ and shear strain rate $\dot{\gamma}$, rate of input work can be written:

$$\dot{W} = (\tan\phi_{cv}')\sigma_n'\dot{\gamma} \tag{2.8}$$

where $\tan\phi'_{cv}$ is the constant of proportionality. Combining Equations 2.7 and 2.8 gives $\frac{\tau}{\sigma'_n} = \tan\phi'_{cv}$ which is same with Equation 2.4. The same hypothesis is used for a soil sample in simple shear. However the input work includes $\sigma'_n\dot{\varepsilon}_v$ since dilation takes place and normal stress does work as well as shear stress. Therefore the following equation can be written:

$$\dot{W} = \sigma'_n\dot{\varepsilon}_v + \tau\dot{\gamma} = (\tan\phi'_{cv})\sigma'_n\dot{\gamma} \tag{2.9}$$

As known before $\tan\phi' = \frac{\tau}{\sigma'_n}$ and angle of dilation is given by $\tan\psi = -\frac{\dot{\varepsilon}_v}{\dot{\gamma}}$. Therefore Equation 2.9 can be written:

$$\tan\phi' = \tan\phi'_{cv} + \tan\psi \tag{2.10}$$

The obtained equation is slightly different from sawtooth model result but validates that friction angle is function of friction at constant volume and dilatancy angle.

### 2.1.3. Rowe's Theory

Rowe (1962) used a different stress-dilatancy concept from Taylor but approximately obtained similar results. Rowe examined the properties of regular assemblies of spheres and obtained expressions for both stress ratio $\frac{\sigma'_1}{\sigma'_3}$ and strain rate ratio $-\frac{\dot{\varepsilon}_3}{\dot{\varepsilon}_1}$ in terms of the geometry of packing. Rowe assumed that sliding takes place on a sawtoothed plane (Figure 2.8) and stress, strain ratios are functions of $\alpha$ and $\beta$ angles. The functions are such that $\alpha$ can be eliminated to give the following equation:

$$\frac{\sigma'_1}{\sigma'_3} = \frac{\tan(\phi_\mu + \beta)}{\tan\beta}\frac{-\dot{\varepsilon}_3}{\dot{\varepsilon}_1} \tag{2.11}$$

where $\phi_\mu$ is the fundamental angle of friction for grain to grain contact. Rowe adopted the minimum energy hypothesis to obtain $\beta = \frac{\pi}{4} - \frac{\phi_\mu}{2}$. Minimum energy hypothesis assumes that the energy ratio during deformation varies with particle arrangement with its minimum value corresponding to particular deformation state. The same result can also be obtained by assuming a minimum stress ratio at a given strain rate ratio. The final relationship was:

$$\frac{\sigma_1'}{\sigma_3'} = \tan^2\left(\frac{\pi}{4} + \frac{\phi_\mu}{2}\right)\left(\frac{-\dot{\varepsilon}_3}{\dot{\varepsilon}_1}\right) \tag{2.12}$$

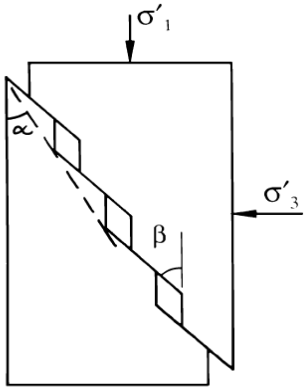


Figure 2.8. Assumed sliding mechanism for for Rowe's stress dilatancy relationship (Rowe 1962)

Equation 2.12 can be written in the short form as:

$$R = KD \tag{2.13}$$

where $D = \frac{\dot{\varepsilon}_3}{\dot{\varepsilon}_1}$, R is the stress ratio and K is a coefficient representing the internal friction which can be explained as:

$$K = \tan^2\left(45 + \frac{\phi_f}{2}\right) \tag{2.14}$$

### 2.1.4. Bolton's Equation

Bolton (1986) conducted an experimental research using plain-strain test and compared his results with data collected from 17 different sands. He compared his results obtained from plain-strain tests with previous theories of Tayor and Rowe. Figure shows there is a good correlation between his results and Rowe and Taylor's theories.

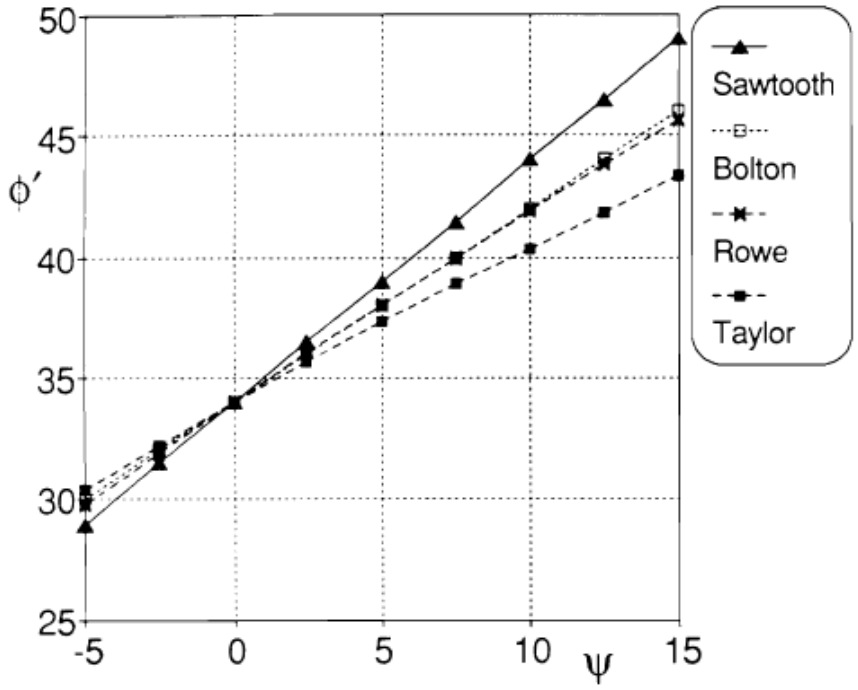


Figure 2.9. Comparisson of Bolton's equation with Taylor and Rowe's theories (Bolton, 1986)

Results showed that the empirical equation proposed by Bolton is in accordance with theories proposed by Taylor and Rowe. Bolton introduced a new relative density index and clarified its use in predicting the behaviour of sands. Using experimental data from various types of sands Bolton concluded that Equation 2.6 overestimates the $\phi'_{peak} - \phi'_{critical}$ value. Bolton presented the following equation for the relationship between the peak friction and dilatancy angles:

$$\phi'_{peak} = \phi'_{cv} + 0.8\psi \tag{2.15}$$

where $\phi_{peak}$ is the peak friction angle, $\phi_{critical}$ is the critical state friction angle of soil and $\psi$ is the angle of dilatancy which is a property of dense sands and correlates with the rate of dilation of the sand. Using the data obtained from plain-strain tests Bolton investigated the effects of relative density and mean effective stress on the angle of dilatancy for sands. Bolton proposed the following empirical equations relating the relative density, mean effective stress and dilatancy angle:

For plain strain tests:

$$\phi'_{\max} - \phi'_{critical} = 0.8\psi = 5I_R \tag{2.16}$$

For triaxial tests:

$$\phi'_{\max} - \phi'_{critical} = 0.8\psi = 3I_R \tag{2.17}$$

where $I_R$ is the relative density index which determined from the following equation:

$$I_R = I_D(Q - \ln p') - R \tag{2.18}$$

In this equation $I_D$ is density index of the sand, Q and R are constant values. Bolton determined that Q=10 and R=1 creat a good definition for all test results. Therefore Equation 2.18 can be written as:

$$I_R = I_D(10 - \ln p') - 1 \tag{2.19}$$

The following figure shows the variation of dilatancy angle with the relative density index in both plain-strain and triaxial tests.

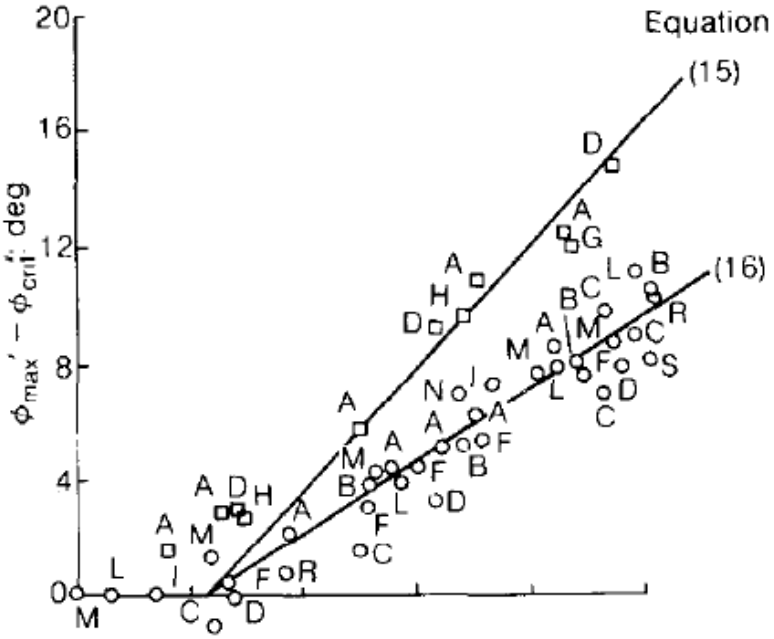


Figure 2.10. Variation of dilatancy angle with relative density index (Bolton, 1986)

Figure above shows the zero dilatancy for the relative density index equivilant to 0.23. In addition Bolton mentioned that then angle of dilatancy is a meaningless parameter in the axisymmetric triaxial compression test as mean strains in any vertical plane are contractile because of the distribution of lateral strains amongst all directions. Hence Bolton recommended to use $(-\frac{d\varepsilon_v}{d\varepsilon_1})_{max}$ as a measure of dilatancy rate in triaxial test and for both test configurations he proposed the following equation:

$$(-\frac{d\varepsilon_v}{d\varepsilon_1})_{\max} = 0.3I_R \tag{2.20}$$

### 2.1.5. Schanz and Vermeer Equation

Schanz and Vermeer (1996) conducted an experimental program using Hostun sand to compare the dilatancy angle values obtained from plain-strain test with triaxial test. Schanz and Vermeer defined the dilatancy angle in triaxial testing by modifying the mechanism used for biaxial state. Figure 2.9 shows the A mechanism with sliding on $\sigma_1 - \sigma_2$ plane and B mechanism with sliding on $\sigma_1 - \sigma_3$ plane. Each sliding mechanism is comprised of a planar deformation. Applying Equation 2.13 to each separate mechanism yields:

$$(\frac{-\dot{\varepsilon}_2}{\dot{\varepsilon}_1})_A = D_A = \frac{R_A}{K} \tag{2.21}$$

$$(\frac{-\dot{\varepsilon}_3}{\dot{\varepsilon}_1})_B = D_B = \frac{R_B}{K} \tag{2.22}$$

where $R_A$=$R_B$=R and $\dot{\varepsilon}_2 = \dot{\varepsilon}_3$ for triaxial testing conditions. In triaxial testing condition there are two contributions to the axial strain:

$$\dot{\varepsilon}_1 = \dot{\varepsilon}_{1A} + \dot{\varepsilon}_{1B} = -\frac{2\dot{\varepsilon}_3 K}{R} \tag{2.23}$$

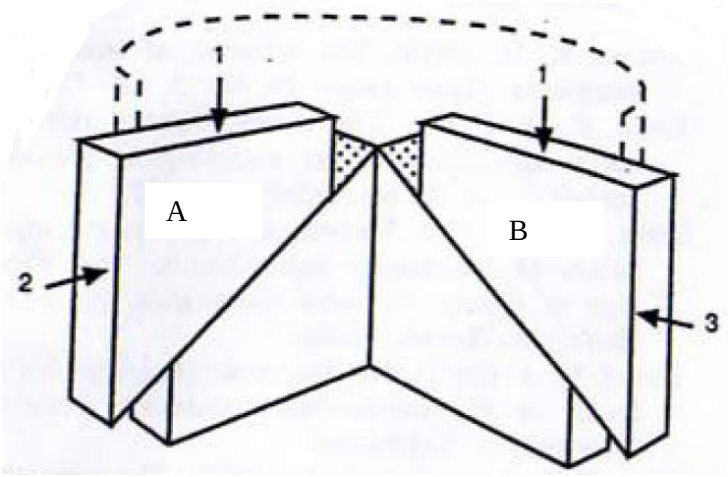


Figure 2.11. Deviation of triaxial dilatancy from biaxial state (Schanz, 1995)

Based on Equation 2.13 proposed by Rowe, D can be written :

$$D = \frac{-2\dot{\varepsilon}_3}{\dot{\varepsilon}_1} \tag{2.24}$$

The difference in definition of D parameter for plain strain and triaxial tests is a factor of two. According to Figure 2.11 volumetric strain rate can be written as:

$$\dot{\varepsilon}_v = \dot{\varepsilon}_{1A} + \dot{\varepsilon}_{1B} = \frac{\dot{\varepsilon}_2}{D_A} + \frac{\dot{\varepsilon}_3}{D_B} \tag{2.25}$$

$$D_A = D_B = -\frac{1-\sin\psi}{1+\sin\psi} \tag{2.26}$$

Therefore Schanz and Vermeer suggested the following equation for calculation of dilatancy angle in triaxial testing:

$$\sin\psi = -\frac{\frac{\dot{\varepsilon}_v}{\dot{\varepsilon}_1}}{2-\frac{\dot{\varepsilon}_v}{\dot{\varepsilon}_1}} \tag{2.27}$$

They also supported the finding that dilatancy angle is almost same in plain-strain and triaxial tests. This rule is also valid for the peak friction angle obtained from plain-strain and triaxial tests but looser sands tend to give results closer to Mohr-Coulomb failure criterion. They also concluded that for practical purposes the critical state friction angle obtained from triaxial tests should be taken as a unique value for a cohesionless soil and initial relative density and confining pressure do not affect it. In addition using the rate of dilation proposed by Bolton (Equation 2.20) they presented the following equation relating the relative density index and dilatancy angle:

$$Sin\psi = -\frac{0.3I_R}{2+0.3I_R} = \frac{I_R}{6.7+I_R} \tag{2.28}$$

### 2.1.6. Chakraborty-Salgado Equation

Chakraborty and Salgado (2010) investigated the relationship between peak friction angle, critical state friction angle and dilatancy angle at low confining pressures using plain-strain compression and triaxial compression tests data. They mentioned that previous works done specially by Bolton do not contain any data for low confining pressures. However in many practical cases such as interpretation of in-situ tests at shallow depths or estimating soil response at shallow depths more detailed relationships for peak friction, critical state friction and dilatancy angles are required. They defined three ranges of confinement: $p' \langle 50$ kPa; $50 \le p' \le 100$ kPa; and $p' \rangle 100$ kPa. They separated the data to five groups according to the relative densities. Specimens were classified to very loose (0-15%), loose (15-35 %), medium (35-65%), dense (65-85%) and very dense (85-100%). The most complete data used for their research was Touyora sand data which included tests at very low confining pressures. They used critical state friction angle of $\phi'_{cv} = 32.8$ for

triaxial and $\phi'_{cv} = 36$ for PS conditions. They plotted $\phi'_{peak} - \phi'_{cv}$ versus $I_D$ and $I_R$ in Figures 2.9 and 2.10 for both triaxial and plain strain conditions. It was observed that Bolton's equation fit well for the data of Toyoura sand used in their research. Results also showed that trixial data points are almost at the same trend with plain-strain data points. They concluded that contribution of dilatancy to shear strength for both cases is almost similar. According to Figure (2.10) peak friction angle can be assumed as summation of critical state friction angle and a part of relative density index. They claimed that for Bolton's equation:

$$\phi'_{peak} = \phi'_{cs} + A_{\psi} I_R \tag{2.29}$$

$A_{\psi} = 3.8$ is valid for both triaxial and plain-strain tests. Therefore by rearranging Equation 2.19 and 2.29, they obtained the following equation:

$$\frac{\phi'_{peak} - \phi'_{cv}}{3.8} + I_D \ln \frac{100 p'}{p'_A} = I_D Q - R \tag{2.30}$$

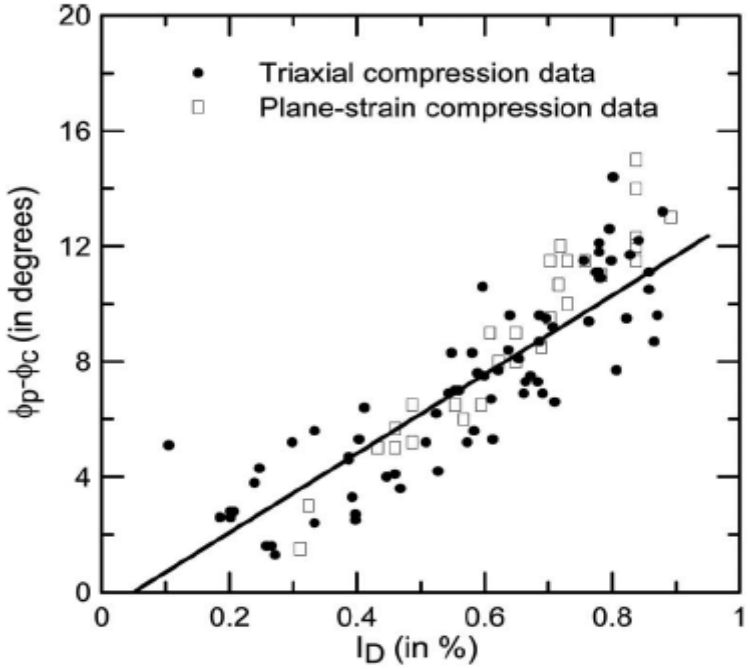


Figure 2.12. Triaxial and plain-strain compression data points for Toyoura sand for determining $A_{\Psi}$ (Chakraborty-Salgado, 2010)

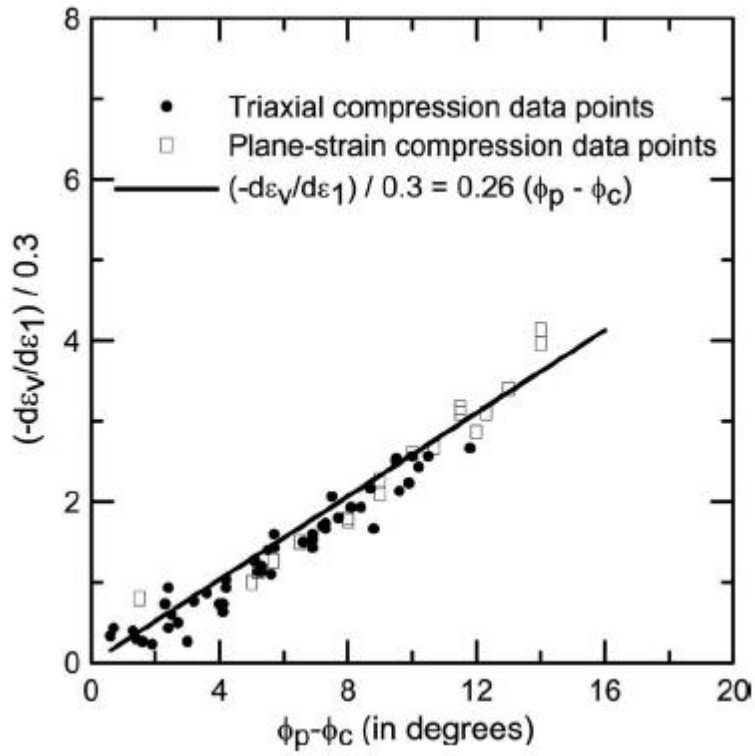


Figure 2.13. Variation of $\phi'_p - \phi'_c$ with $I_R$ (Chakraborty-Salgado, 2010)

Variation of R and Q values with confining stress in triaxial compression tests on Toyoura sand was observed by Chakraborty and Salgado. The Q values varied in the 7.7-10 range when R was set to 1. As it is shown in Figure (2.14), the value of Q drops with considerably with decreasing confining stress.

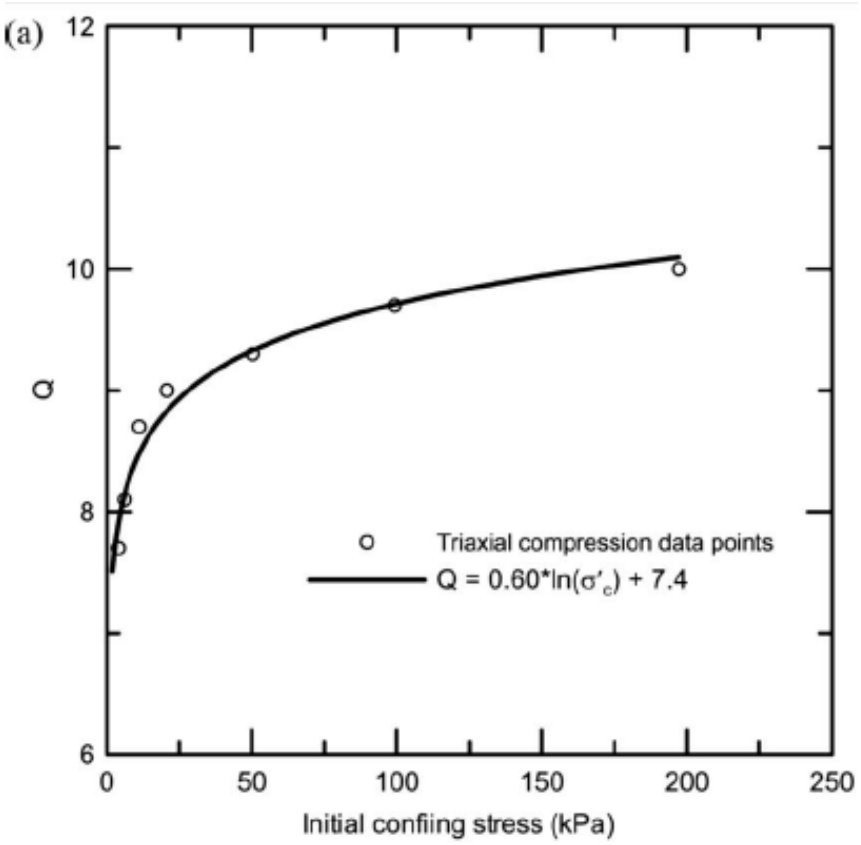


Figure 2.14. Variation of Q value with increasing effective confining stress for triaxial compression tests (Chakraborty-Salgado, 2010)

Based on the observations they suggested a simple empirical equation between Q and $\sigma_c'$ in triaxial compression tests as follows:

$$Q = 7.4 + 0.6 \ln \sigma_c' \tag{2.31}$$

Therefore Equation 2.31 can be substituted into Equation 2.30 which may be used to calculate the peak friction and dilatancy angles in case of low confining pressures:

$$\frac{\phi'_{peak} - \phi'_{cs}}{3.8} + I_D \ln \frac{100\,p'}{P'_A} = I_D(7.4 + 0.6 \ln \sigma_c') - R \tag{2.32}$$

### 2.1.7. Vaid and Sasitharan Equation

Vaid and Sasitharan (1991) investigated the effects of stress path in the triaxial test on stress and dilatancy of sand since in many geotechnical problems field loading may not be in the same direction with the deposition direction of sand as in the case in triaxial compression test and field stress paths may include loadings that have angle $\alpha$ to the vertical direction. Therefore Vaid and Sasitharan conducted consolidated drained triaxial tests using both compression ($\alpha = 0$) and extension ($\alpha = 90$) modes of loading which are possible loading modes in triaxial test. The material used for testing was Erksak sand passed No.10 sieve and retained on No.100 sieve. Erksak sand was sheared along various stress paths wich included increasing and decreasing mean effective stress. Samples were prepared with different relative densities using vibratory method which made specimens possess high degree of uniformity. Consolidation stresses varied between 100-2400 kPa.

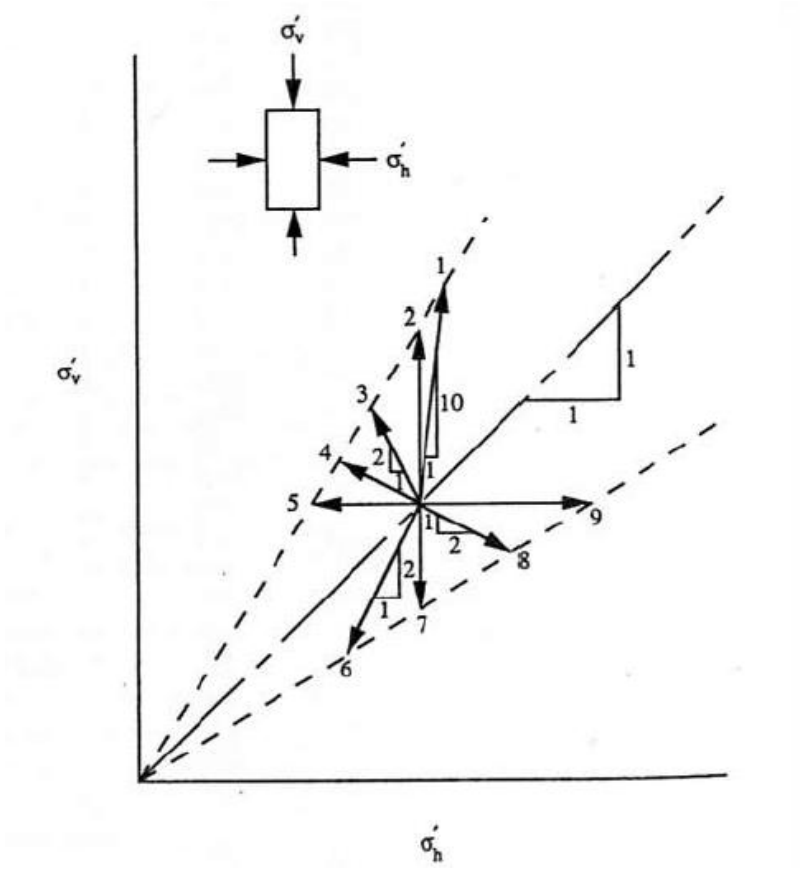


Figure 2.15. Schematic view of stress paths (Vaid and Sasitharan, 1991)

Results showed that the maximum rate of dilatancy $-\left(\frac{d\varepsilon_v}{d\varepsilon_a}\right)_{\max}$ occurred when stress-strain curve reached the peak independent of stress path or loading direction. In addition the rate of dilatancy in triaxial extension tests showed to be smaller than triaxial compression tests. Results showed a similar relationship between peak friction angle $\phi'_p$ and maximum rate of dilatancy, $-\left(\frac{d\varepsilon_v}{d\varepsilon_a}\right)_{max}$, regardless of stress paths.

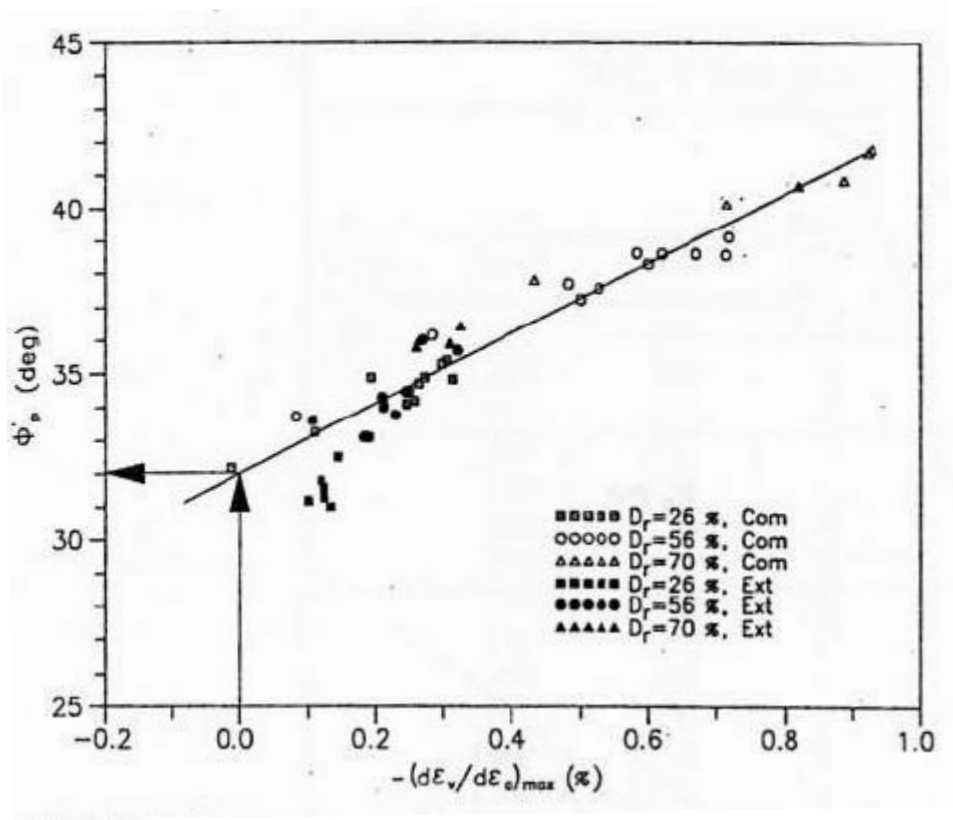


Figure 2.16. Relationship between peak friction angle and maximum rate of dilatancy $d\varepsilon_v/d\varepsilon_a$ in compression and extension tests (Vaid and Sasitharan, 1991)

Based on the results shown in Figure 2.16 Vaid and Sasitharan proposed the following linear relationship which related the peak friction angle, angle of shearing at constant volume and maximum rate of dilation:

$$\left|\frac{d\varepsilon_v}{d\varepsilon_a}\right|_{\max} = 0.1(\phi'_{peak} - \phi'_{cv}) \tag{2.33}$$

Vaid and Sasitharan defined the angle of dilation for triaxial compression test as:

$$\psi = \sin^{-1}\left[\frac{-d\varepsilon_v}{d\gamma}\right] \tag{2.34}$$

$$= \sin^{-1}\left[\frac{-d\varepsilon_v}{d\varepsilon_1 - d\varepsilon_3}\right] \tag{2.35}$$

In triaxial compression:

$$d\varepsilon_1 = d\varepsilon_a \tag{2.36}$$

$$d\varepsilon_3 = d\varepsilon_r = \frac{d\varepsilon_v - d\varepsilon_a}{2} \tag{2.37}$$

Substituting equations 2.36 and 2.37 into equation 2.35 gives:

$$\psi = \sin^{-1}\left[\frac{2}{\frac{3}{\left|d\varepsilon_v / d\varepsilon_a\right|} + 1}\right] \tag{2.38}$$

Similarly for triaxial extension test:

$$d\varepsilon_3 = d\varepsilon_a \tag{2.39}$$

$$d\varepsilon_1 = d\varepsilon_r = \frac{d\varepsilon_v - d\varepsilon_a}{2} \tag{2.40}$$

Substituting Equation 2.39 and 2.40 into Equation 2.35 gives:

$$\psi = \sin^{-1}\left[\frac{2}{\frac{3}{\left|d\varepsilon_v / d\varepsilon_a\right|} - 1}\right] \tag{2.41}$$

Using Equations 2.38 and 2.41 dilatancy angles were calculated and plotted against peak friction angle. It was noted that a unique linear relationship occurred between peak friction angle and maximum dilatancy angle. Therefore they modified the relationship proposed by Bolton with relates the peak friction angel with critical state and dilatancy angles and presented the following equation:

$$\phi'_p = \phi'_{cv} + 0.33\psi \tag{2.42}$$

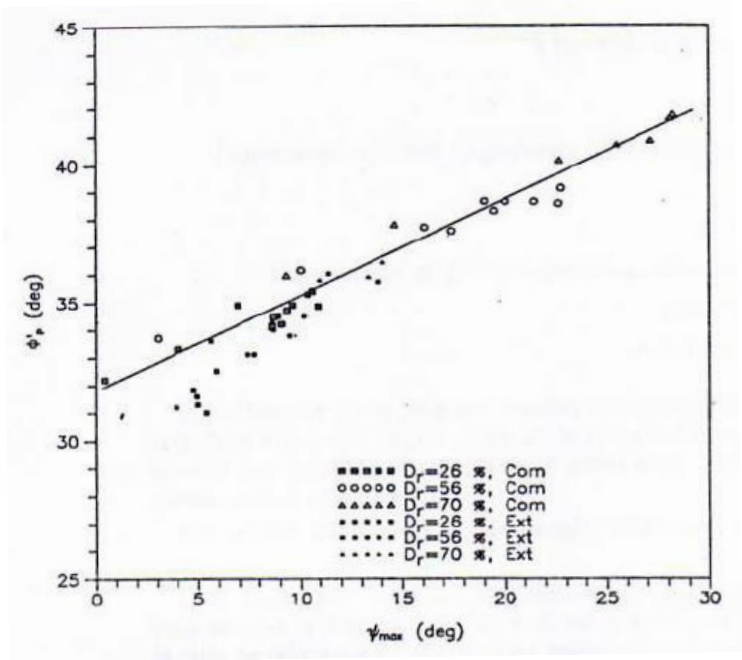


Figure 2.17. Relationship between peak friction angle and maximum dilatancy angle for compression and extension trixial tests (Vaid and Sasitharan, 1991)

The relationships presented by Vaid and Sasitharan found to be valid over a wide range of confining stresses varying from 50 to 2500 kPa.

### 2.1.8. Fukushima and Tatsuoka Research

Fukushima and Tatsuoka (1984) conducted a series of drained triaxial compression tests at very low confining pressures on saturated samples of sand. They investigated the dependency of peak friction angle and deformation characteristics of sands on confinement value. They tried to confirm their results using stress-dilatancy relations at failure.

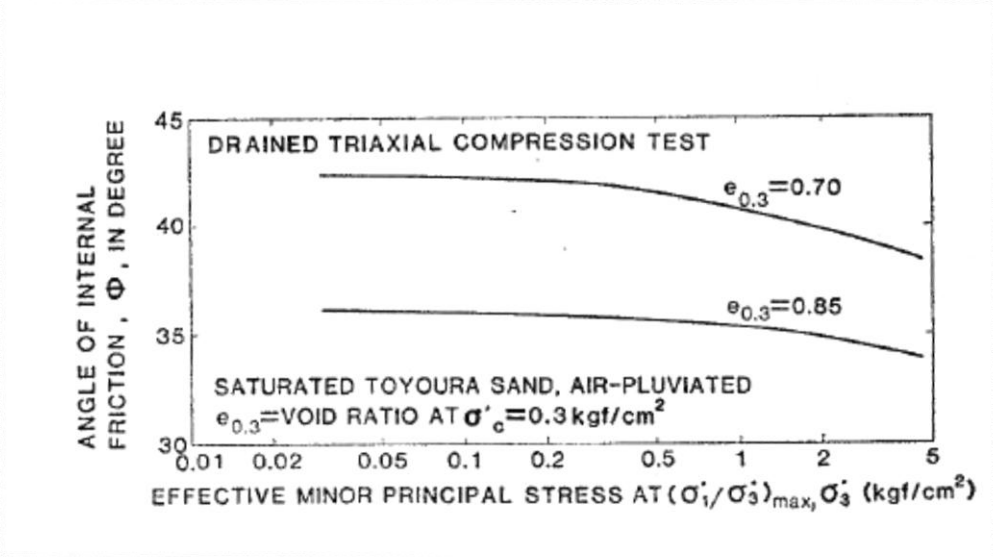


Figure 2.18. Relationship between peak friction angle and $\sigma'_3$ for e=0.7 and 0.85 (Fukushima and Tatsuoka, 1984)

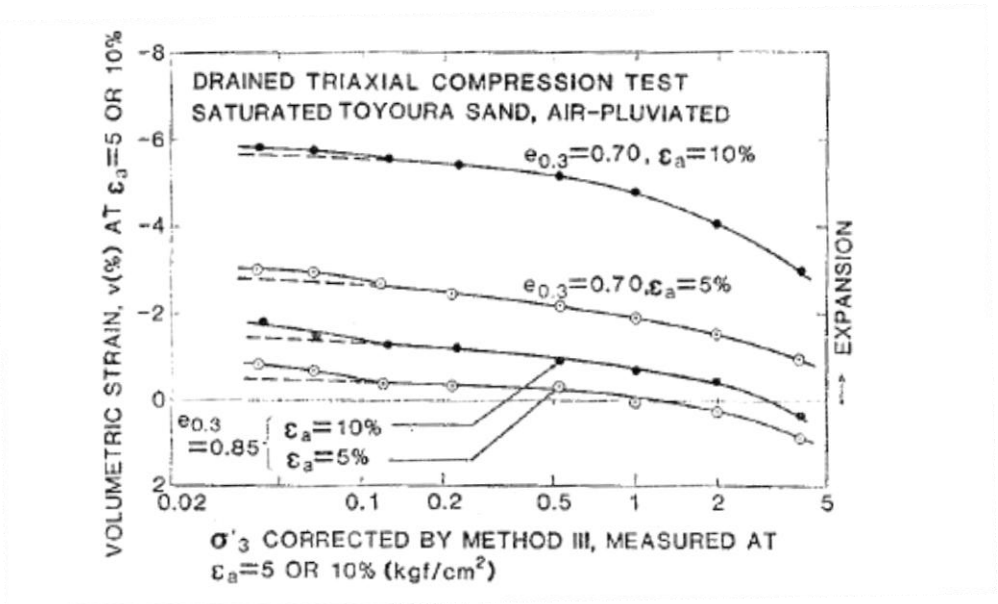


Figure 2.19. Volumetric strain values versus $\sigma'_3$ (Fukushima and Tatsuoka, 1984)

Fukushima and Tatsuoka concluded that the angle of internal friction of saturated Toyoura sand does not vary too much with the change in effective horizontal stress when $\sigma_3'$ is lower than 50 kPa (Figure 2.18). Specialy the variation of peak friction angle with the variation of effective horizontal stress was found to be very small when $\sigma_3'$ was around 10 kPa.

In addition as observed in figure the dilatant behavior of Toyoura sand seemed to change slightly with confinement when $\sigma_3'$ was lower than 50 kPa.

## 2.2. At Rest Lateral Earth Pressure Coefficient of Overconsolidated Cohesionless Soils

Theories that deal with the calculation of lateral earth pressures are central to the design of many geotechnical structures, such retaining walls, abutments, deep excavations, and tunnels. Especially for the estimation of lateral thrust acting on many geotechnical engineering structures at no deformation states, it is vital to be able to calcultate the at rest lateral earth pressures. That is why earth pressure theories is an important research area in soil mechanics. After Jaky's well-known equation for the at rest earth pressure of normally consolidated soils, numerous researchers proposed theories for the estimation of the at rest earth pressure of overconsolidated soils. Some of the most notable works on the at rest earth pressure of overconsolidated cohesionless soils are presented below:

### 2.2.1. Wroth (1973) Equation:

Wroth (1973) proposed the following equation for determining the at rest earth pressure coefficient of overconsolidated sands based on evaluatin of the in situ measurements of initial stresses and deformation characteristics. His equation is commonly used by geotechnical engineers in design of earth retaining structures:

$$K_{0(OC)} = K_{0(NC)} OCR - \left[\frac{\mu}{1-\mu}\right](OCR-1) \qquad (2.35)$$

where $K_{0(NC)}$ is obtained from the following equation (Jaky equation):

$$K_{0(NC)} = 1 - \sin\phi \tag{2.36}$$

$\mu$ is the poisson ratio of the soil. We can assume $\mu = 0.1 - 0.3$ for loose sands and $\mu = 0.3 - 0.4$ for dense sands. $K_{0(NC)}$ is the at rest earth pressure coefficient for normaly consolidated sands and OCR is the overconsolidation ratio.

### 2.2.2. Meyerhof (1976) Equation:

Later Meyerhof (1976) conducted experimental and theoretical investigation on the bearing capacity and settlement of deep foundations. He proposed a semi-empirical formula for approximate estimation of $K_0$ for overconsolidated soils. His equation for estimating the at rest lateral earth pressure coefficient of overconsolidated soils includes the peak friction angle and overconsolidation ratio of the soil:

$$K_{0(OC)} = (1 - \sin\phi)\sqrt{OCR} \tag{2.37}$$

### 2.2.3. Mayne-Kulhawy (1982) Equation

Mayne and Kulhawy expressed the difficulty for the prediction of at rest earth pressure of overconsolidated soils as they undergo a complex stress history of loading and unloading. Mayne and Kulhawy collected reported $K_0$ data from the literature and presented the data with the form shown in Figure 2.20 Dashed lines in Figure 2.20 show the variation of $K_{0(unloading)}/K_{0(loading)}$ with overconsolidation ratio for different soil types where α is the slope of the dashed line. Therefore α can be obtained from the following equation:

$$\alpha = \frac{\log(K_{0u}) - \log(K_{0nc})}{\log(OCR)} \tag{2.38}$$

Results showed that α appears to be constant with OCR. Considering results of both sand and clay samples they determined an average value of 0.509 for α.

They proposed an upper limit for $\alpha$ which equals one. They suggested that the parameter $\alpha$ is uniquely dependant on the effective stress peak friction angle of the soil. In order to evaluate the suitability of their proposition,the researchers plotted the collected $K_o$ data against their corresponding $\sin\phi'$ values (Figure 2.21).

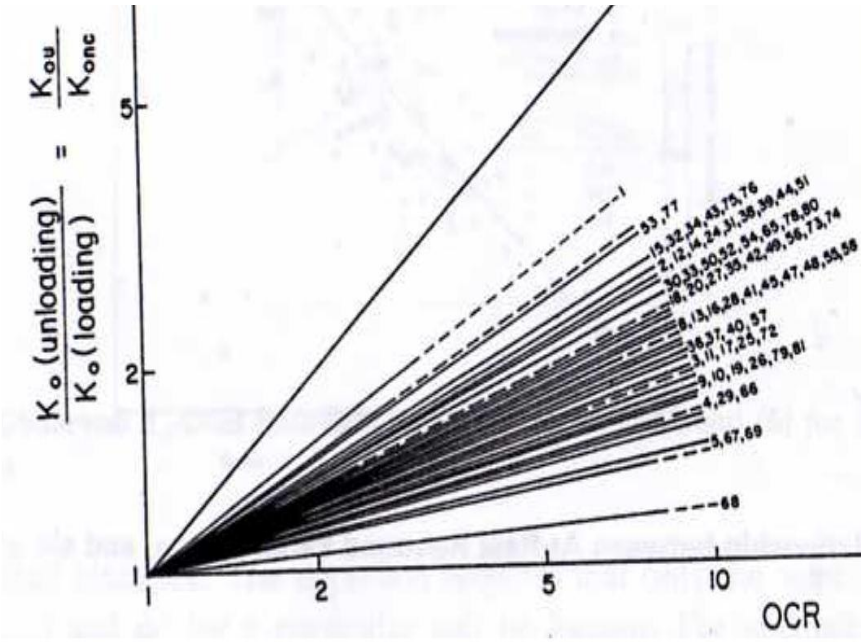


Figure 2.20. Relationship between $K_0$ and OCR for cohesionless soils during unloading (Mayne and Kulhawy, 1982)

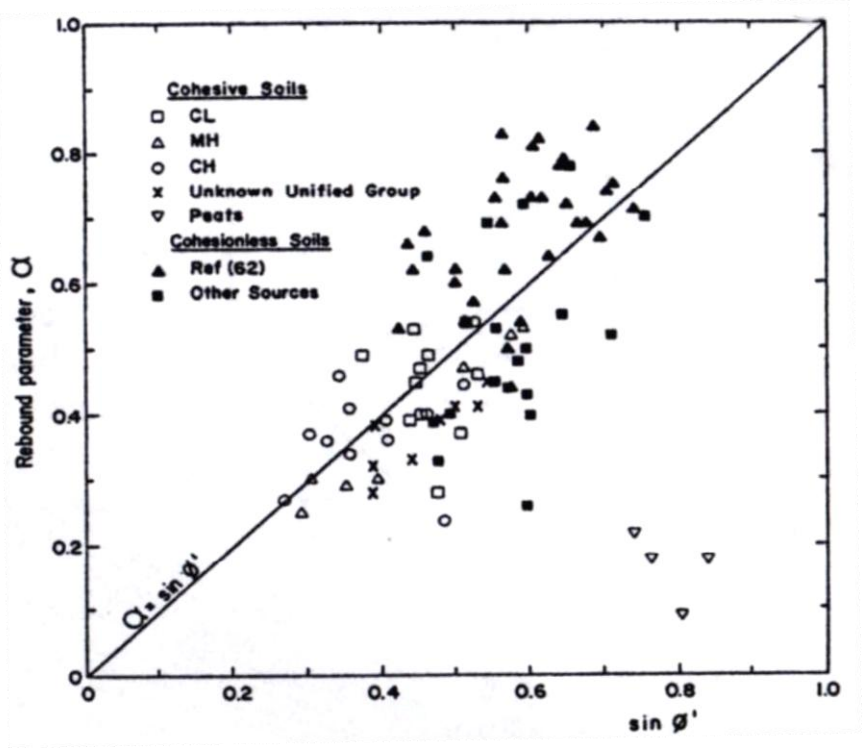


Figure 2.21. Relationship between $\alpha$ and $\sin\phi'$ for clays and sands (Mayne and Kulhawy, 1982)

Results showed that $\alpha$ can be defined with the following equataion:

$$\alpha = \sin\phi' \tag{2.39}$$

Therefore they presented the following equation for estimating at rest earth pressure coefficient of overconsoliated soils:

$$K_{0u} = (1-\sin\phi')OCR^{\sin\phi'} \tag{2.40}$$

### 2.2.4. Chau-Ping Yang (1991) Equation

Chau-ping (2001) mentioned that at rest earth pressure coefficient is a deformation parameter while related equations in the literature evaluate the at rest earth pressure coefficient from the view point of shear strength. Therefore he investigated the

deformation mechanism of soils to explore the nature of $K_0$. His research included a triaxial testing program using standard Ottawa sand. He conducted several experiments with different relative densities and overconsolidation ratios. He observed the variation of $C_c$ and $C_s$ which are compression and swell indexes during the loading and unloading of the sample with the effective vertical stress.

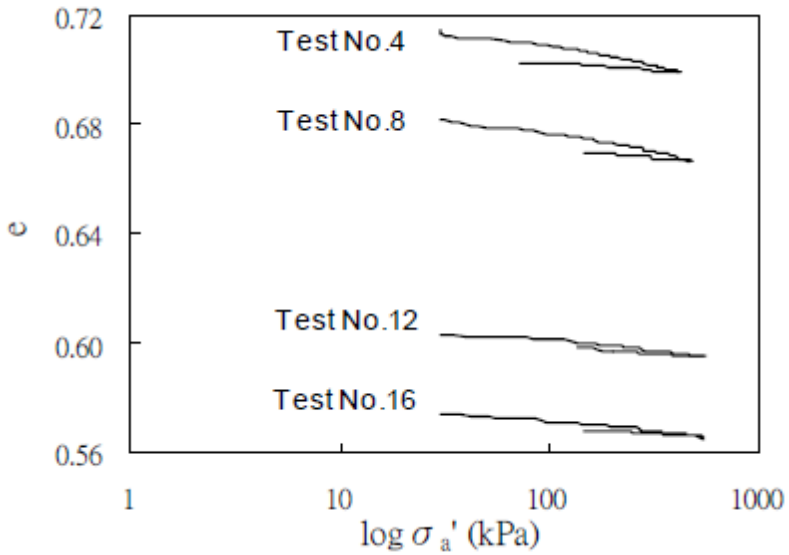


Figure 2.22. Variation of void ratio with effective vertical stress in $K_0$ triaxial test (Chau-Ping Yang, 2001)

Based on experimental results Chau-Ping yang suggested that at rest earth pressure coefficient of sands can be obtained from the following empirical equation:

$$K_{0u} = A.(C_c - C_s).\log(OCR) + (1 - \sin\phi') \qquad (2.41)$$

where A is a parameter varying with relative density of the sand. The value of A for specimens with relative densities of 30%, 75% and 90% are 115, 127 and 144 respectively.

### 2.2.5. Daramola (1980) Equation

Daramola (1980) discussed the difficulties associated with the selection of appropriate value for the Poisson's ratio in Wroth (1973) equation as density and stress-state conditions affect the elastic properties of the sand. Therefore he tried to find a more appropriate parameter instead of Poisson's ratio based on the information during $K_0$ unloading of sands. Daramola (1980) conducted several tests in stress path cell using samples of Ham river sand. Samples were prepared at various relative densities. Axial and lateral deformations of the sample were obtained using transducers. It was tried to keep the samples at $K_0$ condition (zero lateral strain) by increasing the cell pressure. Samples were $K_0$-consolidated to an effective vertical stress of 700 kPa and unloaded to effective vertical stresses of 400, 200 and 100 kPa before they were sheared. Therefore the specimens were overconsolidated by overconsolidation ratios of 1.75, 3.5 and 7 respectively.

Stress paths during loading and unloading of the samples were monitored. Figure 2.23 shows the plot of the stress path with the slope of unloading stress path as $\beta$. Ratio of the effective horizontal stress change to effective vertical stress change was shown as $\lambda$. Therefore $\lambda$ was defined with the following equation:

$$\lambda = \frac{1-\beta}{1+\beta} \tag{2.42}$$

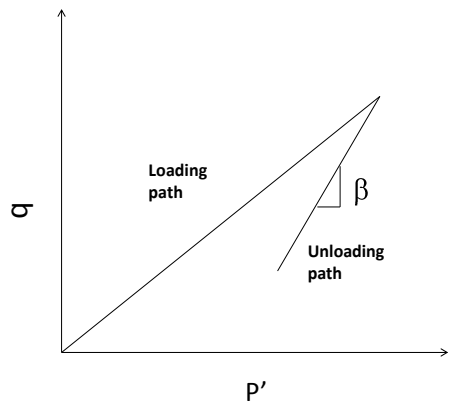

Figure 2.23. Stress path during loading and unloading of (Daramola, 1980)

Daramola modified Wroth equation by replacing $\frac{\mu}{1-\mu}$ with $\lambda$. Therefore Equation 2.35 was written as the following equation:

$$K_{0(OC)} = K_{0(NC)}OCR - \lambda(OCR - 1) \tag{2.43}$$

The value of $\beta$ was obtained from the series of unloading paths plotted against initial void ratio of the samples as shown in Figure 2.24 .

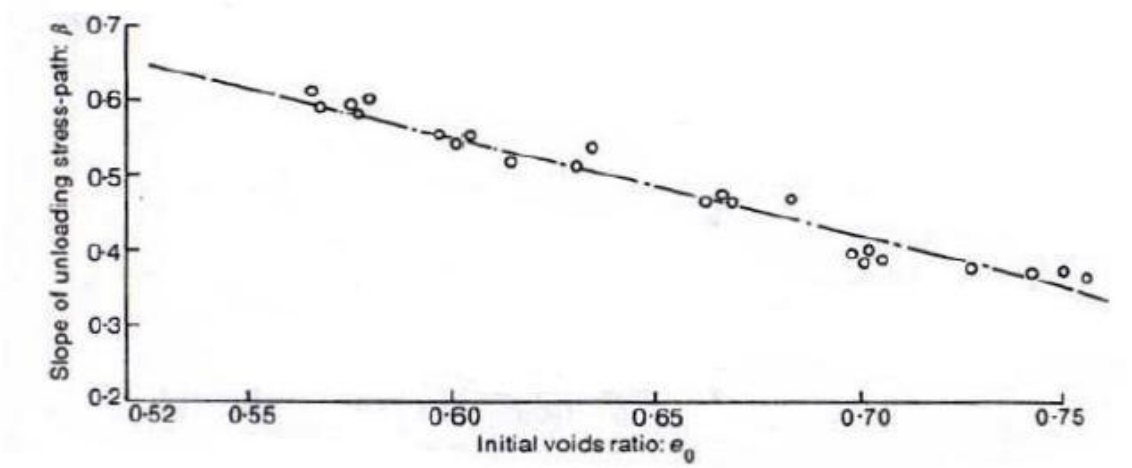


Figure 2.24. Variation of slope of unloading path with initial void ratio (Daramola, 1980)

### 2.2.6. Hanna-Al-Romhein (2008) Study

Hanna and Al-Romhein (2008) conducted physical modelling experiments using a testing tank and a model retaining wall with cohesionless backfill. Model retaining wall was installed in the upper part of the tank. Five pressure transducers were installed on the modeled retaining wall in order to obtain the lateral earth pressure distribution on the wall.

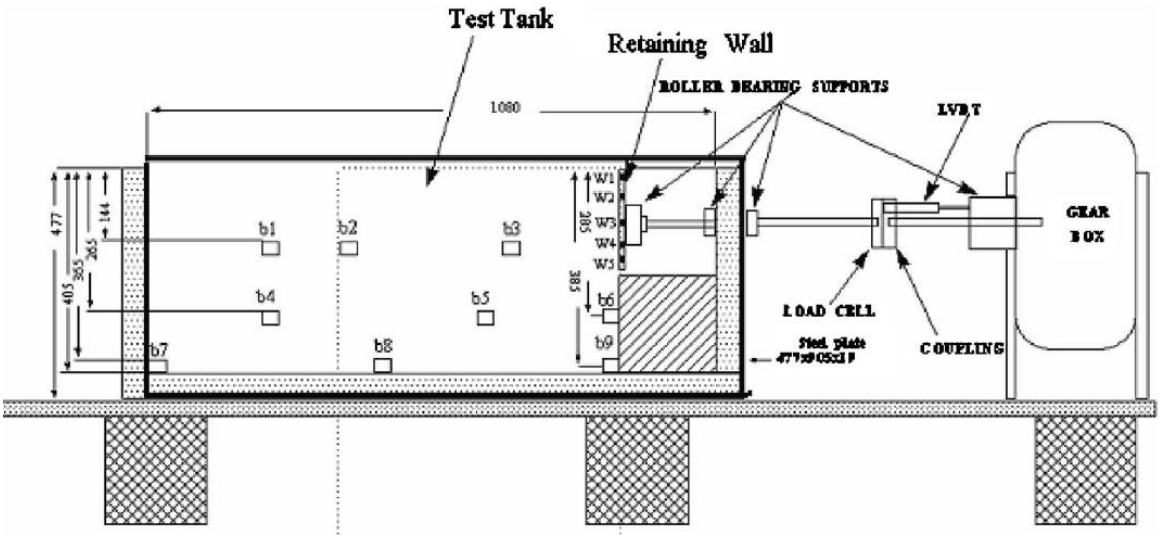


Figure 2.25. View of the experimental setup (Hanna and Al-Romhein, 2008)

Standard Ottawa sand was used in this research and sand sample was prepared by air pluviation method. Sand backfill was loaded and unloaded to reach the required overconsolidation ratio. Later by measuring the values of effective vertical and effective horizontal stresses using pressure transducers following equation was presented for estimating the at rest earth pressure coefficient of cohesionless soils using the peak friction angle and overconsolidation ratio of the soil:

$$K_{0(OC)} = (1-\sin\phi)OCR^{(\sin\phi-0.18)} \tag{2.44}$$

Hanna and Al-Romhein (2008) compared their equation with equations of Wroth (1973), Mayne-Kulhawy (1982) and Meyerhof (1976). It was noted that the values predicted by Hanna and Al-Romhein (2008) empirical equation agreed well with experimental values obtained from Wroth, Mayne-Kulhawy and Meyerhof.

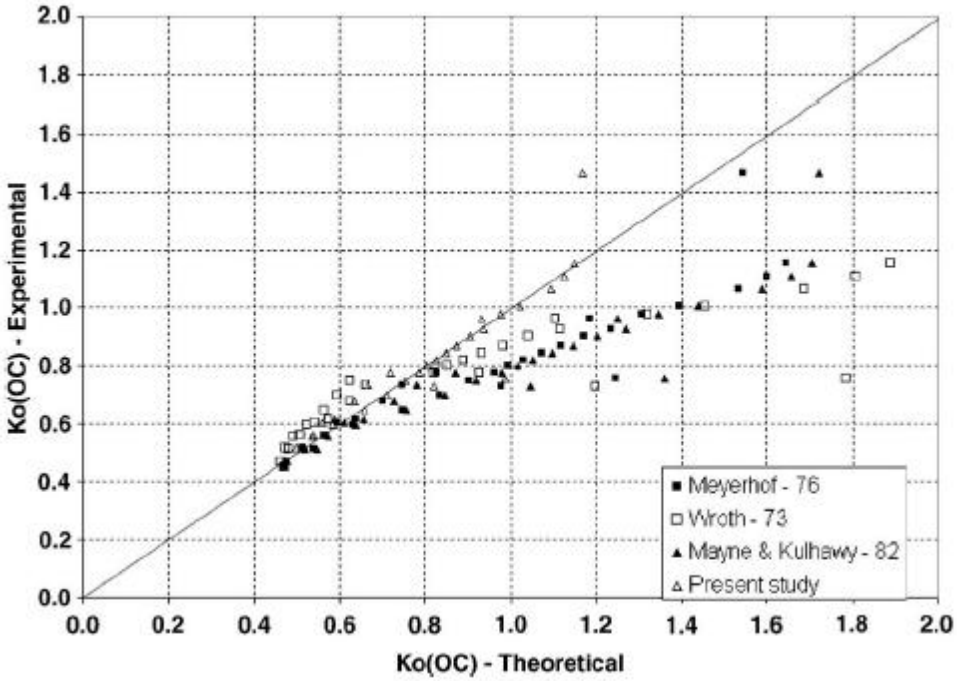


Figure 2.26. Comparison between theoretical and experimental values of $K_0$ (Hanna and Romhein, 2008)

Based on Hanna and Romhein (2008), at rest lateral earth pressure coefficient increases significantly with OCR and theoretical values which were compared with experimental results were in good agreement up to OCR values of 3.

# 3. Methodology

The objective of this research was to investigate the strength parameters and at rest lateral earth pressure coefficient of cohesionless soils. For this purpose a testing program that includes CD triaxial tests was prepared. The reconstituted samples were initially consolidated under $K_o$ conditions after which they were sheared under drained conditions to obtain the corresponding strength parameters Parameters such as relative density and overconsolidation ratio (OCR) were varied between the tests. Therefore $K_0$ triaxial test has been selected as the testing method in this research.

## 3.1. $K_0$ Triaxial Testing Program

Within the course of this research program, more than 80 CD tests were conducted under $K_o$ conditions. Relative density, OCR, vertical effective stress at the end of consolidation ($\sigma'_{vc}$) were the variables in the planned testing program. The aim in conduction CD tests on cohesionless samples was to track the variation of void ratio changes and to confirm the zero lateral strain state. All triaxial tests were conducted according to the ASTM (D7181) standard. Automatic triaxial testing apparatus was used for the experimental program. Automatic triaxial testing apparatus is able to consolidate samples without lateral straining by arranging the cell pressure automatically. Cohesionless soil used in testing was prepared in the lab to have the same gradation with the standard Ottawa sand ASTM (C-788) in order to avoid the variation of gradation between samples. Triaxial tests have been conducted on samples having overconsolidation ratios of 1, 2, 4 and 8. Table 3.1 shows the experimental program arranged for this study which includes data regarding the overconslidation ratios of the tests and effective vertical stresses at the end of loading-unloading stages.

Table 3.1. Experimental program

| Test No. | OCR | $\sigma'_{vc}$ (kPa) | $\sigma'_{vpreshear}$ (kPa) | $D_R$ (%) |
|---|---|---|---|---|
| 1 | 1 | 100 | 100 | 63 |
| 2 | 1 | 100 | 100 | 51 |
| 3 | 1 | 50 | 50 | 49 |
| 4 | 1 | 250 | 250 | 49 |
| 5 | 1 | 500 | 500 | 49 |
| 6 | 1 | 200 | 200 | 64 |
| 7 | 1 | 200 | 200 | 49 |
| 8 | 1 | 0 | 1500 | 66 |
| 9 | 1 | 400 | 400 | 100 |
| 10 | 1 | 400 | 400 | 49 |
| 11 | 2 | 400 | 200 | 54 |
| 12 | 2 | 400 | 200 | 73 |
| 13 | 2 | 500 | 250 | 76 |
| 14 | 2 | 500 | 250 | 60 |
| 15 | 2 | 200 | 100 | 76 |
| 16 | 2 | 200 | 100 | 50 |
| 17 | 2 | 200 | 100 | 63 |
| 18 | 2 | 800 | 400 | 73 |
| 19 | 2 | 800 | 400 | 64 |
| 20 | 2 | 800 | 400 | 88 |
| 21 | 2 | 1200 | 600 | 90 |
| 22 | 2 | 1200 | 602 | 59 |
| 23 | 2 | 400 | 200 | 53 |
| 24 | 2 | 50 | 25 | 55 |
| 25 | 2 | 500 | 250 | 51 |
| 26 | 2 | 150 | 75 | 57 |
| 27 | 2 | 100 | 50 | 56 |
| 28 | 2 | 100 | 50 | 78 |
| 29 | 2 | 100 | 50 | 39 |
| 30 | 2 | 100 | 48 | 46 |
| 31 | 4 | 200 | 50 | 51 |
| 32 | 4 | 200 | 50 | 41 |
| 33 | 4 | 100 | 25 | 41 |
| 34 | 4 | 200 | 50 | 76 |
| 35 | 4 | 200 | 48 | 73 |
| 36 | 4 | 200 | 50 | 75 |

Table 3.1. Experimental program (cont.).

| Test No. | OCR | $\sigma'_{vc}$ (kPa) | $\sigma'_{vpreshear}$ (kPa) | $D_R$ (%) |
|---|---|---|---|---|
| 37 | 4 | 200 | 48 | 71 |
| 38 | 4 | 800 | 196 | 53 |
| 39 | 4 | 1000 | 250 | 53 |
| 40 | 4 | 1000 | 250 | 85 |
| 41 | 4 | 1000 | 250 | 80 |
| 42 | 4 | 1000 | 250 | 61 |
| 43 | 4 | 1000 | 250 | 54 |
| 44 | 4 | 1600 | 400 | 68 |
| 45 | 4 | 1600 | 408 | 93 |
| 46 | 4 | 1600 | 400 | 90 |
| 47 | 4 | 800 | 200 | 56 |
| 48 | 4 | 800 | 200 | 61 |
| 49 | 4 | 800 | 200 | 76 |
| 50 | 4 | 800 | 208 | 61 |
| 51 | 4 | 800 | 200 | 73 |
| 52 | 4 | 800 | 200 | 34 |
| 53 | 4 | 400 | 102 | 63 |
| 54 | 4 | 400 | 100 | 56 |
| 55 | 4 | 400 | 100 | 85 |
| 56 | 4 | 400 | 100 | 34 |
| 57 | 4 | 400 | 100 | 83 |
| 60 | 8 | 200 | 25 | 33 |
| 61 | 8 | 200 | 25 | 43 |
| 62 | 8 | 1600 | 200 | 88 |
| 64 | 8 | 1600 | 200 | 63 |
| 65 | 8 | 1600 | 200 | 73 |
| 66 | 8 | 2000 | 250 | 88 |
| 67 | 8 | 2032 | 246 | 68 |
| 68 | 8 | 800 | 96 | 90 |
| 69 | 8 | 800 | 100 | 76 |
| 70 | 8 | 800 | 98 | 56 |
| 71 | 8 | 400 | 51 | 56 |
| 75 | 8 | 3200 | 409 | 98 |
| 76 | 8 | 3200 | 400 | 80 |
| 77 | 8 | 3200 | 400 | 76 |
| 78 | 8 | 3200 | 400 | 75 |
| 79 | 8 | 3200 | 403 | 81 |
| 80 | 8 | 3200 | 410 | 82 |

## 3.2. Testing Material

Standard Ottawa graded sand was selected as the testing material in this research. Grain size distribution of the sample is given in Figure 3.1. Standard Ottawa sand is classified as a poorly graded sand (SP) with the coefficient of uniformity, $C_u$ ,of 2.16 and coefficient of curvature, $C_c$ , of 1.45 .

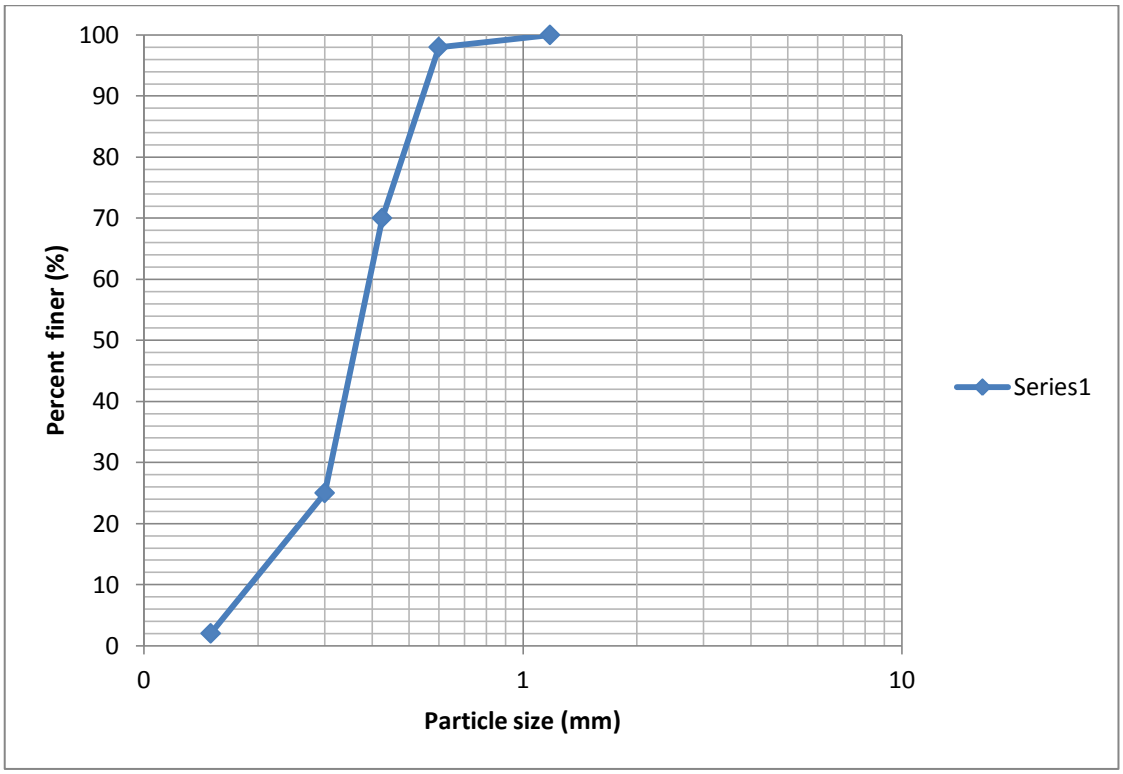


Figure 3.1. Ottawa sand grain size distribution

Relative density tests were conducted for determining the minimum and maximum void ratios of the sand sample according to ASTM D-4253 and ASTM D-4254 standards. Maximum and minimum void ratios of the sample were determined as 0.96 and 0.56 respectively. Ottawa sand is classified as poorly graded sand according to unified soil classification system. Five specific gravity tests were carried out and an average value of 2.67 was determined for the sand used in the experimental program. The dry unit weight of the sand samples used in triaxal tests varied between 14.65 and 17.85 kN/m$^3$.

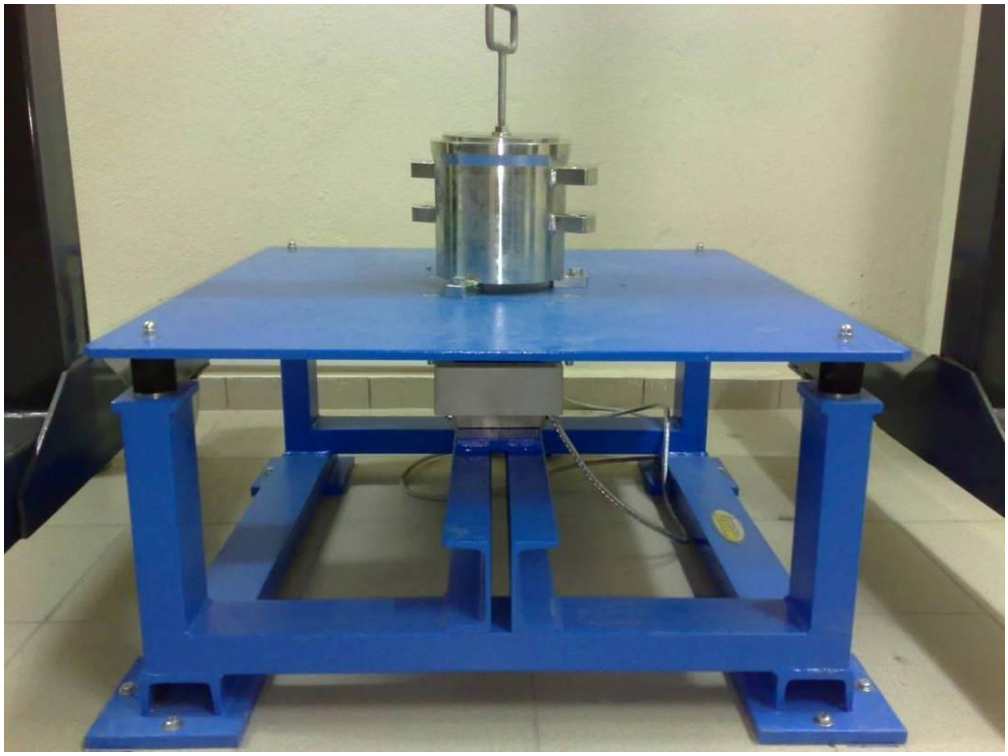

Figure 3.2. Relative density test apparatus

Basic properties of the tested sand have been summarized in the following table:

Table 3.2. Basic properties of the tested sand

| **Sand Type** | **Specific gravity** | **Uniformity coefficient** | **Curvature coefficient** | **Maximum void ratio** | **Minimum void ratio** |
|---|---|---|---|---|---|
| Ottawa graded sand | 2.67 | 2.16 | 1.45 | 0.96 | 0.56 |

### 3.2.1. Particle Shape Analysis of Sand Grains

Particle shape influences soil behavior (Wadell et al.). Cho et al. (2006) investigated the effects of particle shape on different characteristics of sands such as void ratio, critical state friction angle, compressibility under zero lateral strain loading and etc. Therefore it is insightful to obtain shape parameters of sand grains used in experimental research programs. Shape properties of sand particles in this research are analysed according to three important scales which are described below:

(i) Sphericity S: Refers to the global form of the particle and reflects the similarity between particle's dimensions (length, height and width). (Cho et al., 2006)

(ii) Roundness R (angularity): Describes the scale of major surface features which are typically one order of magnitude smaller than the particle size. Roundness is quantified as the average radius of curvature of surface features relative to the radius of the maximum sphere than can be inscribed in the particle. (Cho et al., 2006)

(iii) Smoothness (roughness): Describes the particle surface texture relative to the radius of the particle. (Cho et al., 2006)

Cho et al. suggested the following chart for determining the shape parameters of particles. Sphericity and roundness of the sand particles used in this experimental program were determined according to the proposed chart.

Ottawa graded sand used in this experimental program is within ranges of four sieve gaps. 30 particles from each sieve gap were analysed using the stereomicroscope (Figure 3.4). Sphericity and roundness parameters of the particles in each sieve gap were determined separately.

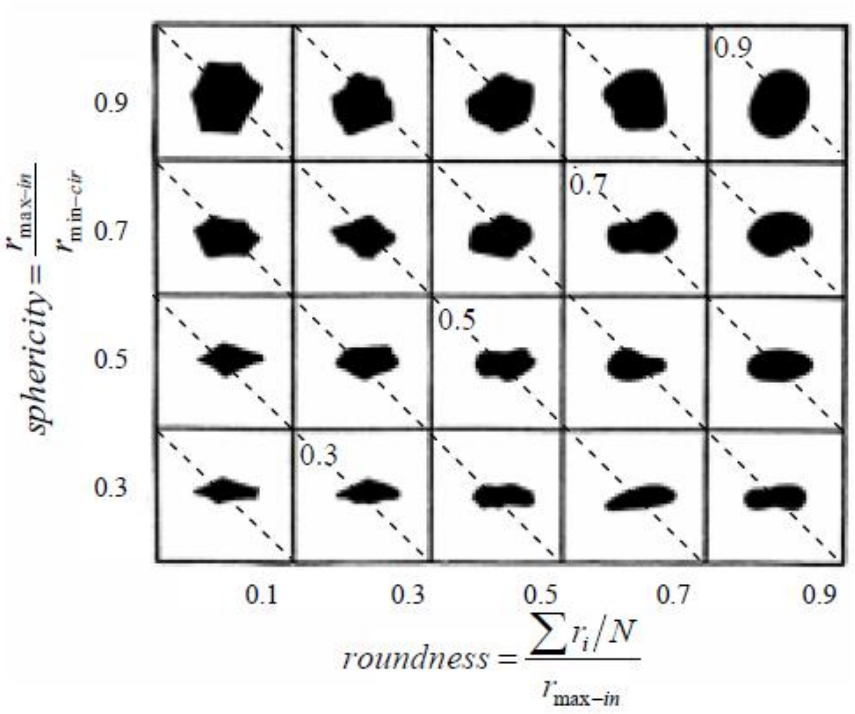


Figure 3.3. Particle shape determination chart (Cho et. al., 2006)

Figure 3.4. Stereomicroscope

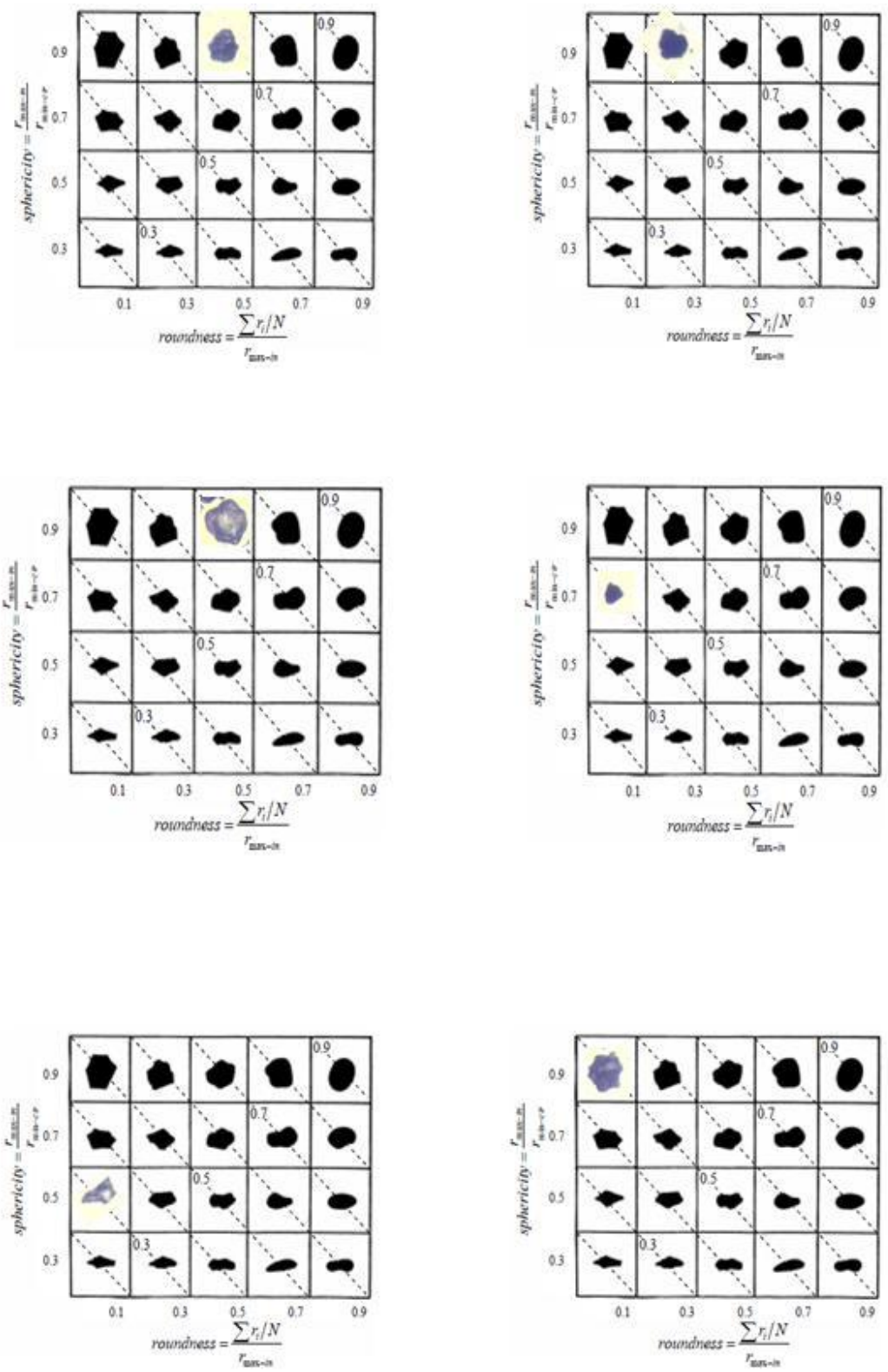


Figure 3.5. Samples of stereomicroscope photographs on shape determination chart

Based on the shape determination chart proposed by Cho et al. The sphericity and roundness of the sand particles within different sieve gaps which were used in Ottawa graded sand production were determined.

Table 3.3. Sphericity and roundness of sand particles

| **Sieve Gap** | **16-30** | **30-40** | **40-50** | **50-100** |
|---|---|---|---|---|
| **Sphericity** | 0.76 | 0.8 | 0.72 | 0.78 |
| **Roundness** | 0.38 | 0.34 | 0.36 | 0.38 |

## 3.3. Sample Preparation

Air pluviation technique was selected as the sample preparation method in this experimental program. In this method dry sand falls through a funnel from a predetermined height so that the required void ratio for the sand sample could be achieved. Funnel is moved up as the sand is pluviating to keep the raining height constant and thus to achieve uniformity throughout the sample. According to Kolbuzewsky (1948), air-pluviated sample's density is proportional to the height of the fall. Accordingly a series of air-pluviation tests were performed to define the variation of void ratio with raining height. Obtained relationship as shown in Figure.3.6 can be considered to be linear. Obtained equation is given below:

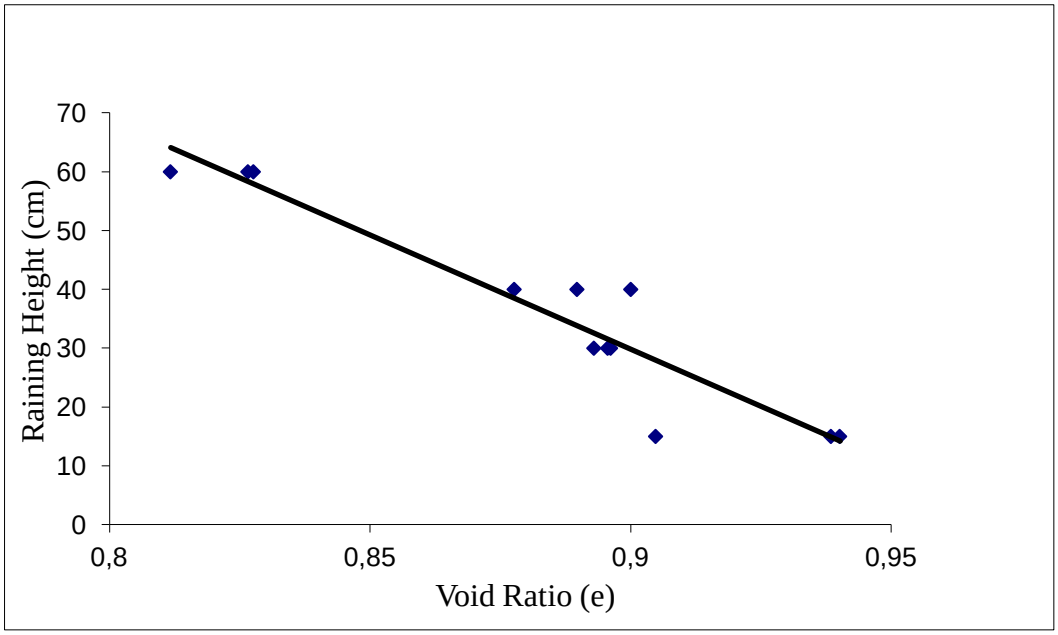


Figure 3.6. Variation of the void ratio with raining height

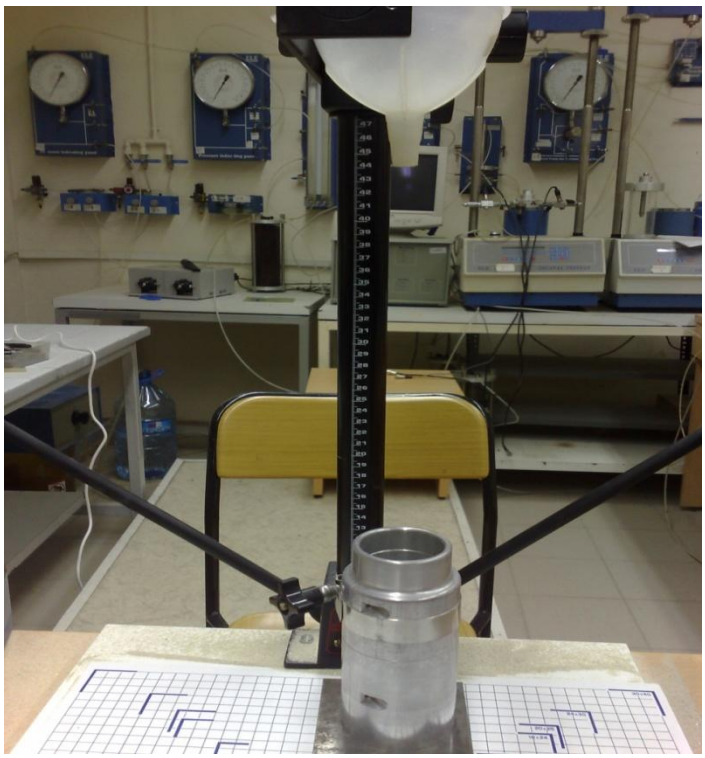

Figure 3.7. Air-pluviation set-up for sample preparation

$$h = -388.53e + 379.5 \qquad (3.1)$$

where h is the raining height in centimeters and e is the void ratio of the sample prepared by pluviation.

### 3.4. Automatic Triaxial Testing Apparatus

Automatic triaxial apparatus consists of two automatic flow pumps and a computer controlled loading frame (Figure. 3.8). Loading frame contains a control system and the components to generate the force on the sample. Loading frame, which is also called the load trac also measures the force and displacement during the test. Automatic flow pumps are also called flow tracs. Flow tracs are intelligent units composed of a flow pump, a pressure sensor and a control board.

Figure.3.8. Automatic triaxial system

Flow pumps in flow tracs (Figure. 3.9) regulate pressure and volume in test cell. Flow tracs contain precision micro stepper motor which moves a piston in a water filled cylinder. Pressure transducers are mounted at the end of the cylinder. They determine the signals being sent to the stepper motor. The number of motor steps is used to calculate the volume changes. Flow tracs are capable of maintaining the desired pressure within 0.35 kPa. Pressure increments can increase and decrease in any pattern by any amount. The count readings from sensors are converted to engineering units. Calibration factors provide this conversion.

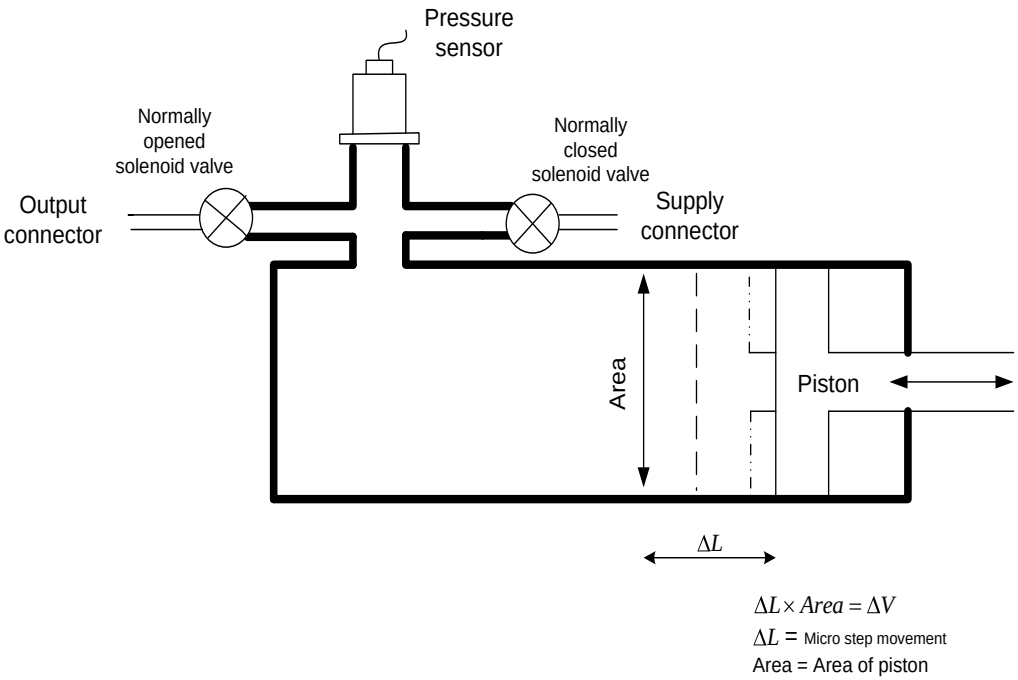


Figure 3.9. Schematic of a flow trac unit

### 3.5. Triaxial Testing Procedure

$K_0$ consolidated drained triaxial test was selected as the testing method in this research. Automatic triaxial apparatus conducts consolidated drained triaxial tests in four stages as:

(i) Initialisation

(ii) Saturation

(iii) Consolidation

(iv) Shearing

### 3.5.1. Initialisation Phase

During the initialization phase a small horizontal and vertical stress along with the pore pressure is applied to the specimen. It is done in order to observe that the apparatus functions properly and there is no leakage of water from the valves of the apparatus. This phase takes about 20 minutes.

### 3.5.2. Saturation Phase

In saturation phase cell and pore pressures are increased incrementally while effective stress on the specimen is kept constant in order to achieve the maximum saturation ratio. When the increase in the cell pressure is applied the system monitors the increase in pore pressure automatically. According to ASTM (D-7181) pore pressure parameter is obtained from the following equation:

$$B = \frac{\Delta u}{\Delta \sigma_3} \tag{3.2}$$

where $\Delta u$ is the change in the specimen pore pressure that occurs when cell pressure changes and specimen drainage valves are closed and $\Delta \sigma_3$ is the change in cell pressure.

Before applying the next cell pressure increment the pore pressure is raised and held constant in order to maintain the effective stress on the specimen. This results in higher B values. Minimum Skempton value of B=0.95 has been achieved in all experiments.

### 3.5.3. Consolidation Phase:

Consolidation phase started after samples reached the minimum Skempton value of 0.95. This step was run in all tests without lateral straining ($K_0$ consolidation). Automatic

triaxial system arranges the cell pressure in order to prevent lateral straining of the sample during the loading and unloading of the sample. It means that cell pressure increased by the automatic system when the sample is being loaded vertically and decreases while the sample is being unloaded. Samples have been loaded and unloaded with a constant stress ratio of 5 kPa/min. Samples were loaded and unloaded during the consolidation phase to gain overconsolidation ratios of 1, 2, 4 and 8.

Hence at rest earth pressure coefficient of sand samples could be monitored during the whole consolidation phase (loading and unloading) by dividing the effective horizontal stress value to the effective vertical stress value in $K_0$ triaxial tests.

$$K_0 = \frac{\sigma'_h}{\sigma'_v} \tag{3.3}$$

where $K_0$ is the at rest earth pressure coefficient, $\sigma'_h$ is the effective horizontal stress and $\sigma'_v$ is the effective vertical stress.

### 3.5.4. Shearing Phase

In this stage samples were sheared under drained conditions by increasing the vertical stress with the constant strain rate of $2.5\times10^{-2}$ %/min. According to ASTM (D-7181) shear strain rate has been obtained from the following equation:

$$\dot{\varepsilon} = \frac{4\%}{10t_{90}} \tag{3.4}$$

where $\dot{\varepsilon}$ is the shear strain rate and $t_{90}$ is the time corresponding to 90% primary consolidation.

Samples were sheared until they reached the maximum axial strain value of 20%. Critical state behavior of the sand was well observed by reaching this axial strain value.

## 3.6. Triaxial Test Corrections

There are some important corrections which have to be done to obtain realistic results from triaxial tests.

1. Piston area correction
2. Rubber membrane correction
3. Sample area correction

### 3.6.1. Piston Area Correction

Piston which applies the vertical stress to the sample is influenced by the buoyancy force trying to move the piston in the reverse direction. In order to omit the effect of buoyancy in vertical stress calculations, effective area of the piston has been measured by filling the cell with water only and applying pressure to the piston. Buoyancy force has been measured while the cell pressure was increasing. Results were plotted and the effective area of the piston was determined from the slope of the line relating the cell pressure and produced buoyancy force as shown in Figure 3.11.

Based on the results from Figure 3.11 the effective area of the piston was determined as 153 $mm^2$. Therefore buoyancy force could be calculated from the following equation:

$$F_b = 0.153\sigma_c + 6.25 \tag{3.5}$$

where $F_b$ is the buoyancy force in Newtons and $\sigma_c$ is the cell pressure in kPa. Calculated buoyancy force was subtracted from the total load value.

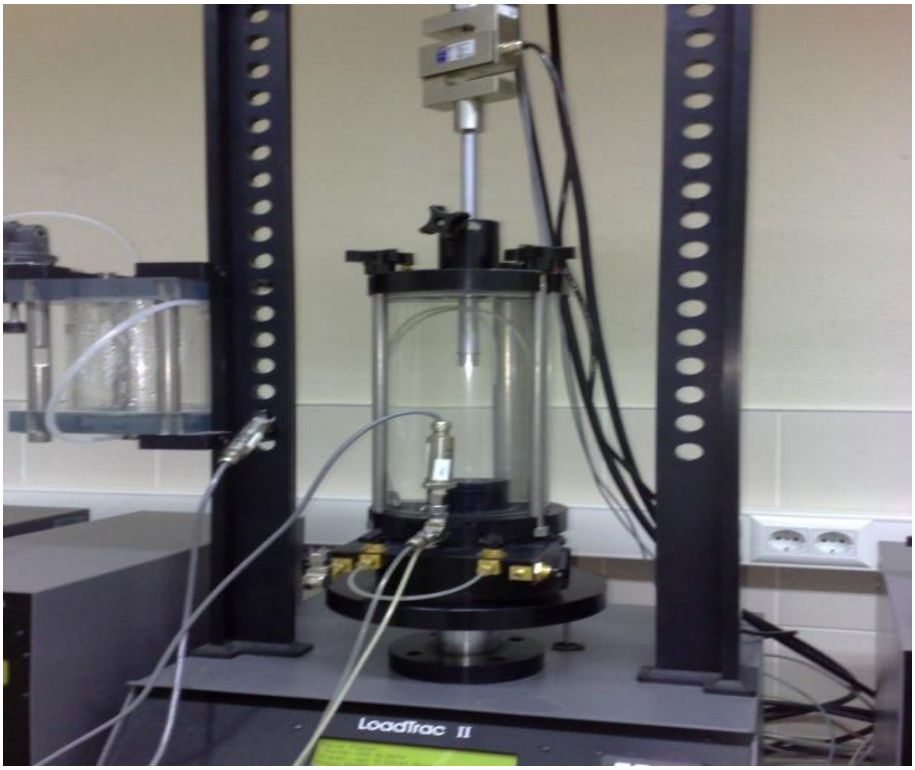


Figure 3.10. Piston area correction test

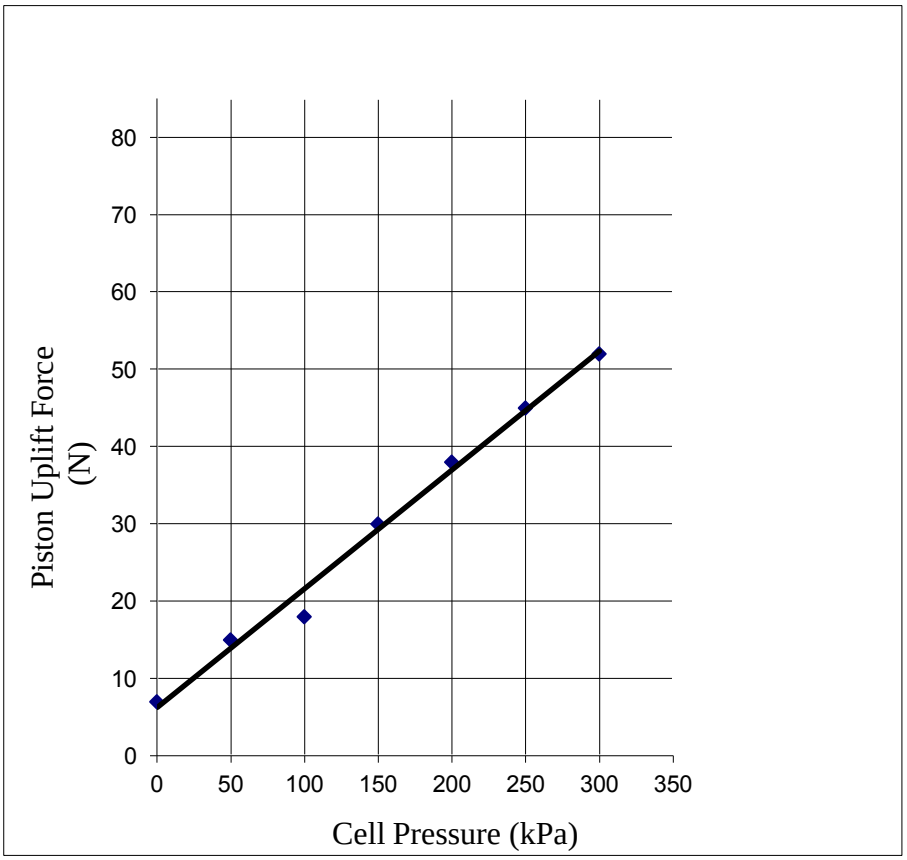


Figure 3.11. Variation of uplift force with cell pressure

### 3.6.2. Correction for the Rubber Membrane

Thickness of the membrane restraint can influence the radial stress applying to the sample. According to ASTM (D-4767), the following equation is used to correct the principal stress difference for the effect of rubber membrane:

$$\Delta(\sigma_1 - \sigma_3) = (4E_m t_m \varepsilon_1) / D_c \tag{3.6}$$

where $\Delta(\sigma_1 - \sigma_3)$ is the correction to be subtracted from the measured deviator stress, $D_c$ is the diameter of the sample after consolidation, $E_m$ is the young's modulus for the membrane material, $t_m$ is the membrane thickness and $\varepsilon_1$ is the axial strain. In order to find Young's modulus for the latex membrane, tensile test has been done pulling the membrane and measuring the observed strain. Young's modulus is obtained from Equation 3.7. Results showed a value of 1450 kPa for the Young's modulus of the membranes used in the triaxial testing program.

$$E_m = \left(\frac{F}{A_m}\right) / \left(\frac{\Delta L}{L}\right) \tag{3.7}$$

where $E_m$ is the Young's modulus of the membrane material, F is the force applied to stretch the membrane, L is unstretched length of the membrane, $\Delta L$ is the change in length of the membrane and $A_m$ is the area of the membrane which can be calculated from the following equation:

$$A_m = 2t_m W_s \tag{3.8}$$

where $t_m$ is the thickness of the membrane and $W_s$ is the width of the circumferential strip.

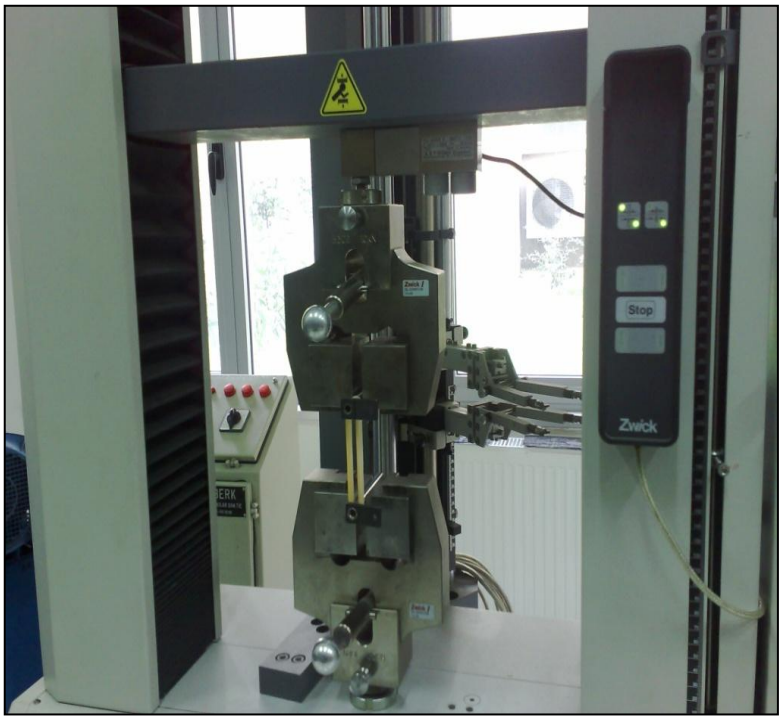


Figure 3.12. Tensile test

### 3.6.3. Correction for Sample Area

There are two kinds of area correction for the samples being tested which depends on the shape the sample takes during the shearing phase.

1. Uniform area correction (Figure 3.14)
2. Parabolic area correction. (Figure 3.15)

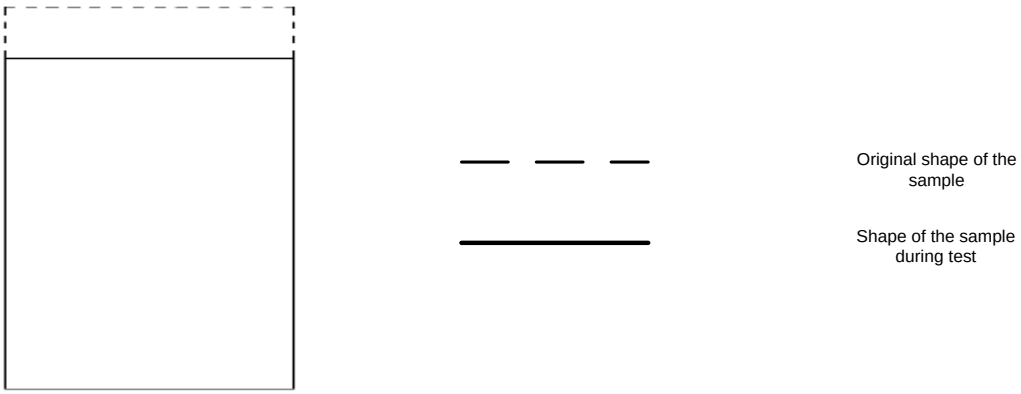


Figure 3.13. None area correction

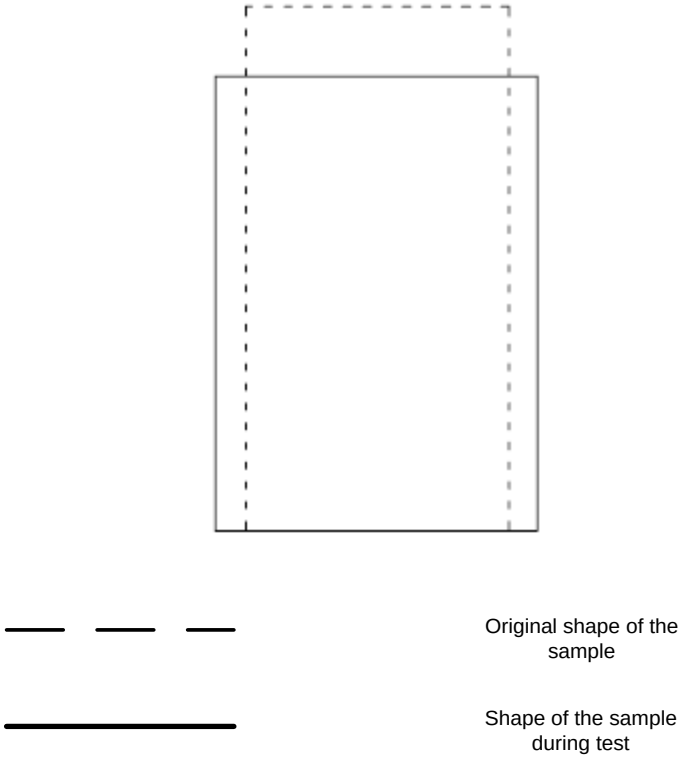


Figure 3.14. Uniform area correction

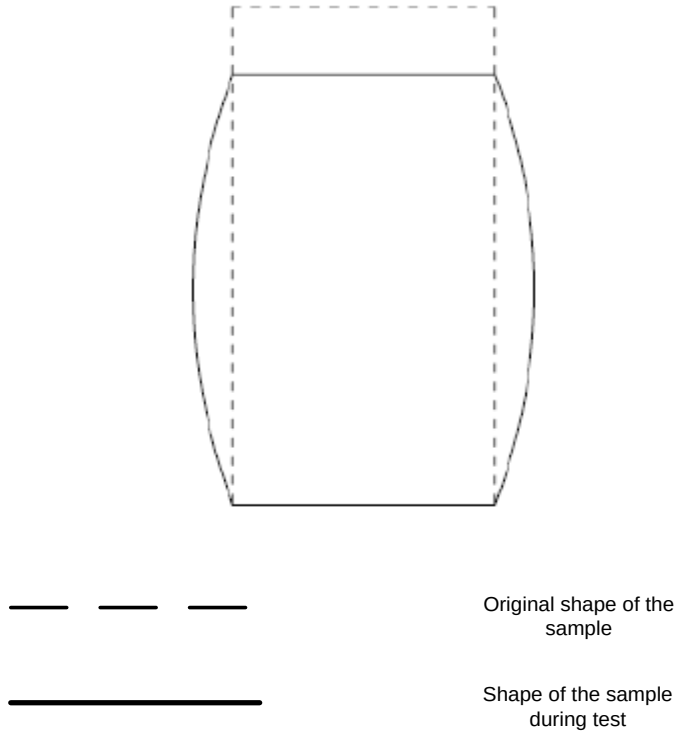


Figure 3.15. Parabolic area correction

Sand samples' shapes were parabolic during the shearing phases (Figure 3.16). Therefore the sample area under the applied vertical loads varied as the sample shape changed into parabolic form. In order to correct the area change in vertical stress calculations, following equation has been used:


Figure 3.16. Parabolic shape of the sample during shearing

$$A_c = A_0 \frac{1-\varepsilon_v}{1-\frac{5}{3}\varepsilon_1} \tag{3.9}$$

where $A_c$ is the corrected area for the sample, $A_0$ is the initial area of the sample, $\varepsilon_v$ is the volumetric strain during shearing and $\varepsilon_a$ is the axial strain. Volumetric strain is obtained from the following equation:

$$\varepsilon_v = \frac{\Delta V_s}{V_c} \tag{3.10}$$

where $\Delta V_s$ is the volume change of the sample during the shearing phase and $V_c$ is the volume of the sample after the consolidation phase. Axial strain is also obtained from the following equation:

$$\varepsilon_1 = \frac{\Delta h}{h_c} \tag{3.11}$$

where :

$\Delta h$ = change in height of the specimen during loading

$h_c$ = height of sample after consolidation which can be obtained from the following equation:

$$h_c = h_0 - \Delta h_0 \tag{3.12}$$

where $h_0$ is the initial height of the sample and $\Delta h_0$ is the change of height in the specimen at the end of the consolidation phase.

### 3.7. Information About the Triaxial Tests

After conducting triaxial tests, obtained raw data is corrected by applying the appropriate corrections factors. After all corrections, data is analysed in detail. Data includes information about time, load, cell pressure motor steps counter and pore pressure motor steps counter. Cell pressure and pore pressure step numbers allows the calculation of the sample volume changes. Area and length of the sample are measured at the beginning of each test. Therefore the following properties can be determined for each sample:

(i) Maximum effective vertical stress ($\sigma'_{v\max}$): Vertical stress is calculated from the following equation:

$$\sigma_v = \frac{F_c}{A_c} \tag{3.13}$$

where $\sigma_v$ is the total vertical stress (kPa), $F_c$ is the corrected load (N) and $A_c$ is the corrected area of the sample ($m^2$). Therefore effective vertical stress could be obtained from Equation 3.14:

$$\sigma'_v = \sigma_v - u \tag{3.14}$$

where $\sigma'_v$ (kPa) is the effective vertical stress (kPa) and u (kPa) is the pore water pressure.

Variation of the effective vertical stress versus axial strain is monitored in all tests and peak value for the effective vertical stress is thus obtained.

(ii) Peak deviatoric stress ($q_{peak}$): Deviatoric stress is obtained using the following equation:

$$q = \sigma_1 - \sigma_3 = \sigma'_1 - \sigma'_3 \tag{3.15}$$

where q is the deviatoric stress and $\sigma'_3$ is the effective horizontal stress. The peak value for deviatoric stress is obtained by monitoring the variation of the deviatoric stress with axial strain.

(iii) At rest lateral earth pressure coefficient at the end of normal consolidation/ Normally consolidated lateral earth pressure coefficient for at rest state ($K_{0c}$): At rest lateral earth pressure coefficient of the sample is obtained from Equation 3.16:

$$K_{0c} = \frac{\sigma'_h}{\sigma'_v} \tag{3.16}$$

(iv) At rest lateral earth pressure coefficient at the end of the unloading phase / Overconsolidated lateral earth pressure coefficient for at rest state ($K_{0u}$): At rest earth pressure coefficient at the end of unloading corresponds to the at rest lateral earth pressure coefficient of the overconsolidated sample. $K_{ou}$ is calculated using the following equation:

$$K_{0u} = \frac{(\sigma'_h)_{preshear}}{(\sigma'_v)_{preshear}} \tag{3.17}$$

where $(\sigma'_h)_{preshear}$ is the effective horizontal stress at the end of unloading step and $(\sigma'_v)_{preshear}$ is the effective vertical stress at the end of unloading stage.

(v) Peak friction angle ($\phi'_{peak}$): Depiction of the stress state of the sample at the instance of failure using a Mohr circle renders the calculation of peak internal friction angle of the soil possible.

(vi) Dilatancy angle ($\psi$): There are several equations proposed in the literature for determining the dilatancy angle however most the equations have been proposed according to plain-strain test data. Schanz and Vermeer (1995) modified the proposed equations for triaxail testing conditions mentioned in chapter two and proposed the following equation for calculation of dilatancy angle using triaxial test data. Therefore Schanz and Vermeer empirical equation was selected for determining the dilatancy angle value of triaxial tests in the experimental program.

$$\sin\psi = -\frac{\frac{\dot{\varepsilon}_v}{\dot{\varepsilon}_1}}{2-\frac{\dot{\varepsilon}_v}{\dot{\varepsilon}_1}} \tag{2.27}$$

(vii) Critical state friction angle ($\phi'_{cs}$): Critical state friction angle of the sample is calculated by constructing the Mohr circlecorresponding to the residual state.

However, since $\phi'_{cs}$ is a soil constant, it is sufficient to run several triaxial and direct shear tests up to residual state to obtain its value.

According to the obtained parameters from test results mentioned above following relationships were investigated for all experiments:

(i). Variation of the effective vertical stress with axial strain (Figure 3.17)
(ii). Variation of the deviatoric stress with axial strain (Figure 3.18)
(iii). Variation of the mean effective stress with axial strain (Figure 3.19)
(iv). Variation of the radial strain with axial strain (Figure 3.20)
(v). Variation of the effective vertical stress with the at rest lateral earth pressure coefficient (Figure 3.21)
(vi). Variation of the effective vertical stress with void ratio (Figure 3.22)
(vii). Variation of dilatancy angle with axial strain (Figure 3.23)
(viii). Variation of volumetric strain with axial strain (Figure 3.24)
(ix). Variation of $K_0$ with OCR (Figure 3.25)

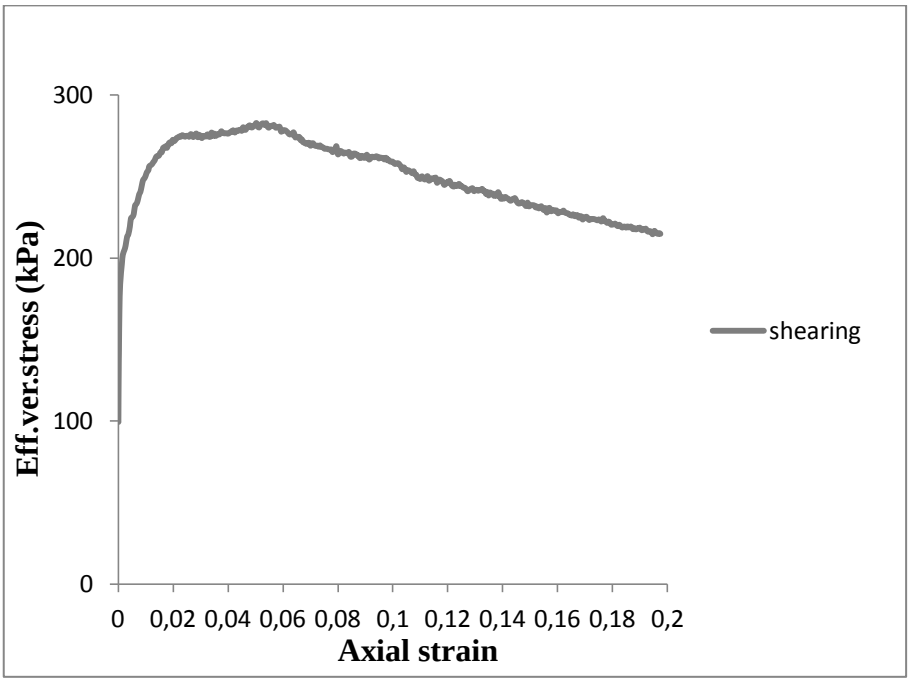


Figure 3.17. Variation of effective vertical stress with the axial strain in a sample test

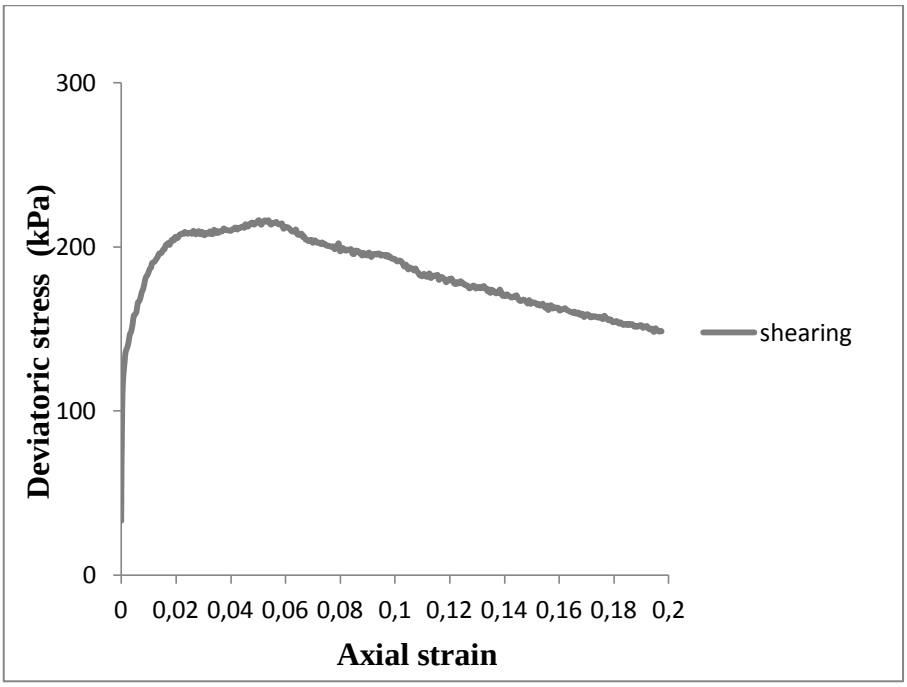


Figure 3.18. Variation of deviatoric stress with the axial strain for a sample test

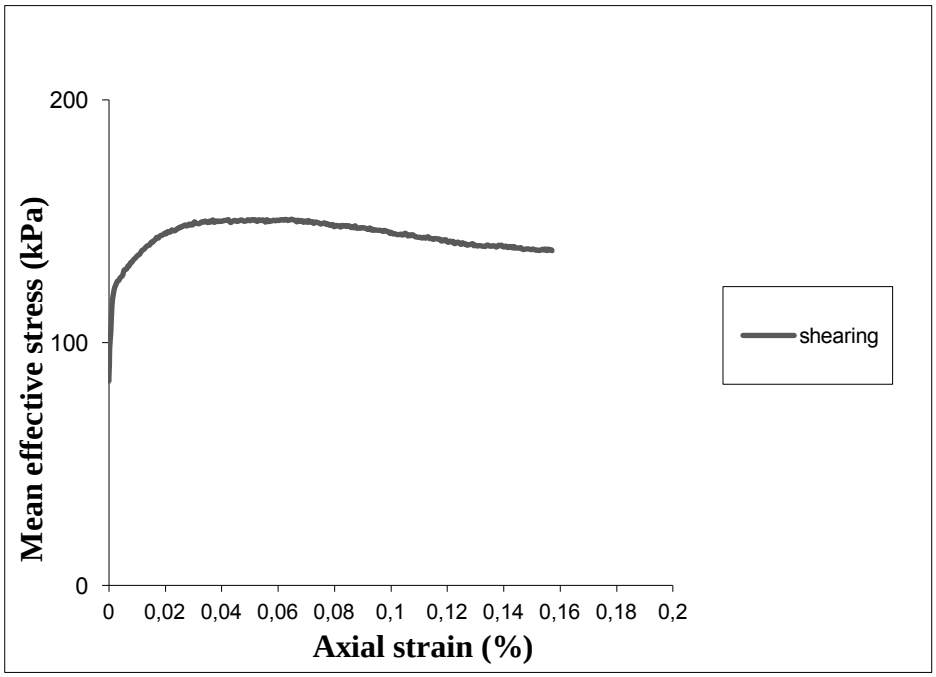


Figure 3.19. Variation of the mean effective stress with axial strain for a sample test

Variation of radial strain versus vertical effective stress is monitored during the loading and unloading stages of the consolidation phase (Figure 3.20). In order to simulate the at rest state during theexperiments, radial strain $\varepsilon_r$ of the specimens should be kept within the range of $\pm 0.005\%$ according to ASTM D-7181. During the loading stage of the consolidation phase the specimen has a tendency to expand laterally while being compressed axially. Therefore cell pressure is increased to keep the radial strains close to zero. On the other hand when the sample is being unloaded the specimen has a tendency to contract laterally while elongating axially. In this condition the cell pressure would be decreased to avoid further contraction of the sample and to keep the radial strains within the range specified by the ASTM standard. Figure 3.20 shows the variations in the radial strain during a $K_o$ loading and unloading phase. The cell pressureis being controlled by the automatic control unit of the triaxial apparatus so that the radial strains do not exceed the ranges required for the satisfaction of the at rest earth pressure condition.

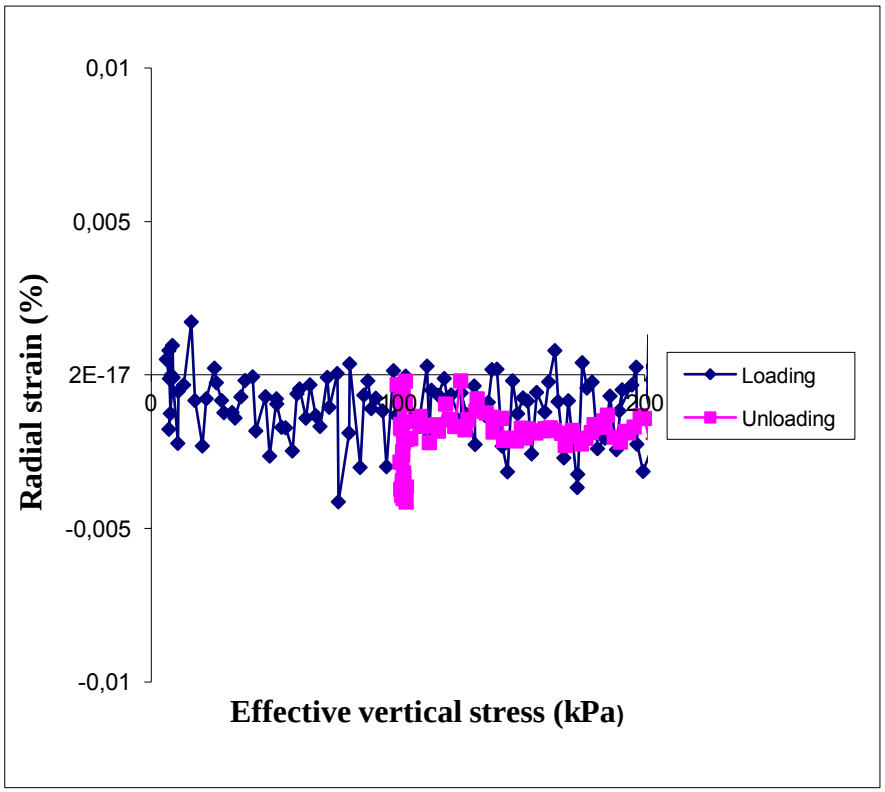


Figure 3.20. Variation of radial strain with the effective vertical stress during the consolidation stage of a sample test

At rest earth pressure coefficient of the soil decreases during the loading stage of the consolidation phase by the increase in the effective vertical stress value. When sample is being unloaded it starts to increase as seen in Figure 3.21.

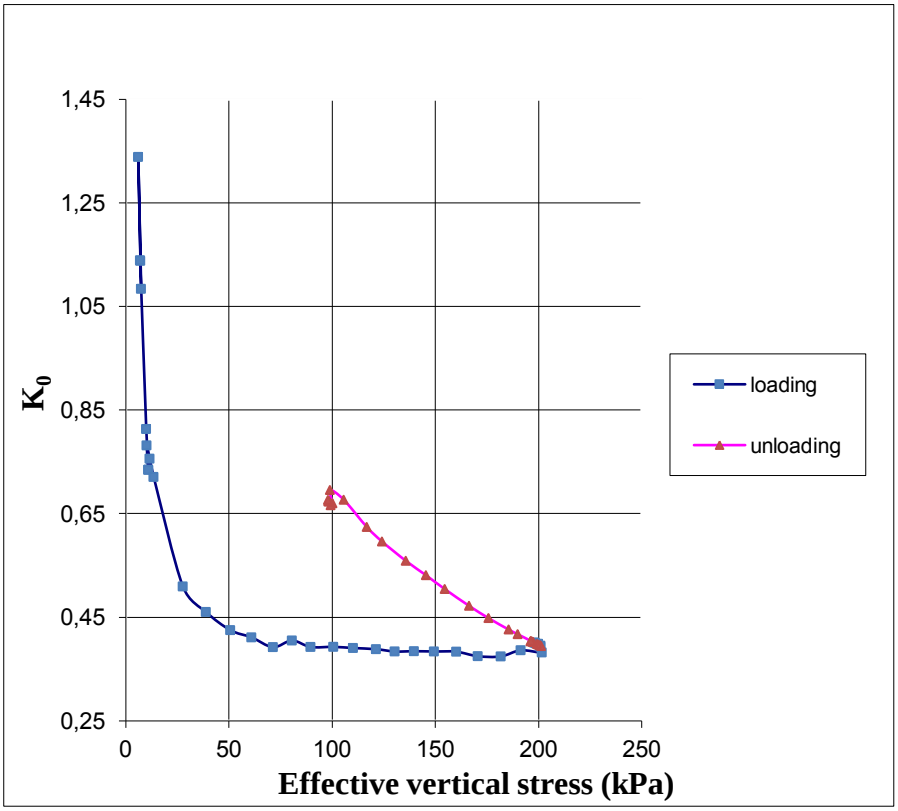


Figure 3.21. Variation of the at rest earth pressure coefficient with effective vertical stress during the consolidation phase for a sample test

The void ratio of the sample starts to decrease as the sample is being consolidated during the consolidation phase. During the unloading stage sample's void ratio starts to increase.

As mentioned in Chapter 3.7 Shanz and Vermeer equation was used to measure the dilatancy angle in the experiments. Strain percentage corresponding to the peak dilatancy angle also corresponds to the instance of failure as stated by Newland et el.

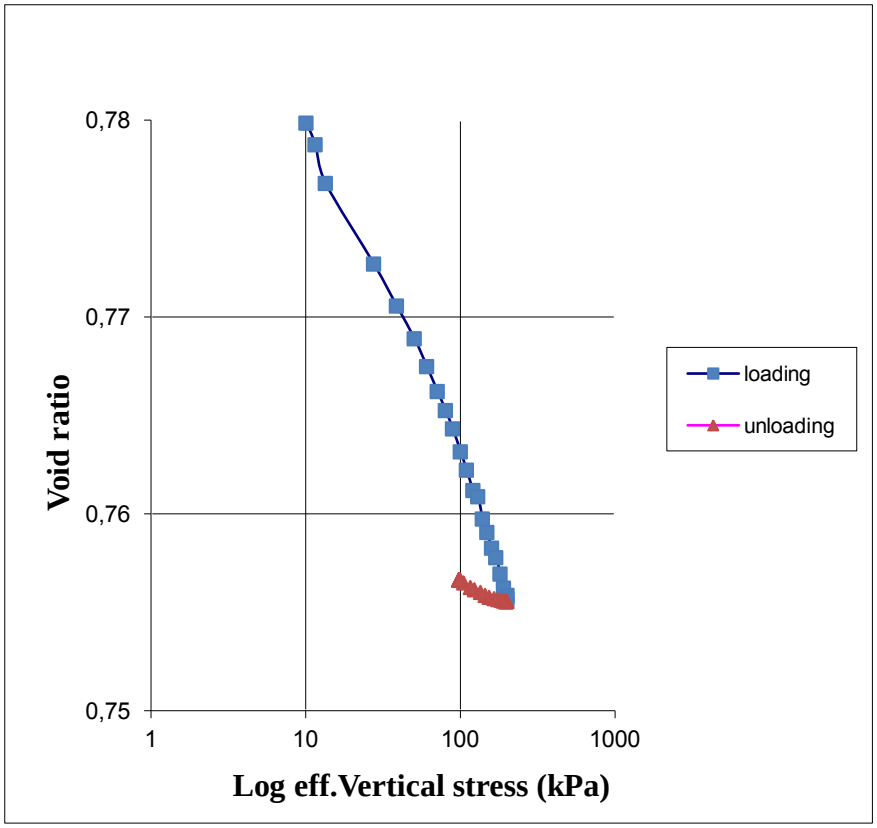


Figure 3.22. Variation of the void ratio with vertical effective stress during the consolidation phase for a sample test

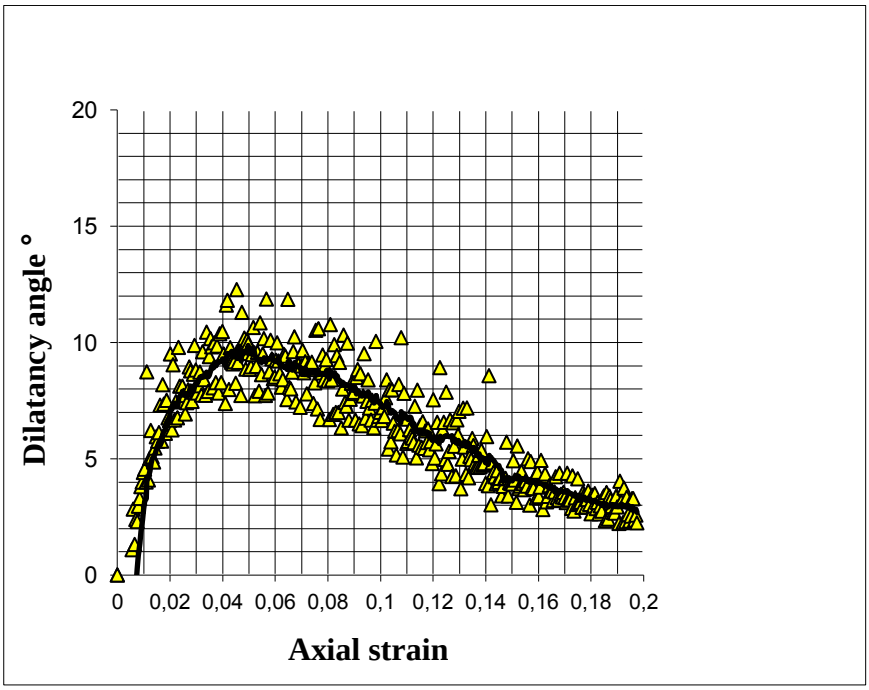


Figure 3.23. Variation of the dilatancy angle with axial strain for a sample test

Volumetric change of the sample during the shearing phase is shown in Figure 3.24. Sample shows a small contraction at the beginning of the shearing phase then it starts to dilate. The maximum slope of the graph corresponds to the maximum dilatancy angle of the soil.

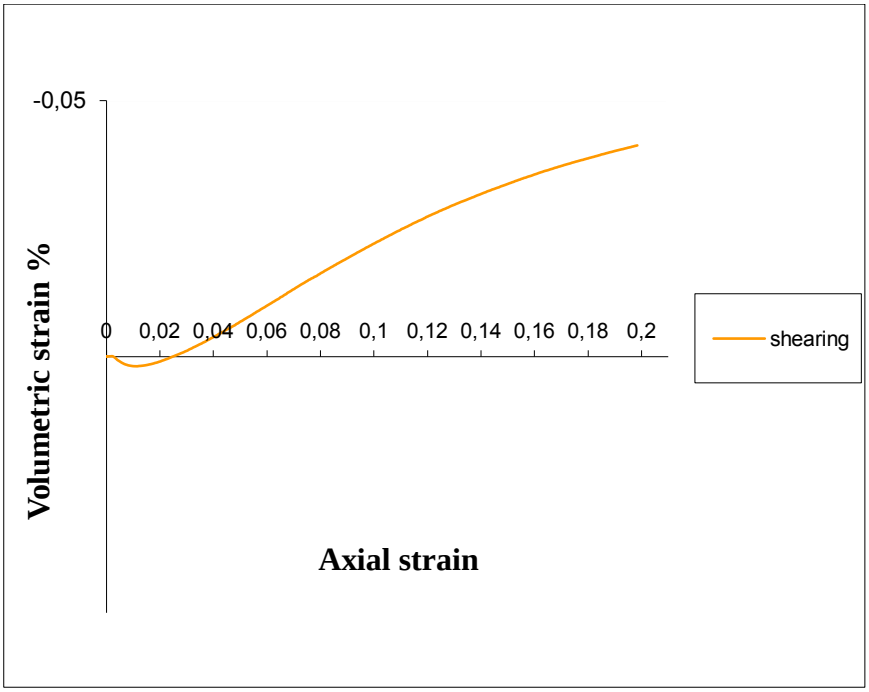


Figure 3.24. Variation of volumetric strain with the axial strain during the shearing phase for a sample test ($D_R$=0.7)

At rest lateral earth pressure coefficient of the sample showed an increase with overconsolidation ratio. A logarithmic trend between the overconsolidation ratio and at rest earth pressure was observed in all experiments.

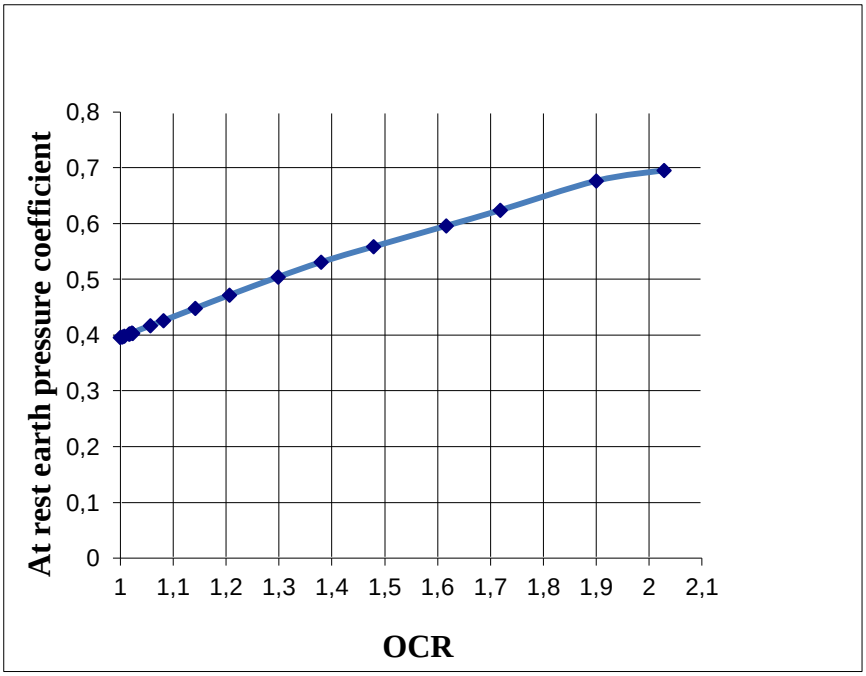


Figure 3.25. Variation of at rest earth pressure coefficient with overconsolidation ratio during the unloading stage of consolidation phase

# 4. EVALUATION OF THE TRIAXIAL TEST RESULTS

Triaxial test results have been evaluated to achieve the following objectives:

(i) Investigate the parameters affecting the strength and dilatancy of sands

(ii) Investigate the parameters affecting at rest earth pressure coefficient of overconsolidated sands

## 4.1. Strength and Dilatancy of Sands

Using an extensive literature review and by analyzing several triaxial tests, parameters that influence the peak friction angle of clean cohesionless soils are found to be critical state friction angle ($\phi'_{cs}$) and dilatancy angle ($\psi$) (Bolton et al., 1986). However, even though $\phi'_{cs}$ is a constant for a specific sand (assuming grains size distribution, particle shape characteristics and mineralogy remain unchanged), $\psi$ varies as the stress state and volume state of the soil changes.That is why the main goal of this research shifted towards investigating the nature of dilatant behavior and to quantifying its variation under different circumstances.

In the literature, it is shown that the dilatancy angle for a specific soil varies with the confining pressure and void ratio. However there is no relationship or function that quantifies this variation. Since it is the first step for the quantification of the peak friction angle, the preliminary goal of this experimental study was to investigate the influences of stress state and volumetric state on the dilatancy angle. Moreover, it was initially believed that plastic work done during the loading-unloading of soils might affect the dilatants behavior.

For this purpose a triaxial testing program was prepared in which samples were tested at different combinations of overconsolidation ratio (1, 2, 4, and 8), relative density (varying from 30% to 100%), and confining pressure (varying from 25 kPa to 1000 kPa). All tests were conducted under $K_o$ consolidation conditions for simulating field conditions as closely as possible.

Table 4.1 lists the details of the triaxial tests conducted during the experimental program. In this table, p′ values were mean effective stress values at the beginning of the shearing phase. These values are calculated using the vertical effective stress applied on the sample prior to shearing and the horizontal effective stress that is a function of the $K_o$ parameter. Relative density is the relative density at the initiation of shearing.

Table 4.1. Details of triaxial tests

| **OCR** | **$D_R$ (%)** | **p' at the end of consolidation(kPa)** |
|---|---|---|
| 1 | 63 | 62 |
| 1 | 51 | 57 |
| 1 | 49 | 32 |
| 1 | 49 | 155 |
| 1 | 49 | 284 |
| 1 | 64 | 112 |
| 1 | 49 | 116 |
| 1 | 66 | 963 |
| 1 | 100 | 226 |
| 1 | 49 | 242 |
| 2 | 54 | 165 |
| 2 | 73 | 134 |
| 2 | 76 | 160 |
| 2 | 60 | 193 |
| 2 | 76 | 71 |
| 2 | 50 | 77 |
| 2 | 63 | 73 |
| 2 | 73 | 290 |
| 2 | 64 | 286 |
| 2 | 88 | 273 |
| 2 | 90 | 338 |
| 2 | 59 | 470 |
| 2 | 53 | 158 |

Table 4.1. Details of triaxial tests (cont.).

| **OCR** | **$D_R$ (%)** | **p' at the end of consolidation(kPa)** |
|---|---|---|
| 2 | 56 | 37 |
| 2 | 78 | 37 |
| 2 | 39 | 41 |
| 2 | 46 | 49 |
| 4 | 51 | 52 |
| 4 | 41 | 49 |
| 4 | 41 | 26 |
| 4 | 76 | 43 |
| 4 | 73 | 45 |
| 4 | 75 | 46 |
| 4 | 71 | 42 |
| 4 | 53 | 185 |
| 4 | 53 | 188 |
| 4 | 85 | 198 |
| 4 | 80 | 191 |
| 4 | 61 | 202 |
| 4 | 54 | 236 |
| 4 | 68 | 359 |
| 4 | 93 | 303 |
| 4 | 90 | 285 |
| 4 | 56 | 181 |
| 4 | 61 | 160 |
| 4 | 76 | 209 |
| 4 | 61 | 169 |
| 4 | 73 | 197 |
| 4 | 34 | 175 |
| 4 | 63 | 88 |
| 4 | 56 | 85 |
| 4 | 85 | 86 |
| 4 | 34 | 83 |
| 4 | 83 | 82 |

Table 4.1. Details of triaxial tests (Cont.).

| OCR | $D_R$ (%) | p' at the end of consolidation (kPa) |
|---|---|---|
| 4 | 61 | 82 |
| 8 | 56 | 31 |
| 8 | 33 | 33 |
| 8 | 43 | 28 |
| 8 | 88 | 162 |
| 8 | 90 | 180 |
| 8 | 63 | 199 |
| 8 | 73 | 209 |
| 8 | 88 | 207 |
| 8 | 68 | 249 |
| 8 | 90 | 82 |
| 8 | 76 | 67 |
| 8 | 56 | 96 |
| 8 | 56 | 46 |
| 8 | 54 | 59 |
| 8 | 55 | 50 |
| 8 | 84 | 52 |
| 8 | 98 | 320 |
| 8 | 80 | 334 |
| 8 | 76 | 366 |
| 8 | 72 | 345 |

### 4.1.1. Effects of Density and Mean Effective Stress on Dilatancy Angle

Relative density is calculated using the following equation:

$$D_R = \frac{e_{\max} - e}{e_{\max} - e_{\min}} \tag{4.1}$$

where $D_R$ is the relative density of the soil, $e_{max}$ is the maximum void ratio of the soil and $e_{min}$ is the minimum void ratio of the soil. $e_{max}$ and $e_{min}$ values for the test sand are reported in Section 3.2.

Even though air-pluviation technique provides a certain amount of control over the density of the samples, with the additional influence of the loading-unloading process during the tests on sample volume, it is not possible to achieve target relative density values with pinpoint precision. That is why in the data analysis part of this thesis, tests will be grouped using relative density ranges. These relative density ranges will cover 5% variations in $D_R$. As a result $\psi$-p′ relationships are obtained for different $D_R$ as given in Figures 4.1 to 4.10.

When these relationships are examined, it is seen that they define a relationship that can be assumed to be linear. That is why in all graphs, the corresponding linear trendlines are shown. Below the figures, the equations for the trendlines are given.

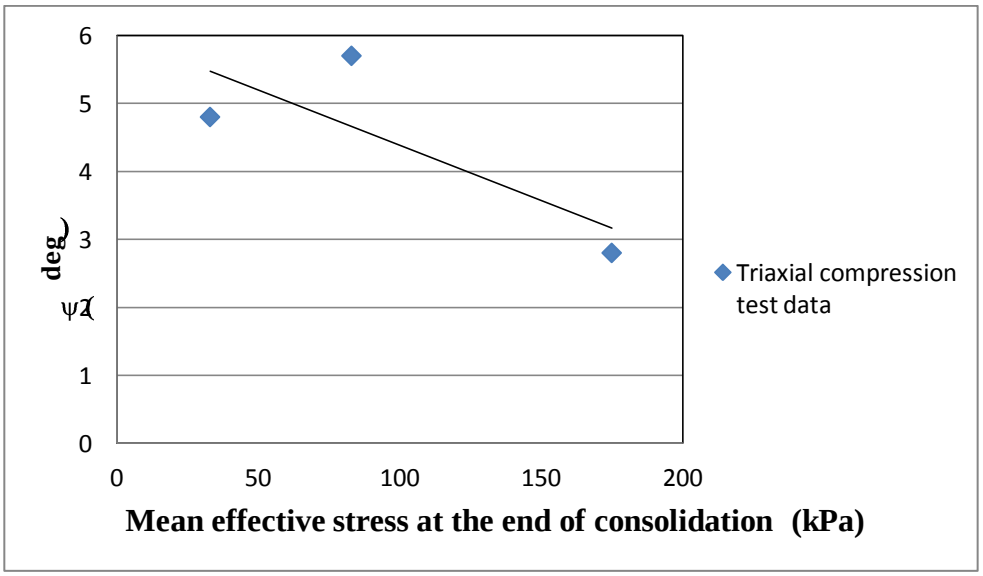


Figure 4.1. Variation of the peak dilatancy angle with mean effective stress for $D_R$=0.30-0.35

For $0.30 < D_R < 0.35$ $\psi = -0.0162p' + 6.0095$ (4.2)

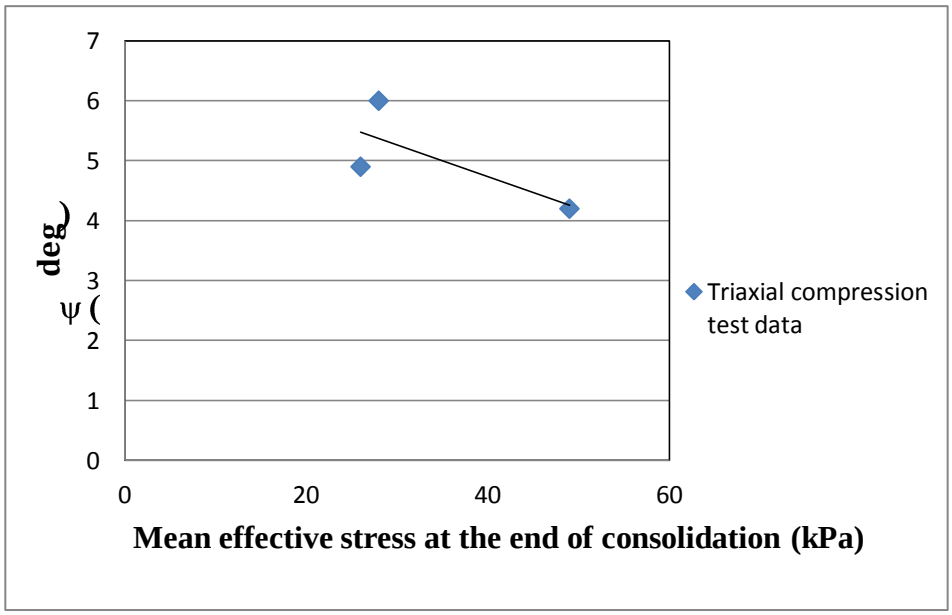


Figure 4.2. Variation of the peak dilatancy angle with mean effective stress for $D_R$=0.40-0.45

For $0.40 < D_R < 0.45$ $\psi = -0.0531p' + 6.8557$ (4.3)

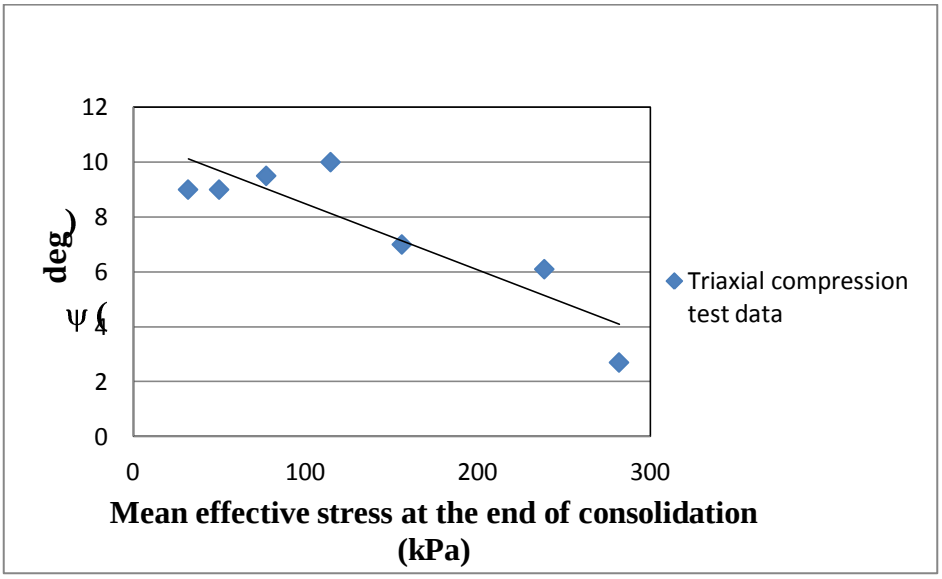


Figure 4.3. Variation of the peak dilatancy angle with mean effective stress for $D_R$=0.45-0.5

For $0.45 < D_R < 0.5$ $\psi = -0.0241p' + 10.887$ (4.4)

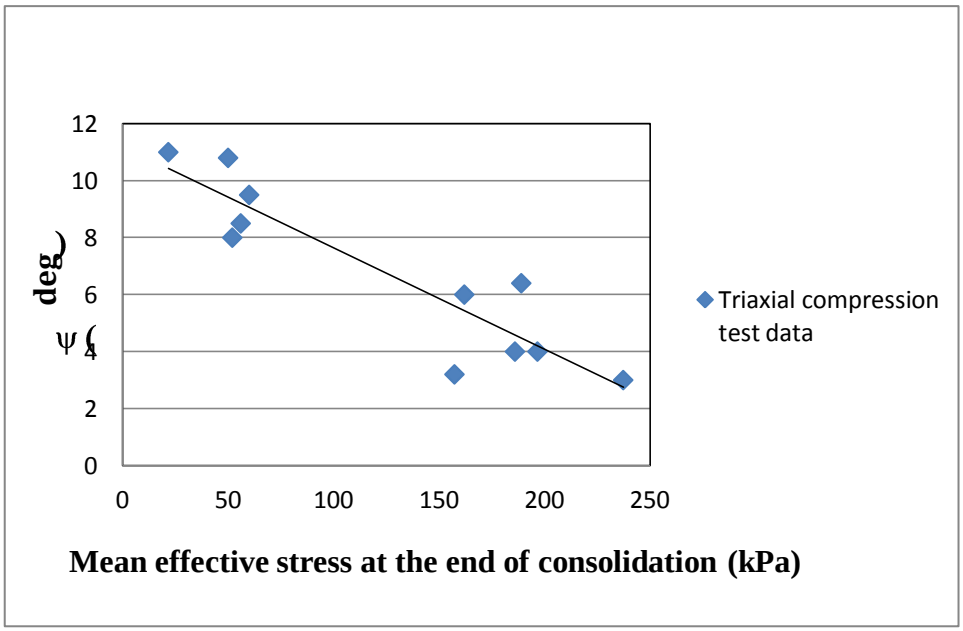


Figure 4.4. Variation of the peak dilatancy angle with mean effective stress at the end of consolidation for $D_R$=0.5-0.55

For $0.5 < D_R < 0.55$ $\psi = -0.0356p' + 11.188$ (4.5)

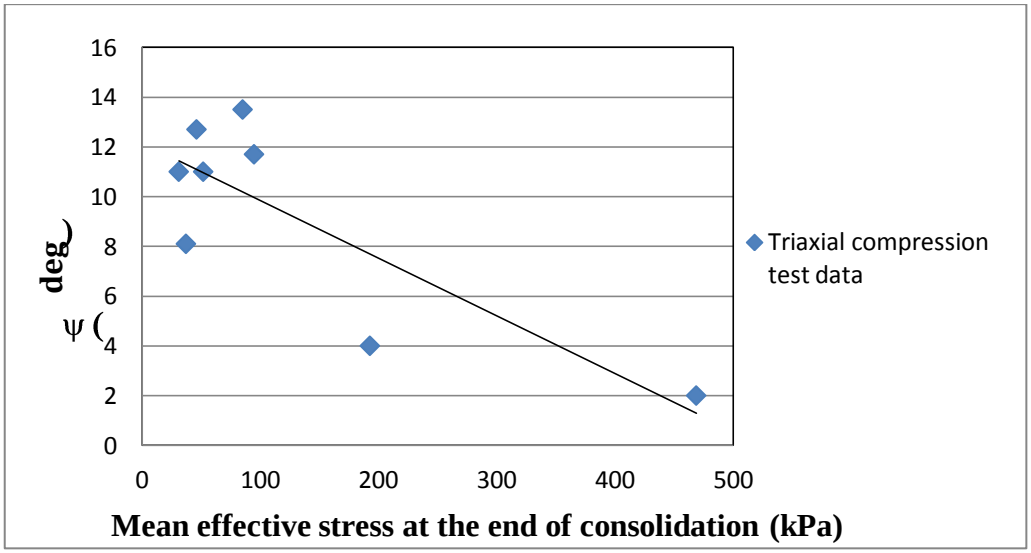


Figure 4.5. Variation of the peak dilatancy angle with mean effective stress at the end of consolidation for $D_R$=0.55-0.6

For $0.55 < D_R < 0.6$ $\psi = -0.0232\,p' + 12.167$ (4.6)

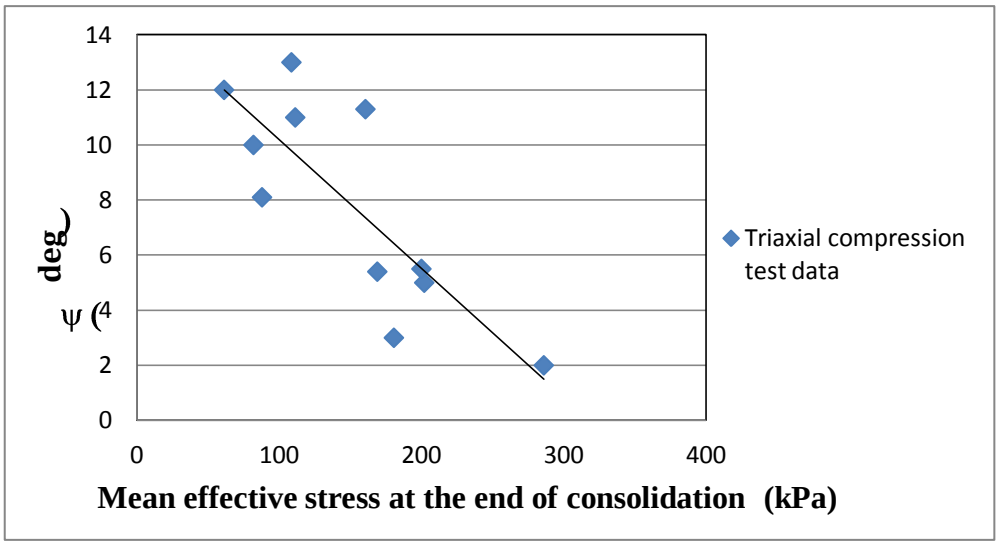


Figure 4.6. Variation of the peak dilatancy angle with mean effective stress at the end of consolidation for $D_R$=0.6-0.65

For $0.6 < D_R < 0.65$ $\psi = -0.0467\,p' + 14.846$ (4.7)

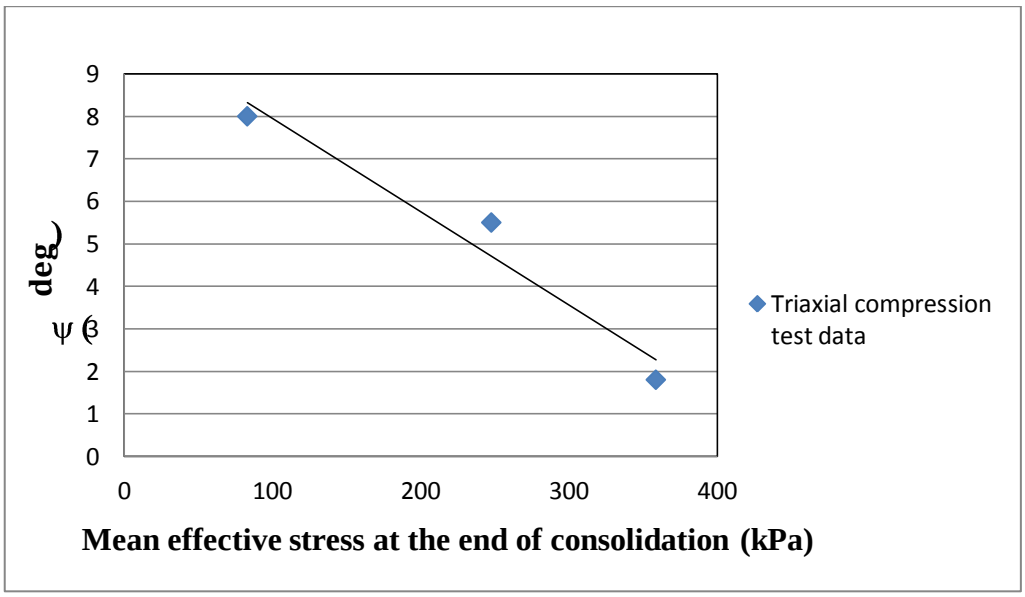


Figure 4.7. Variation of the peak dilatancy angle with mean effective stress at the end of consolidation for $D_R$=0.65-0.7

For $0.65 < D_R < 0.7$ $\psi = -0.0219p' + 10.139$ (4.8)

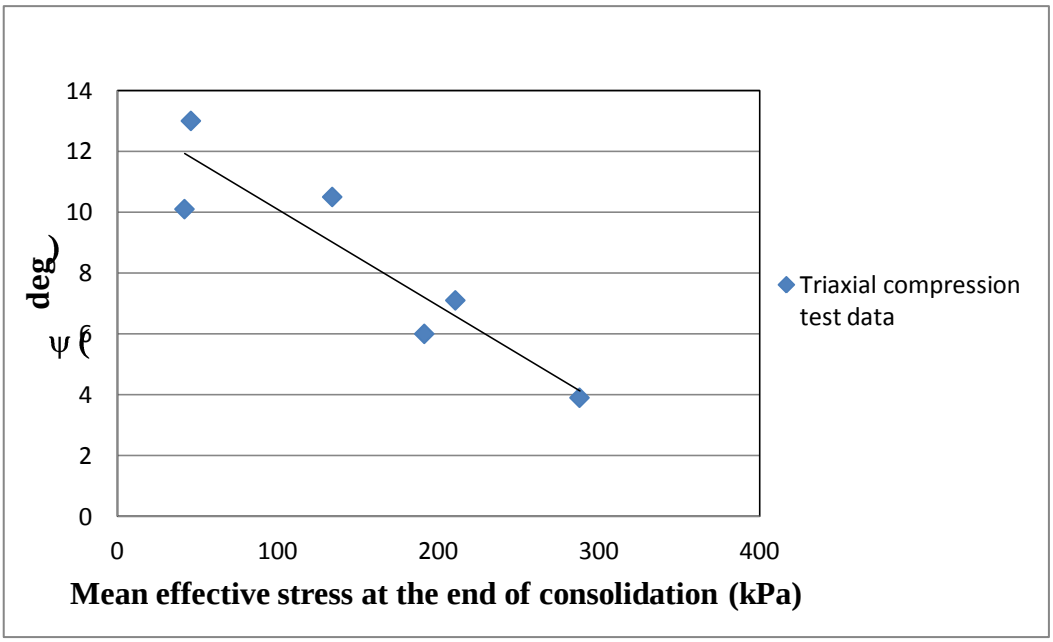


Figure 4.8. Variation of the peak dilatancy angle with mean effective stress for $D_R$=0.7-0.75

For $0.7 < D_R < 0.75$ $\psi = -0.0317p' + 13.254$ (4.9)

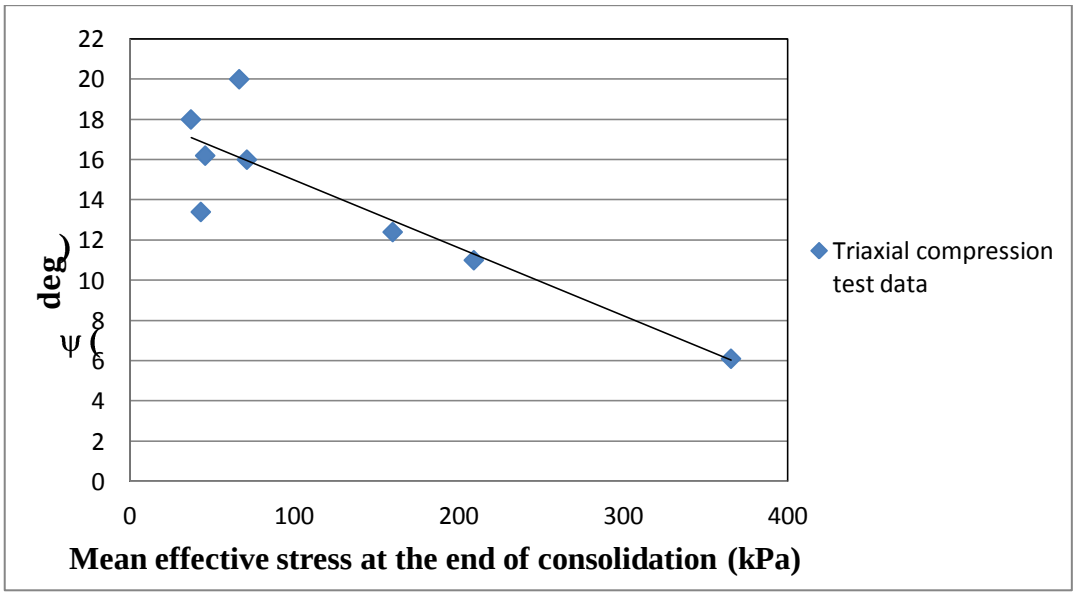


Figure 4.9. Variation of the peak dilatancy angle with mean effective stress for $D_R$=0.75-0.8

For $0.75 < D_R < 0.8$ $\psi = -0.0337p' + 18.354$ (4.10)

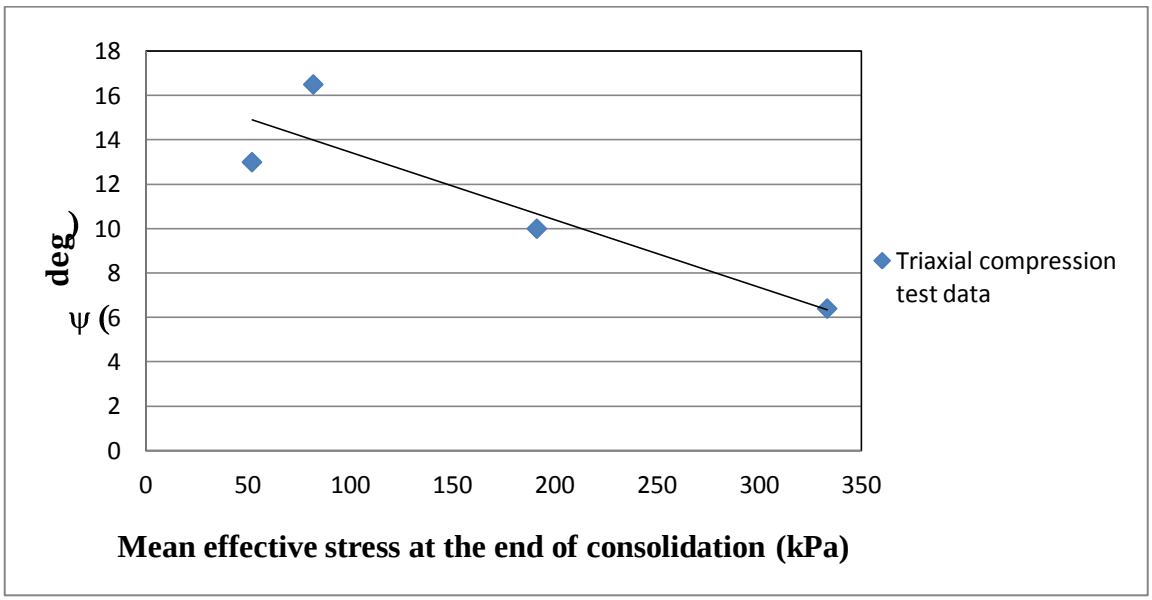


Figure 4.10. Variation of the peak dilatancy angle with mean effective stress for $D_R$=0.8-0.85

For $0.8 < D_R < 0.85$ $\psi = -0.0305p' + 16.489$ (4.11)

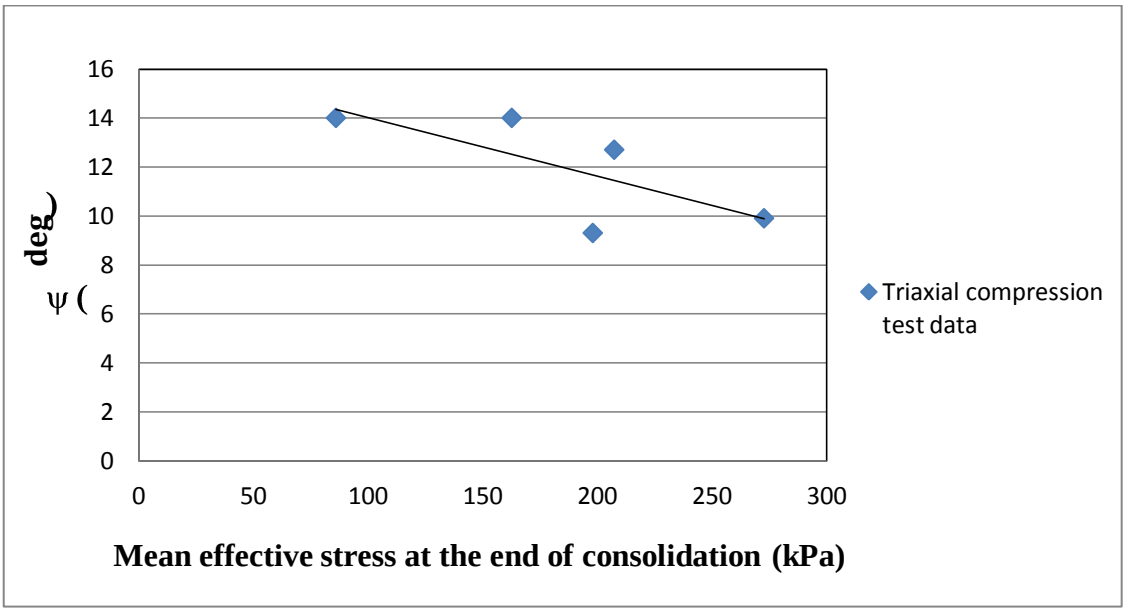


Figure 4.11. Variation of the peak dilatancy angle with mean effective stress for $D_R$=0.85-0.9

For $0.8 < D_R < 0.85$ $\psi = -0.0239p' + 16.414$ (4.12)

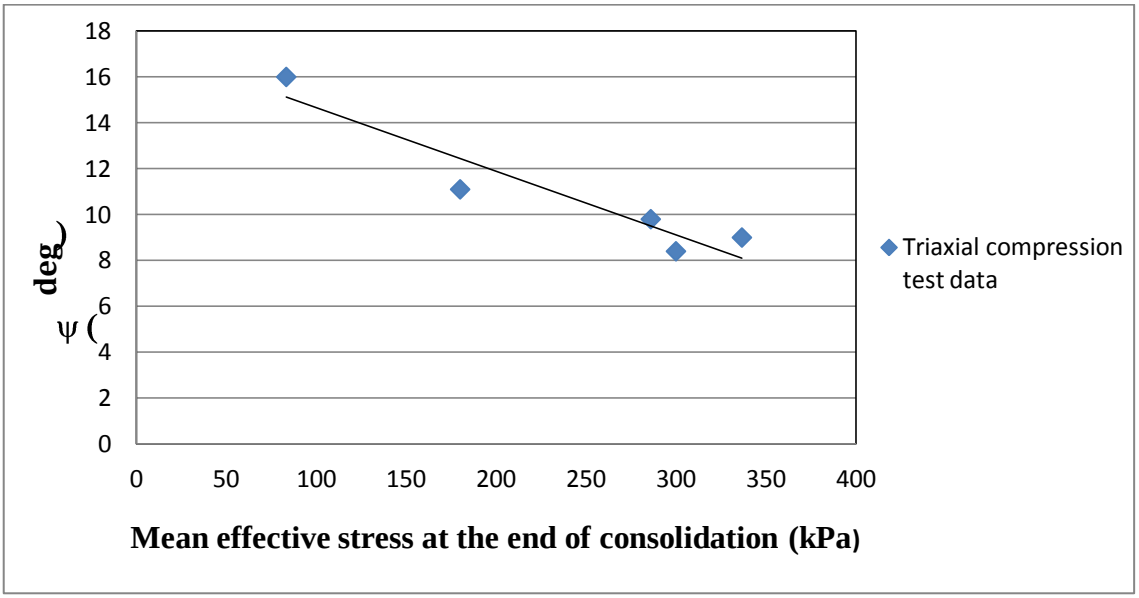


Figure 4.12. Variation of the dilatancy angle with mean effective stress for $D_R$=0.9-0.95

For $0.8 < D_R < 0.85$ $\psi = -0.0277p' + 17.431$ (4.13)

Clearly, all ψ-p′ relationships can be assumed to be linear for the corresponding $D_R$ ranges. Accordingly, considering the forms of these linear relationships a function of the form below can be defined:

$$\psi = \alpha_\psi p' + \beta_\psi \quad (4.14)$$

where $\alpha_\psi$ and $\beta_\psi$ are paremeters are dependent on $D_R$.

Variations of the parameters $\alpha_\psi$ and $\beta_\psi$ with relative density are shown in Figures 4.13 and 4.14:

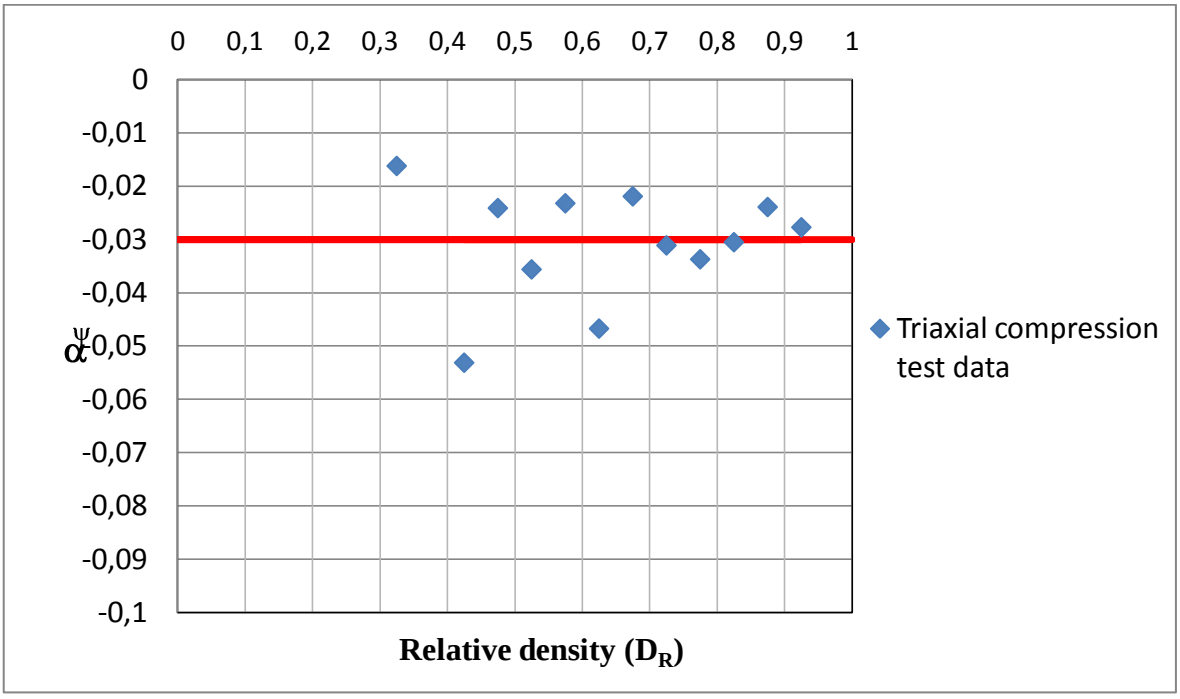


Figure 4.13. Variation of $\alpha_{\psi}$ parameter with relative density

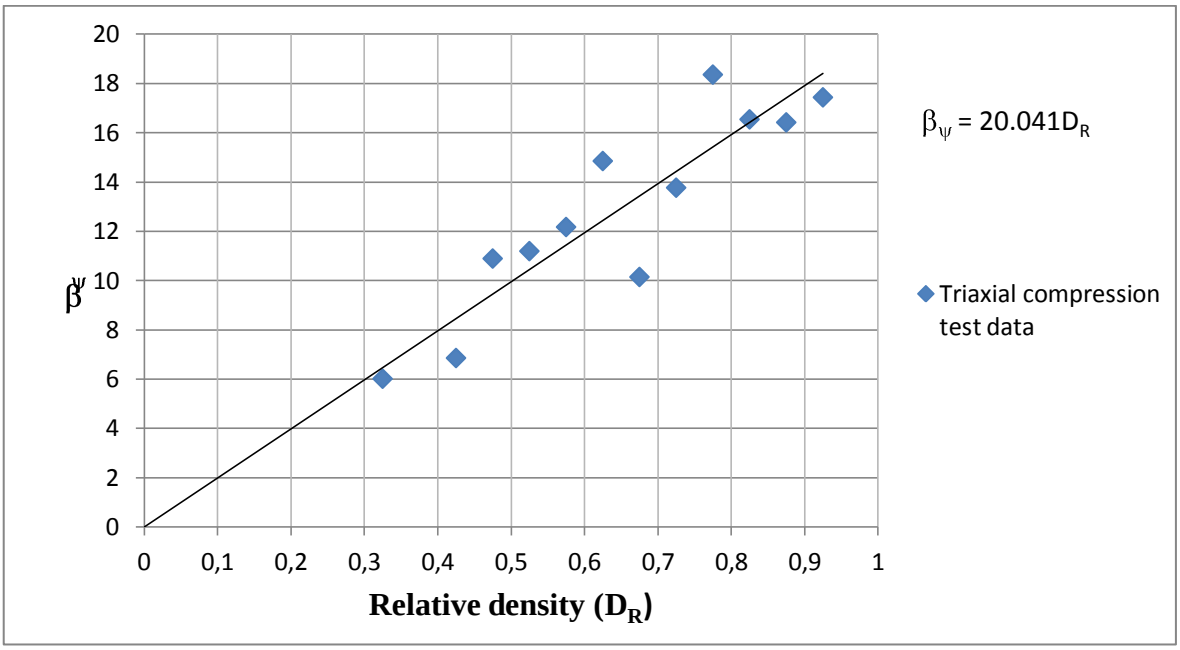


Figure 4.14. Variation of $\beta_{\psi}$ parameter with relative density

Considering the general applicability of the $\alpha_{\psi}$ parameter, it is defined in the form shown below:

$$\alpha_\psi = a_\psi D_R + b_\psi \tag{4.15}$$

Based on the results shown in Figure 4.13 an average value of -0.03 was assumed for $\alpha_\psi$. Therefore:

$$a_\psi = 0 \text{ and } b_\psi = -0.03$$

The reason for assuming a linear relationship between $\alpha_\psi$ and $D_R$ is that later it will be shown that using test data of other researchers the relationship is obtained as a linear relationship. With the form in Eq. 4.15, the equation is rendered more generally applicable.

Accordingly, the following equation was defined for $\beta_\psi$ confirming to linear variation of $\beta_\psi$ with mean relative density values:

$$\beta_\psi = m_\psi D_R + n_\psi \tag{4.16}$$

According to the results shown in figure 4.14:

$$\beta_\psi = m_\psi D_R + n_\psi = 21 D_R \tag{4.17}$$

Therefore $m_\psi = 21$ and $n_\psi = 0$ for the soil being tested.

Combining equations 4.14 and 4.16 gives the following relationship for calculating the angle of dilatancy for any sand:

$$\psi = \left(a_\psi D_R + b_\psi\right) p' + \left(m_\psi D_R + n_\psi\right) \tag{4.18}$$

In the case of the tested sand with the standard Ottawa gradation, considering the values of the constants appropriate for the sand, the form simplifies to

$$\psi = \alpha_\psi p' + \beta_\psi = b_\psi p' + m_\psi D_R \tag{4.19}$$

where $b_\psi = 0.03$ and $m_\psi = 21$ . So equation 4.19 can be written as:

$$\psi = -0.03 p' + 21 D_R \tag{4.20}$$

According to equation 4.20 peak dilatancy angle can be calculated using the mean effective stress and relative density values that are obtained prior to shearing. This increases the applicability of the proposed equation since it is a standard practice to measure or calculate these values.

### 4.1.2. Effects of Density and Mean Effective Stress on Peak Friction Angle

As explained in detail in the literature review section of this thesis, peak friction angle can be assumed to be a combination of critical state friction and dilatancy angles. The proposed form of the relationship, verified by different researchers (Bolton et al.), is given below:

$$\phi'_{\max} = \phi'_{cs} + r\psi \tag{4.21}$$

where r is a constant showing the amount of dilatancy contribution to peak friction angle. The value of the constant r is soil specific. This constant can be expressed in the form shown in Eq. 4.22 by arranging Eq. 4.21:

$$r = \frac{\phi'_{\max} - \phi'_{cs}}{\psi} \tag{4.22}$$

In order to determine the r parameter value, variation of the r parameter with the mean effective stress and relative density of the sand has been investigated. Results were separated based on the relative density ranges and the relationship between mean effective stress and r parameter was monitored.

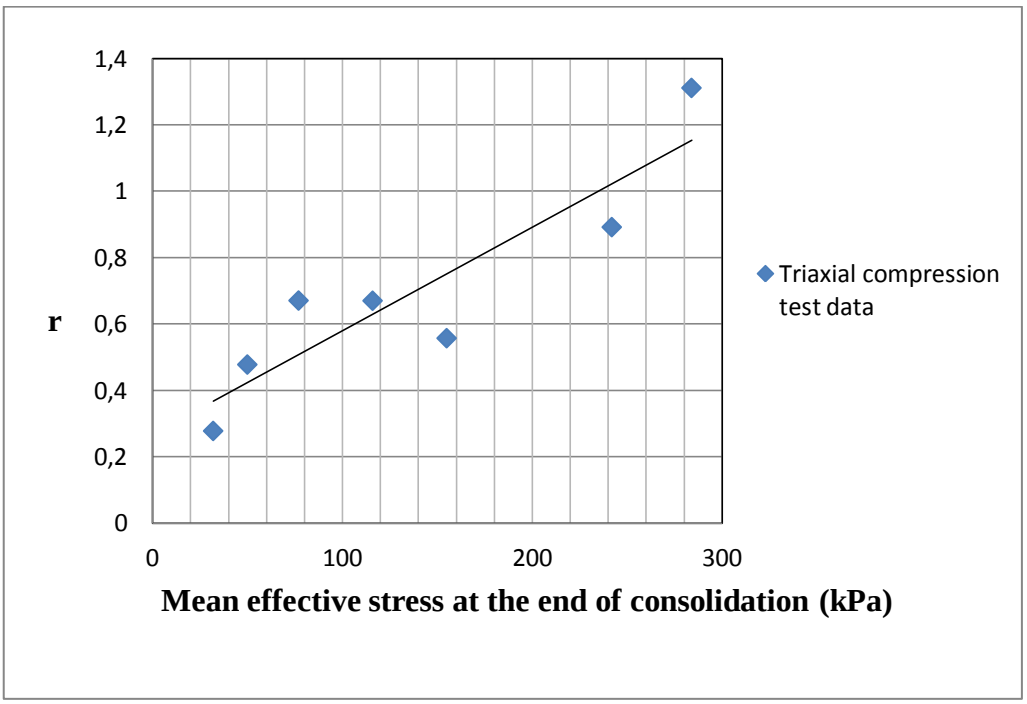


Figure 4.15. Variation of r with mean effective stress for $D_R$=0.45-0.5

For 0.45< $D_R$<0.5 $r = 0.0031p' + 0.2676$ (4.23)

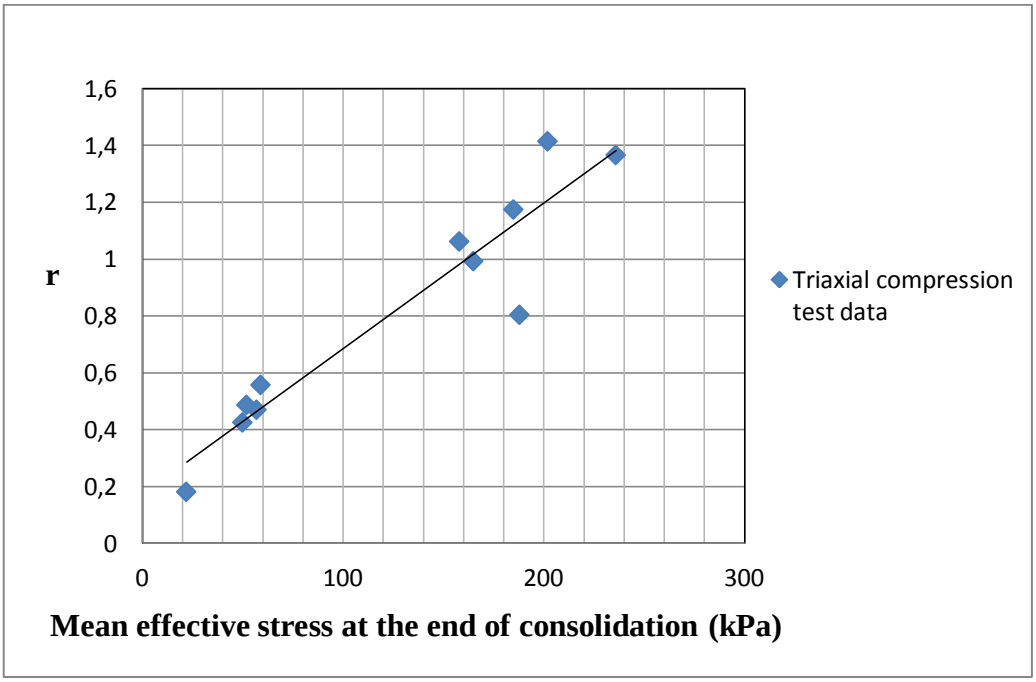


Figure 4.16. Variation of r with mean effective stress for $D_R$=0.50-0.55

For 0.5< $D_R$<0.55 $$r = 0.0051p' + 0.1732$$ (4.24)

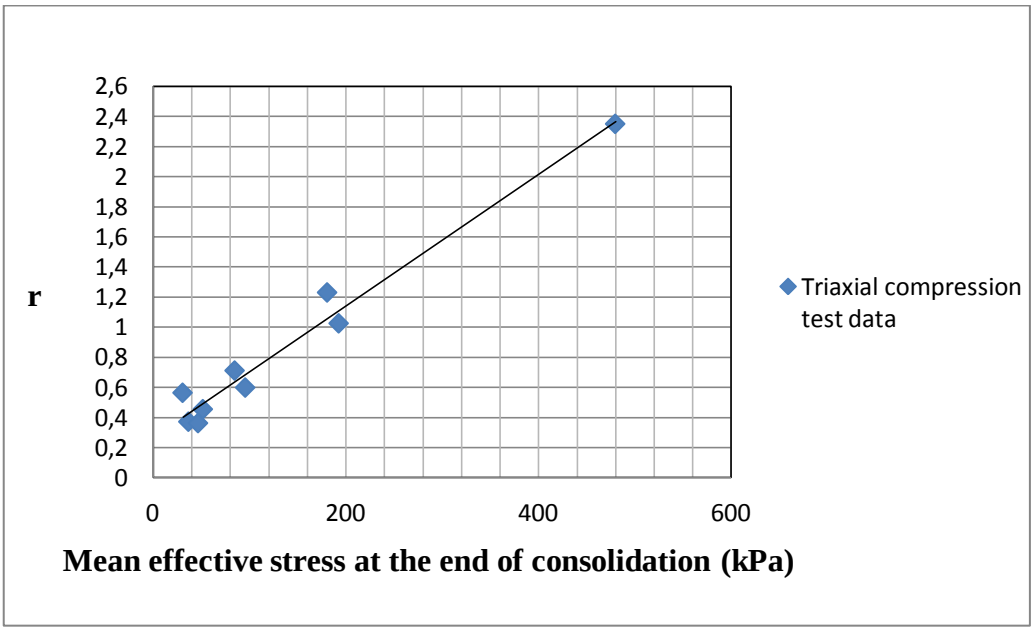


Figure 4.17. Variation of r with mean effective stress for $D_R$=0.55-0.60

For 0.55< $D_R$<0.6 $$r = 0.0044p' + 0.2685$$ (4.25)

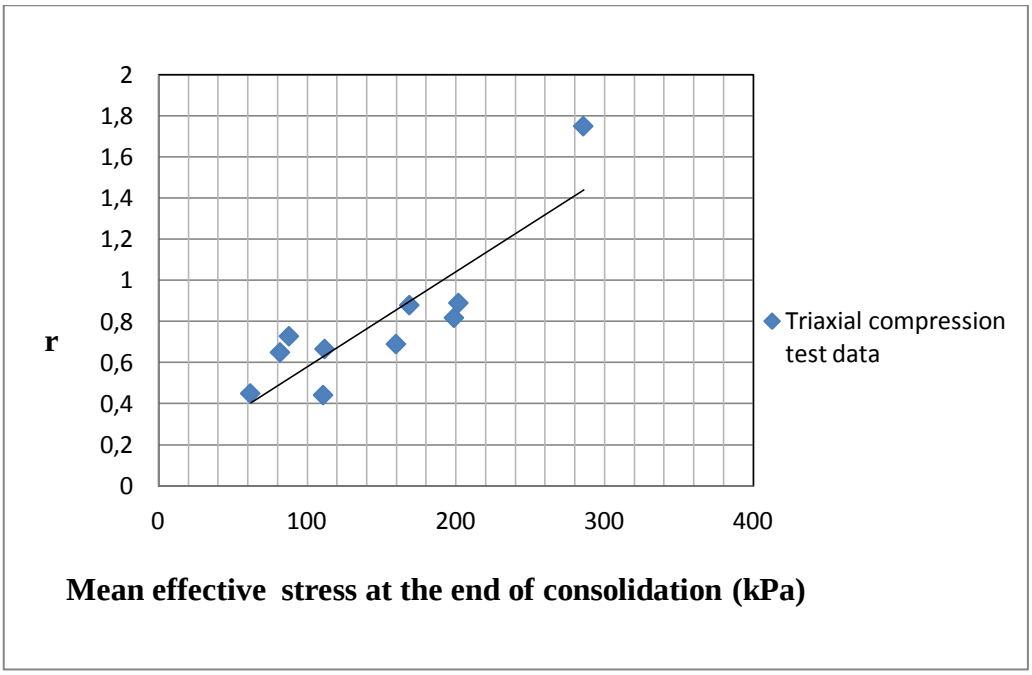


Figure 4.18. Variation of r with mean effective stress for $D_R$=0.60-0.65

For 0.6< $D_R$<0.65 $$r = 0.0046p' + 0.1163$$ (4.26)

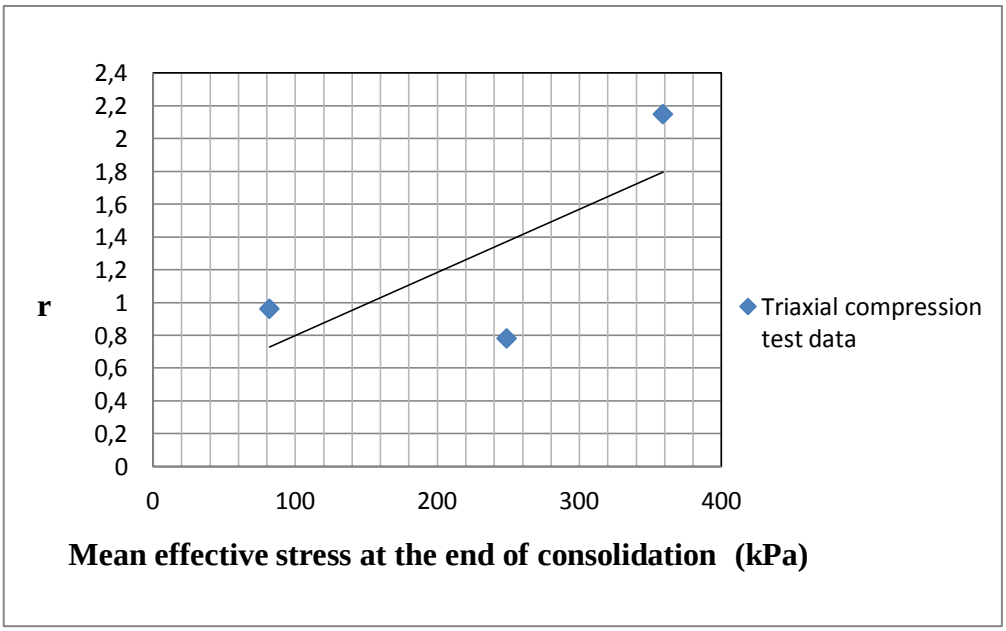


Figure 4.19. Variation of r with mean effective stress for $D_R$=0.65-0.70

For 0.65< $D_R$<0.7 $$r = 0.0038p' + 0.4128$$ (4.27)

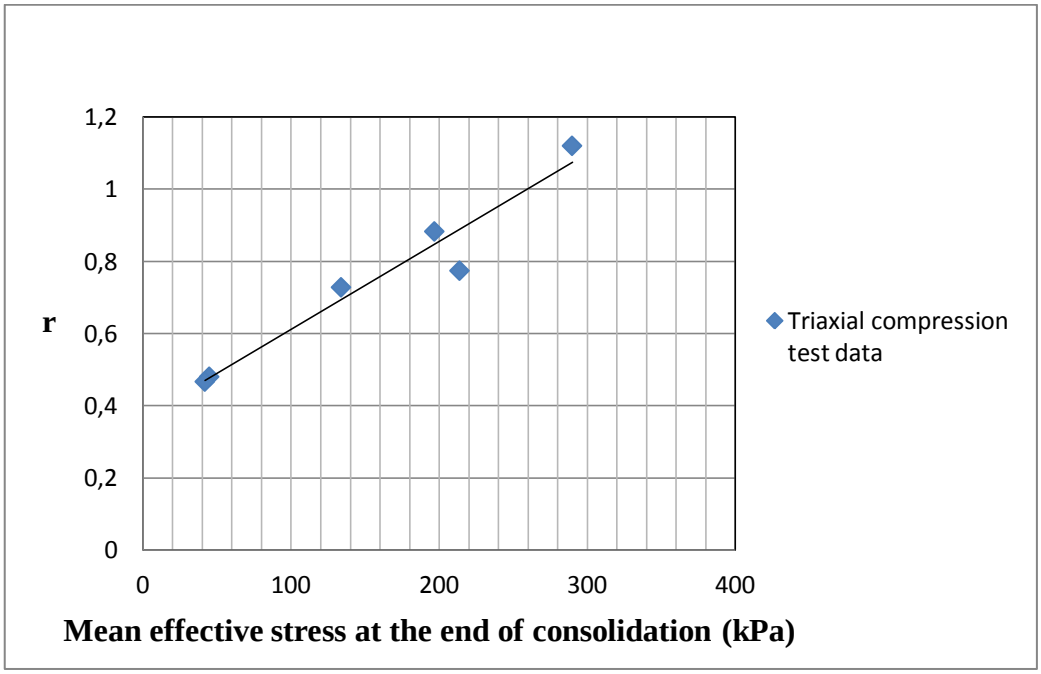


Figure 4.20. Variation of r with mean effective stress for $D_R$=0.70-0.75

For 0.7< $D_R$<0.75 $$r = 0.0024p' + 0.3675$$ (4.28)

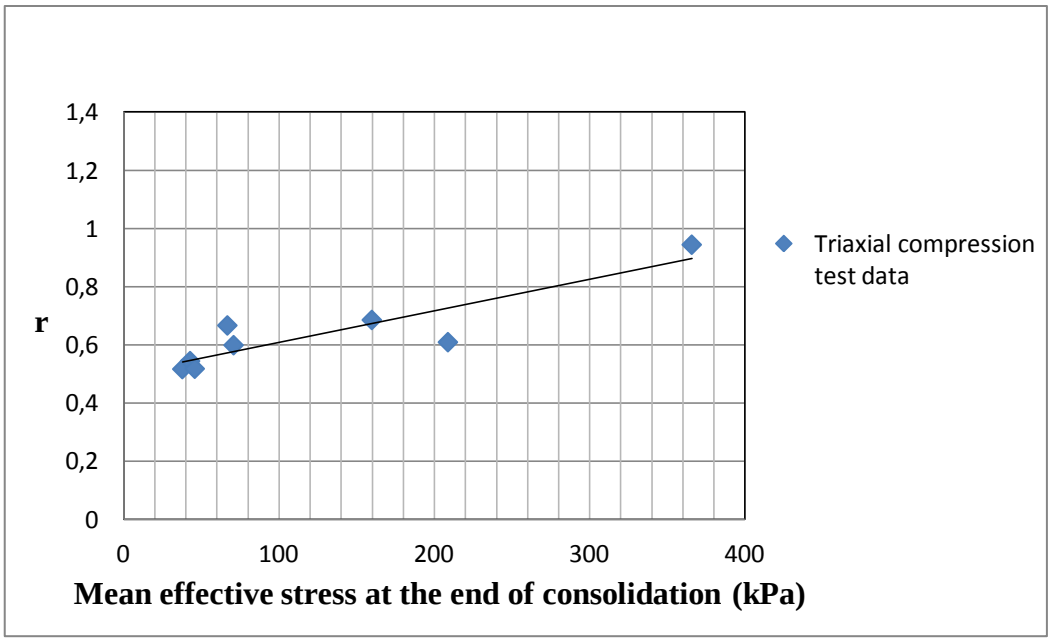


Figure 4.21. Variation of r with mean effective stress for $D_R$=0.75-0.80

For 0.75< $D_R$<0.8 $$r = 0.0011p' + 0.4995$$ (4.29)

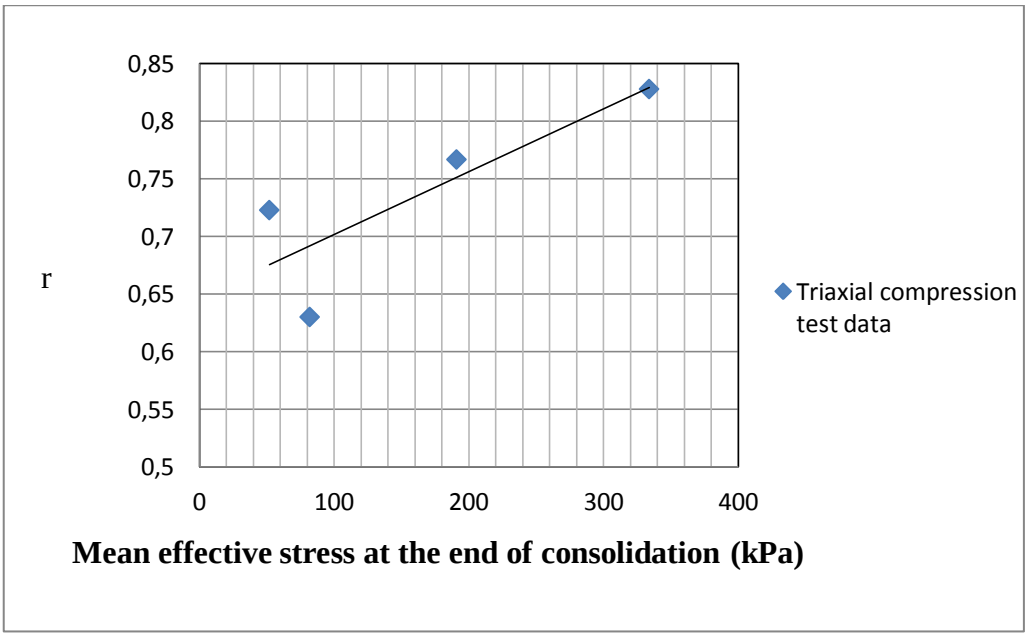


Figure 4.22. Variation of r with mean effective stress for $D_R$=0.80-0.85

For 0.8< $D_R$<0.85 $$r = 0.0005p' + 0.6475$$ (4.30)

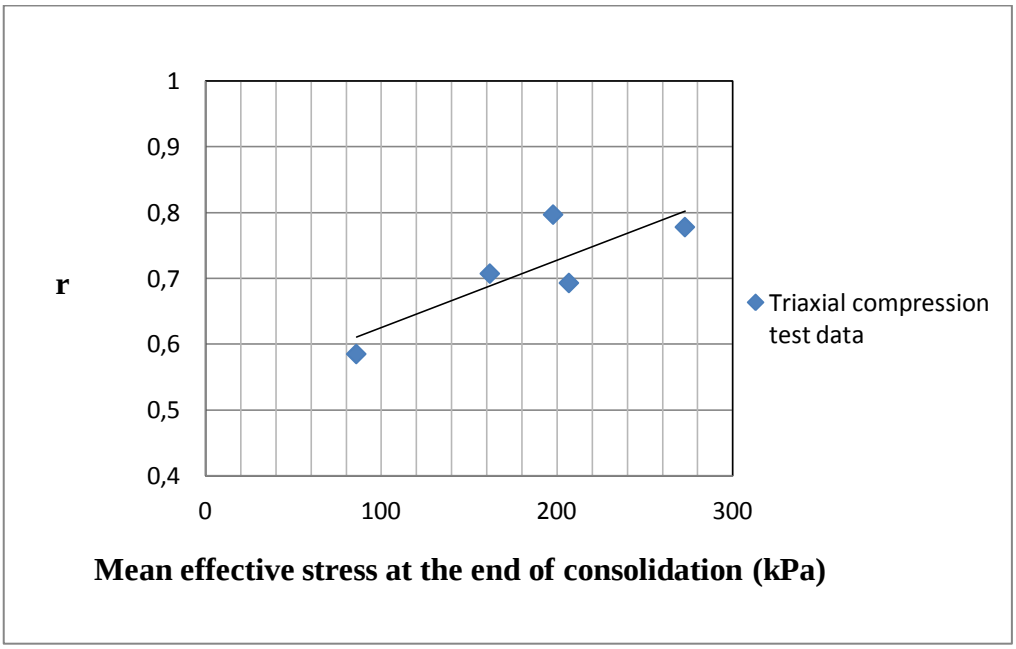


Figure 4.23. Variation of r with mean effective stress for $D_R$=0.85-0.90

For 0.85 < $D_R$ < 0.9 $$r = 0.001p' + 0.5225$$ (4.31)

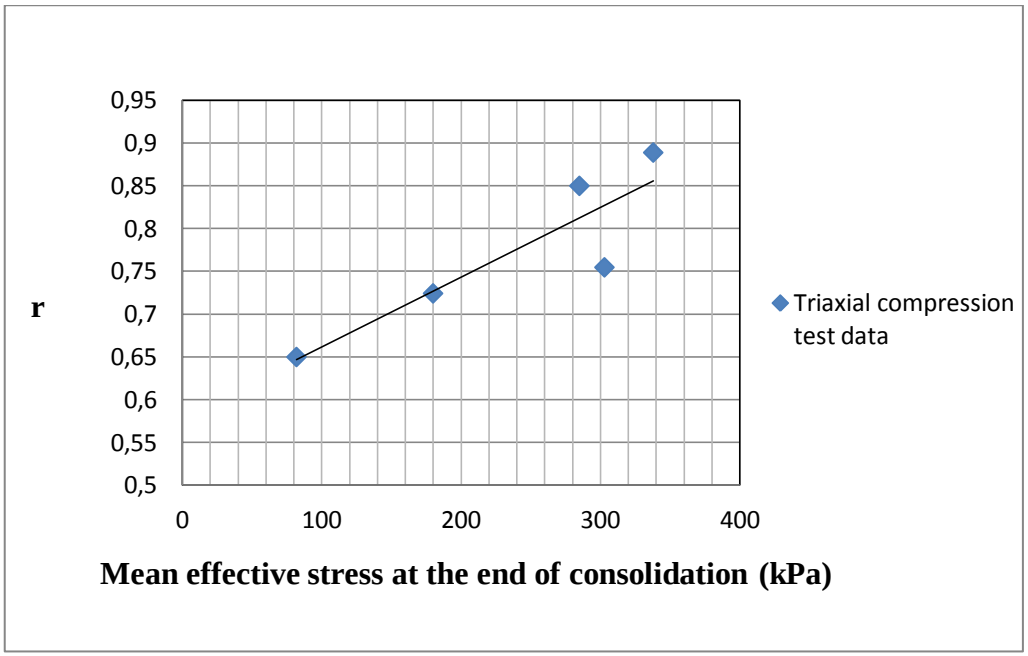


Figure 4.24. Variation of r with mean effective stress for $D_R$=0.90-0.95

For $0.9 < D_R < 0.95$ $$r = 0.0008p' + 0.5796 \quad (4.32)$$

Based on the results above following linear equation was defined between r parameter and mean effective stress:

$$r = \alpha_r p' + \beta_r \quad (4.33)$$

Variations of the parameters $\alpha_r$ and $\beta_r$ are functions of relative density as shown in figures 4.25 and 4.26:

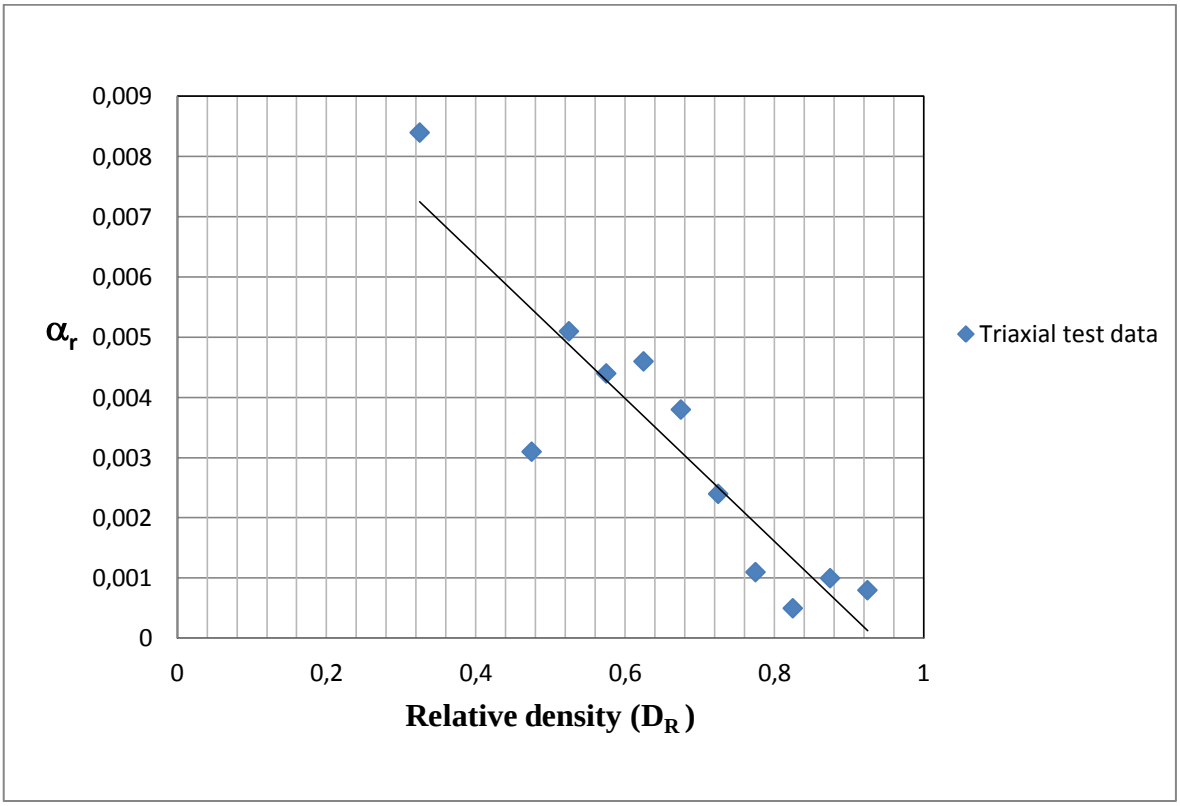


Figure 4.25. Variation of $\alpha_r$ with relative density

According to figure 4.25 following equation has been defined for $\alpha_r$ :

$$\alpha_r = a_r D_R + b_r \qquad (4.34)$$
$$= -0.0119 D_R + 0.0111$$

Therefore: $a_r = -0.0119$ and $b_r = +0.0111$

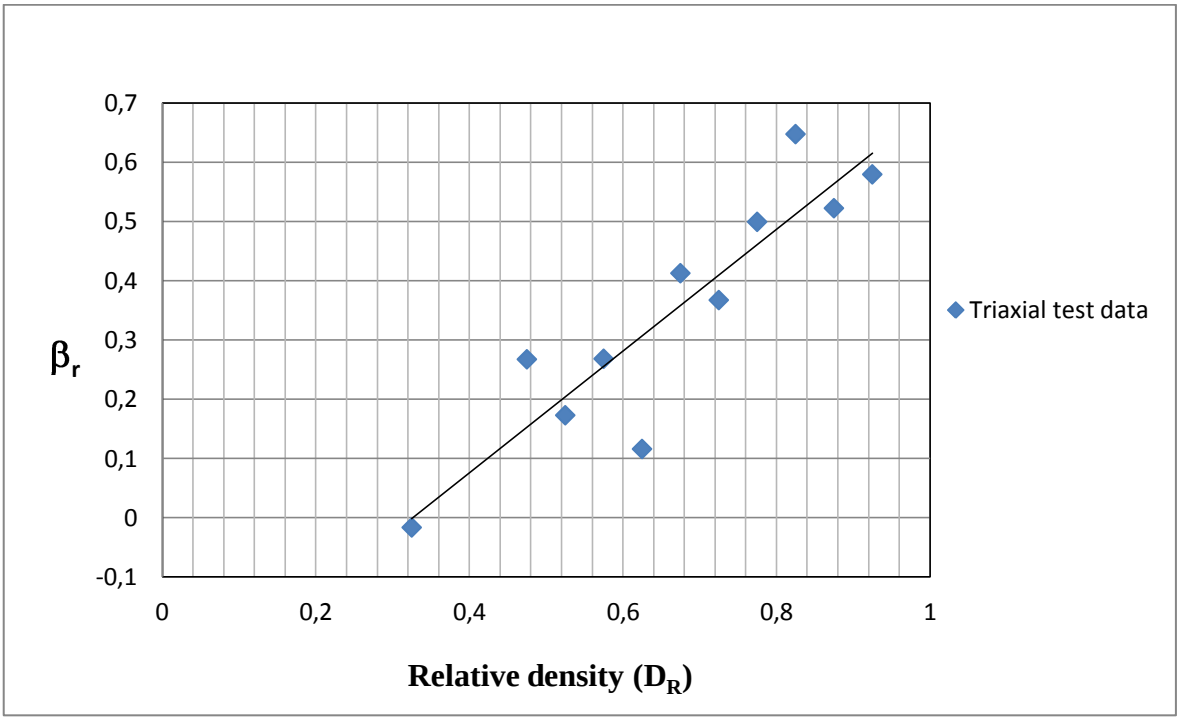


Figure 4.26. Variation of $\beta_r$ with relative density

Based on the linear variation of $\beta_r$ with relative density, following equation was defined for $\beta_r$:

$$\beta_r = m_r D_R + n_r \qquad (4.35)$$
$$= 1.0237 D_R - 0.3351$$

Therefore according to equation 4.35: $m_r = 1.027$ and $n_r = 0.34$.

r parameter was determined by combining equations 4.32, 4.33 and 4.35.

$$r = \alpha_r p' + \beta_r = (a_r D_R + b_r) p' + m_r D_R + n_r \qquad (4.36)$$

It is clear from Eq. 6.33 that proportion of dilatancy contribution to friction angle as represented by the parameter r is dependent on the combination of relative density and mean effective stress. By substituting $a_r$, $b_r$, $m_r$ and $n_r$ into equation 4.36 r parameter can be determined for Ottawa graded sand from the following equation:

$$r = -0.012 D_R p' + 0.011 p' + 1.027 D_R - 0.34 \tag{4.37}$$

In order to calculate $\phi'_{\max}$ equations 4.14 and 4.37 have been combined and added to the critical state friction angle. Therefore $\phi'_{\max}$ can be calculated from thee following equation:

$$\phi'_{\max} = (\alpha_\psi p' + \beta_\psi).(\alpha_r p' + \beta_r) + \phi'_{cs} \tag{4.38}$$

And combining Eq. 4.38 with Eqs. 4.16, 6.17, 4.34, and 4.35 we get the equation for calculating the peak friction angle:

$$\phi'_{\max} = f\ \ p', D_R\ = \left[\ a_\psi D_R + b_\psi\ \ p' +\ m_\psi D_R + n_\psi\ \right]\left[\ a_r D_R + b_r\ \ p' +\ m_r D_R + n_r\ \right] + \phi'_{cs} \tag{4.39}$$

Here in Eq. 4.39 $a_\psi$, $b_\psi$, $m_\psi$, $n_\psi$, $a_r$, $b_r$, $m_r$, $n_r$, and $\phi'_{cs}$ are constants that are dependent on the soil gradation, mineralogy, and shape. Therefore either they must be obtained by testing or their calculations must be linked to gradation and shape parameters.

Even though Eq. 4.39 links $\phi'_{max}$ to both $D_R$ and p′, there are studies in the literature that links $\phi'_{max}$ to only $D_R$. For this purpose in Figure 4.27 the variation of peak friction angle with relative density for all tests is given. It was observed that peak friction angle decreases with decreasing relative density and reaches the critical state friction angle value when relative density reaches zero. Based on Figure 4.27 the following empirical equation

used by different researchers (Bolton, Vaid et al.) can be presented showing the relationship between peak friction angle, critical state friction angle and relative density.

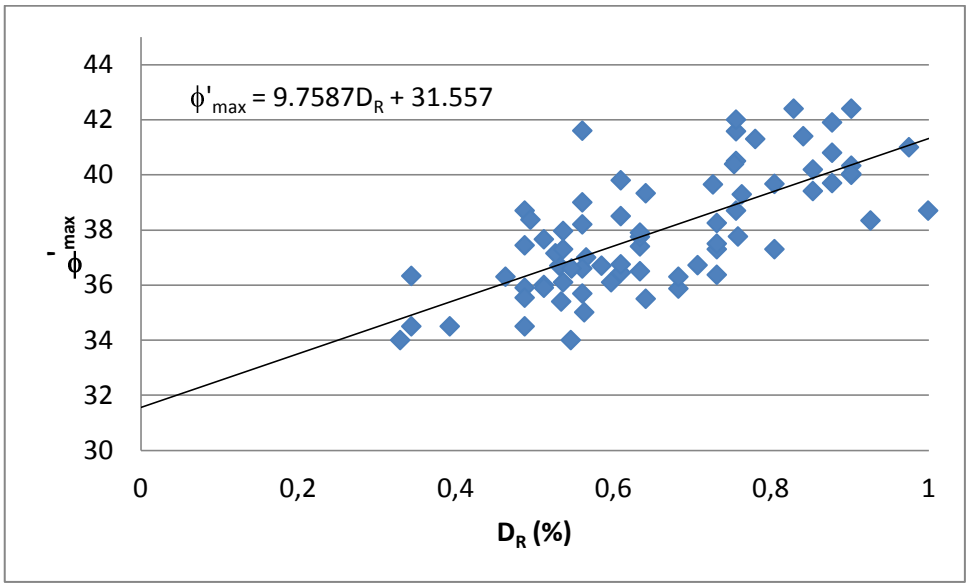


Figure 4.27. Variation of peak friction angle with mean relative density value

$$\begin{aligned} \phi'_{\max} &= \phi'_{cs} + hD_R \\ &= \phi'_{cs} + 9.8D_R \\ &\cong \phi'_{cs} + 10D_R \end{aligned} \tag{4.40}$$

where h is a constant which equals 10 for Ottawa graded sand. Here in the presented form peak friction angle is a function of only relative density. But it is clear from the deviation of the data points it is only possible to use relative density as a crude estimation of peak friction angle. It is known that dilatancy angle is a function of relative density and confinement. Therefore it is not possible to discard confinement effect from the calculation of the peak friction angle. The influence of the confinement on the peak friction angle is in Eqs. 4.38 and 4.39. and the corresponding graphs. It is natural that there is a proportionality between the peak friction angle and relative density since relative density is one of the two variables that control the peak friction angle function. For this purpose for different ranges of $D_R$, variations of peak friction angle with mean effective stress are shown in Figure 4.28 to 4.32. Clearly peak friction angle drops with the increase in the

mean effective stress. Therefore, Eq. 4.39 as proposed by various researchers (Bolton et al.) can only be used as a crude estimation and the obtained relationships would be dependent on the stress ranges used in the tests.

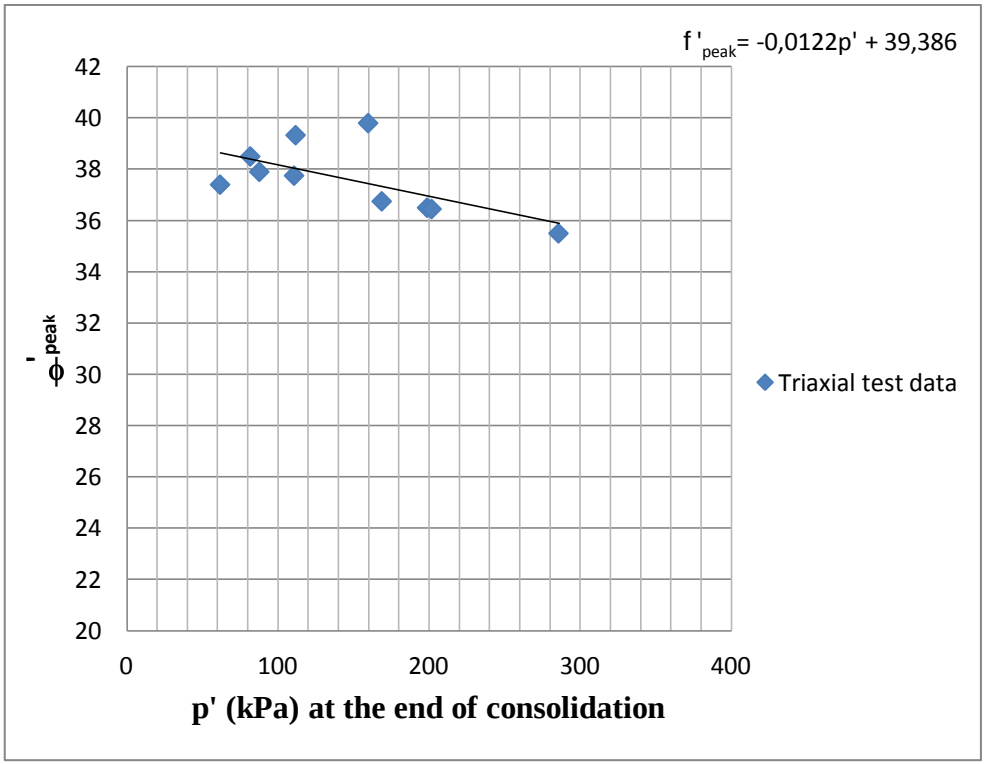


Figure 4.28. Variation of peak friction angle with mean effective stress for $D_R$=0.6-0.65

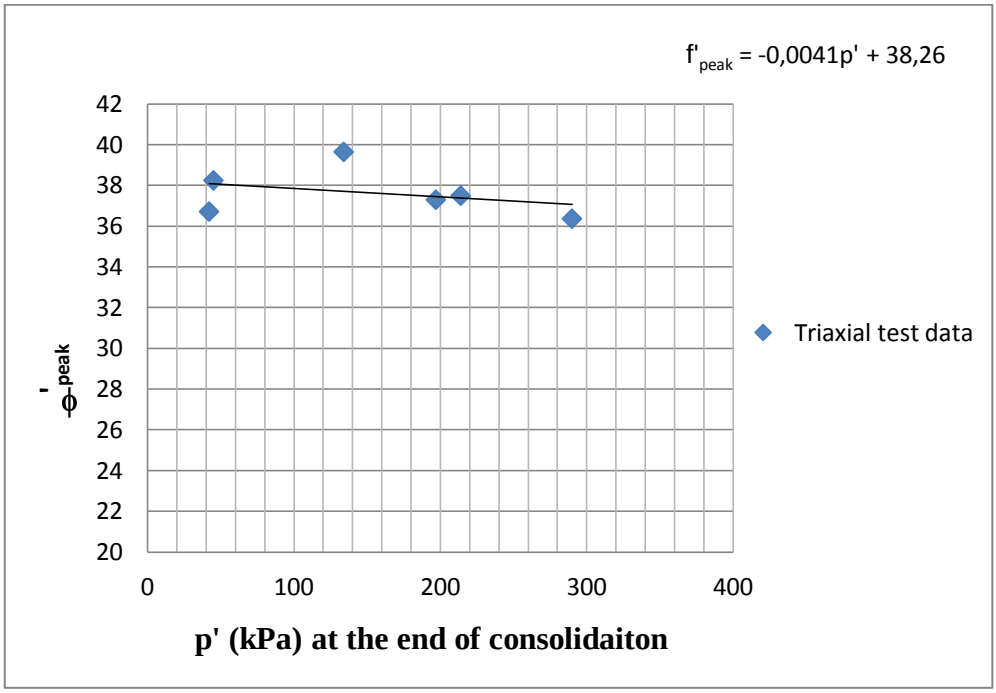


Figure 4.29. Variation of peak friction angle with mean effective stress at the end of consolidation for $D_R$=0.7-0.75

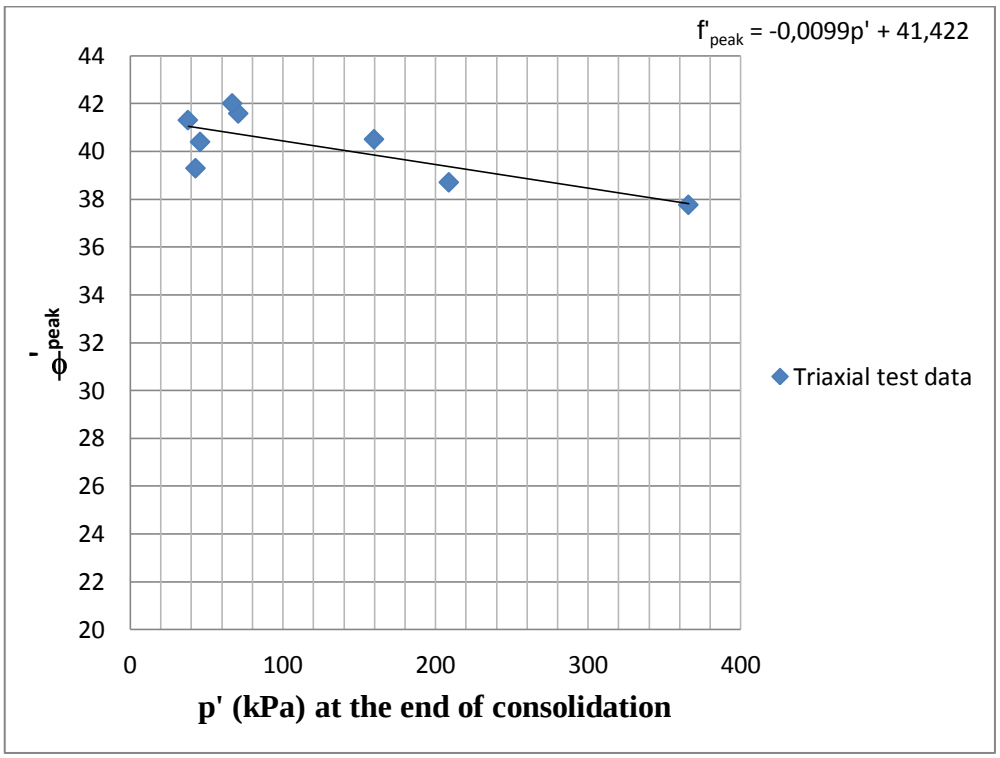


Figure 4.30. Variation of peak friction angle with mean effective stress at the end of consolidation for $D_R$=0.75-0.8

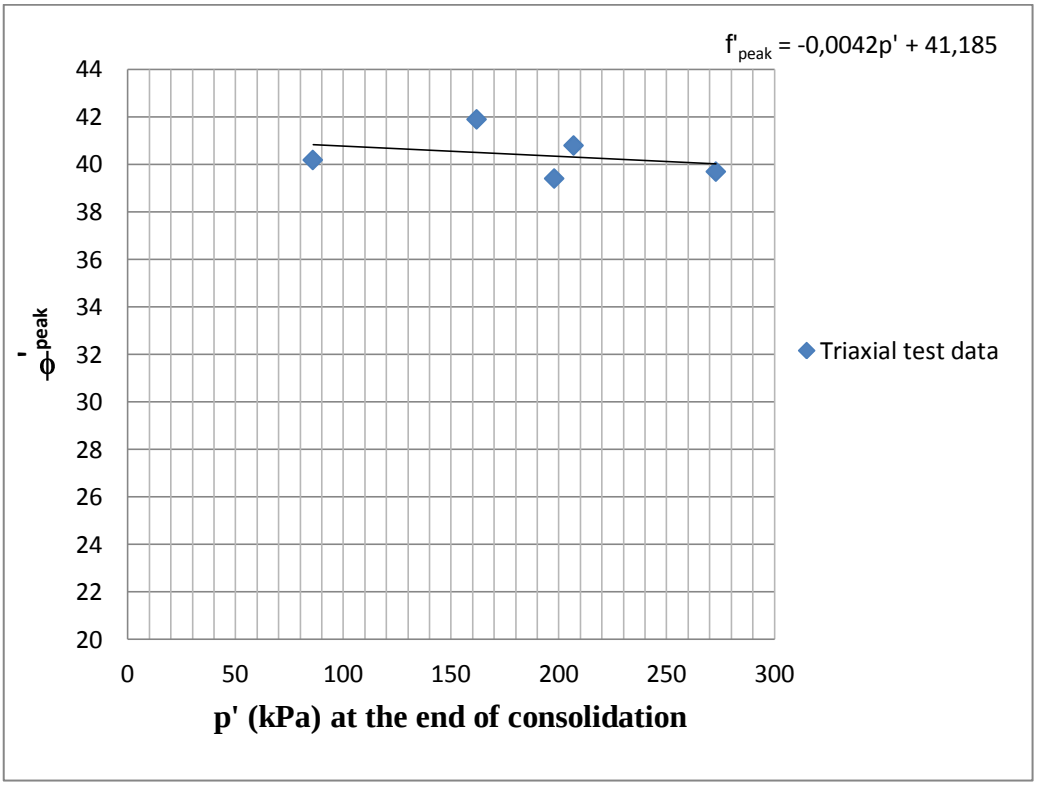


Figure 4.31. Variation of peak friction angle with mean effective stress at the end of consolidation for $D_R$=0.85-0.9

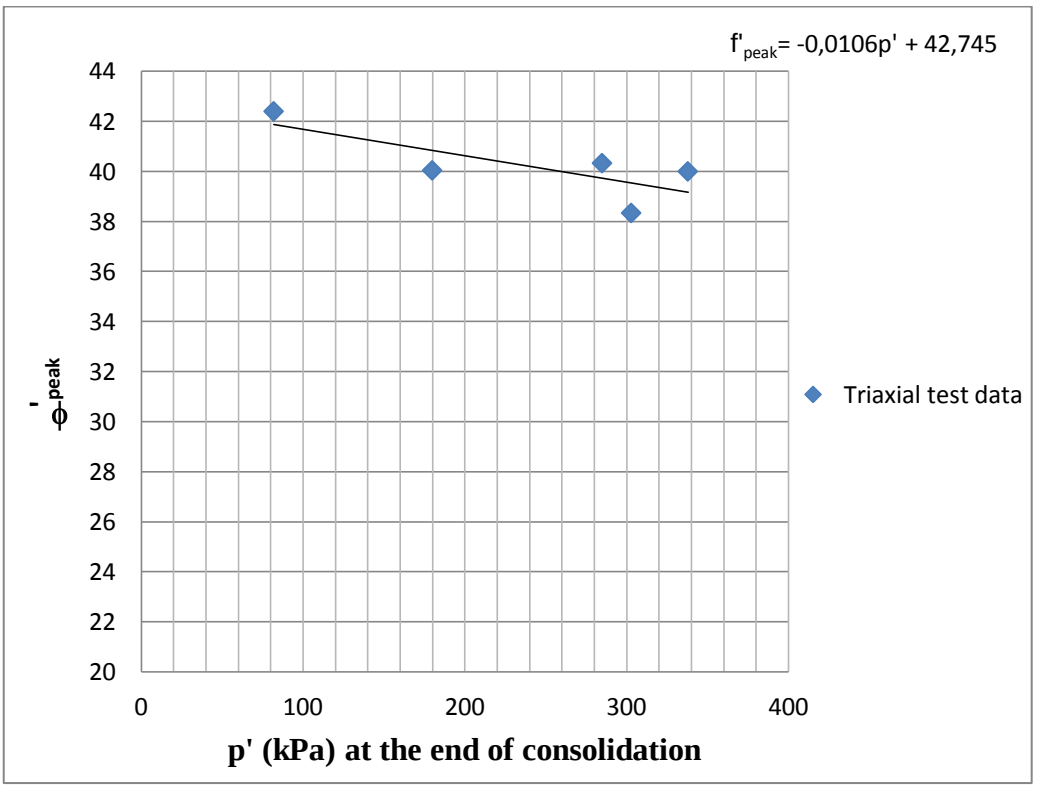


Figure 4.32. Variation of peak friction angle with mean effective stress for $D_R$=0.9-0.95

## 4.2. At Rest Lateral Earth Pressure Coefficient of Overconsolidated Sands

At rest earth pressure coefficient of cohessionless soils has been investigated in this research using $K_0$ consolidation data of triaxial tests. At rest earth pressure coefficient of the sample has been measured during the consolidation phase for all tests. Variation of at rest earth pressure coefficient with various parameters such as overconsolidation ratio, mean effective stress and relative density has been studied elaborately. Experimental results have been compared with commonly used empirical equations which are proposed by Wroth (1973), Meyerhof (1976), Mayne and Kulhawy (1982). Finally based on the experimental values a new empirical equation has been proposed.

Wroth (1973) presented the following equation for calculating at rest earth pressure of overoconsolidated soils:

$$K_{0(OC)} = K_{0(NC)} OCR - \left[\frac{\mu}{1-\mu}\right](OCR - 1) \tag{2.35}$$

where $K_{0(OC)}$ is the at rest earth pressure coefficient of overconsolidated soil, $K_{0(NC)}$ is at rest earth pressure of normally consolidated soil, OCR is overconsolidation ratio and $\mu$ is poisson ratio.

Later Meyerhof (1976) suggested equation using peak friction angle and overconsolidation ratios of the soils:

$$K_{0(OC)} = (1 - Sin\phi')\sqrt{OCR} \tag{2.37}$$

Meyerhof equation was modified later by Mayne and Kulhawy (1982):

$$K_{0(OC)} = (1 - Sin\phi')OCR^{1-Sin\phi'} \tag{2.38}$$

Experimental program consisted of $K_0$ triaxial tests using overconsolidation ratios of 1, 2, 4 and 8. Saturated samples were loaded and unloaded to obtain the required overconsolidation ratios before shearing. Therefore at rest earth pressure coefficient of overconsolidated samples could be compared with proposed empirical equations for OCR valus of 1, 2, 4 and 8. Figure 4.36 shows the experimental $K_0$ values compared with Wroth equation:

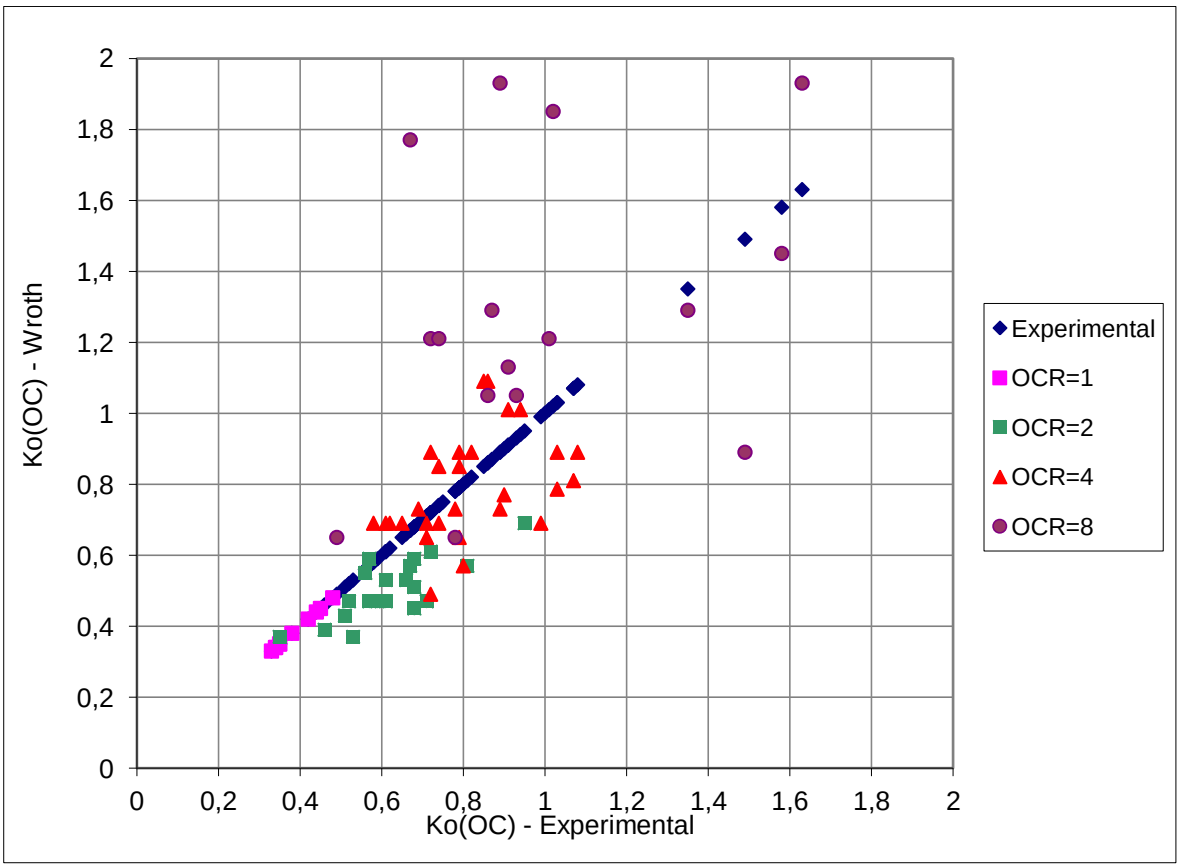


Figure 4.36. Comparisson of experimental results with Wroth equation

As observed in Figure 4.36, Wroth equation underestimate the value of at rest earth pressure coefficient for OCR=2 and 4 values and overestimate the at rest earth pressure coefficient for sands which have been overconsolidated with overconsolidation ratio of 8.

Figure 4.37 shows the values for at rest earth pressure coefficients of overconsolidated samples measured from triaxial tests versus $K_0$ valus calculated from Meyerhof equation. As observed in the figure, Meyerhof equation underestimates the at rest earth pressure coefficient up to the overconsolidation ratio of 4 but mostly overestimates it for overconsolidation ratio of 8.

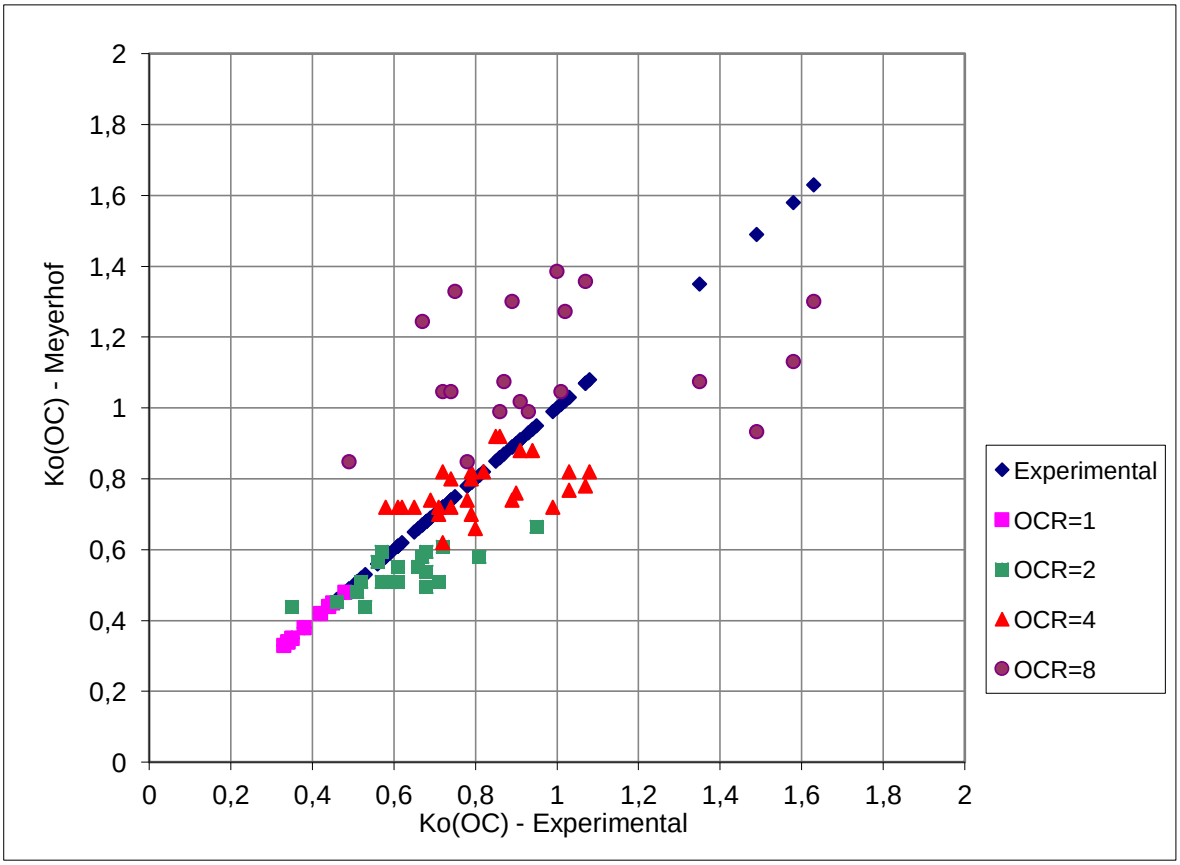


Figure 4.37. Comparisson of experimental results with Meyerhof equation

Figure 4.38 shows the values of experimental at rest earth pressure coefficients versus at rest earth pressure coefficients obtained from Mayne-Kulhawy equation. Results showed that at rest earth pressure coefficients calculated using Mayne-Kulhawy empirical equation are well below the experimental values for all overconsolidation ratios in this experimental program.

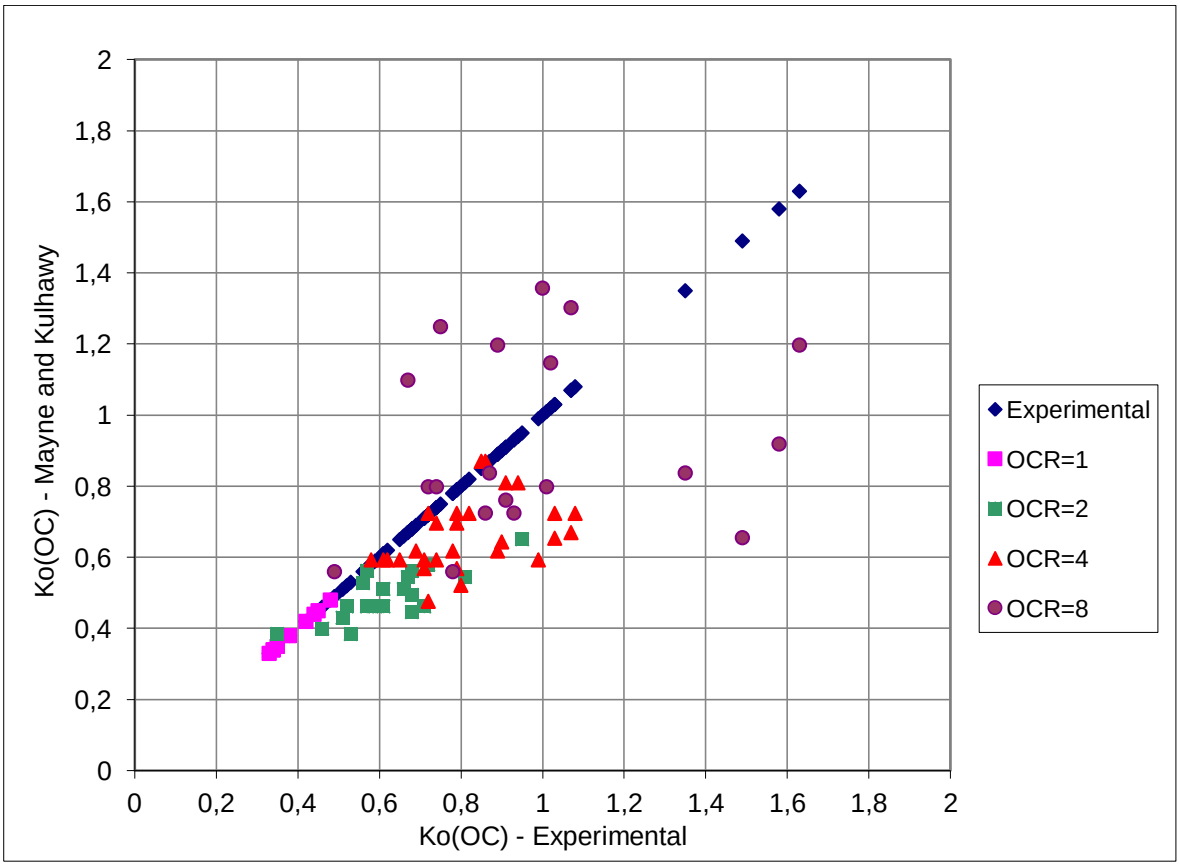


Figure 4.38. Comparisson of experimental results with Mayne-Kulhawy equation

A statistical analysis has been performed on the experimental data versus values obtained from common empirical equations. It is observed that empirical equations overestimate or underestimate the value of at rest earth pressure coefficient based on the overconsolidation ratio (OCR). The following table shows the evaluation results:

Table 4.2. Statistical comparison of experimental values with empirical formulas

| **OCR** | **1** | **2** | **4** | **8** |
|---|---|---|---|---|
| **Mayne-Kulhawy equation** | Almost same with experimental results | 19 % underestimation | 17 % underestimation | 8 % underestimation |
| **Meyerhof equation** | Almost same with experimental results | 12 % underestimation | 4 % underestimation | 22 % overestimation |
| **Wroth equation** | Almost same with experimental results | 22 % underestimation | 7 % underestimation | 51 % overestimation |
| **Proposed empirical equation** | Almost same with experimental results | 5 % Underestimation | 3 % Underestimtion | 4 % Overestimation |

Statictical analysis showed that Meyerhof equation gives more realistic results in comparison with the other empirical results. Wroth equation presents at rest earth pressure coefficients close to experimental results up to overconsolidation value of 4 but overestimates the at rest pressure coefficient for overconsolidation ratio of 8.

Variation of at rest earth pressure coefficient with peak friction angle, dilatancy angle, relative density and overconsolidation ratio was monitored. Resutls showed that dilatancy angle does not have any effect on $K_0$ and there is no relationship between dilatancy angle and at rest earth pressure coefficient. Variation of $K_0$ with overconsolidation ratio and peak friction angle has also been investigated.

Figure 4.39 shows the variation of at rest earth pressure coefficient with overconsolidation ratio and peak friction angle. At rest earth pressure coefficient for sands having the same overconsolidation ratio tends to decrease with increasing peak friction angle.

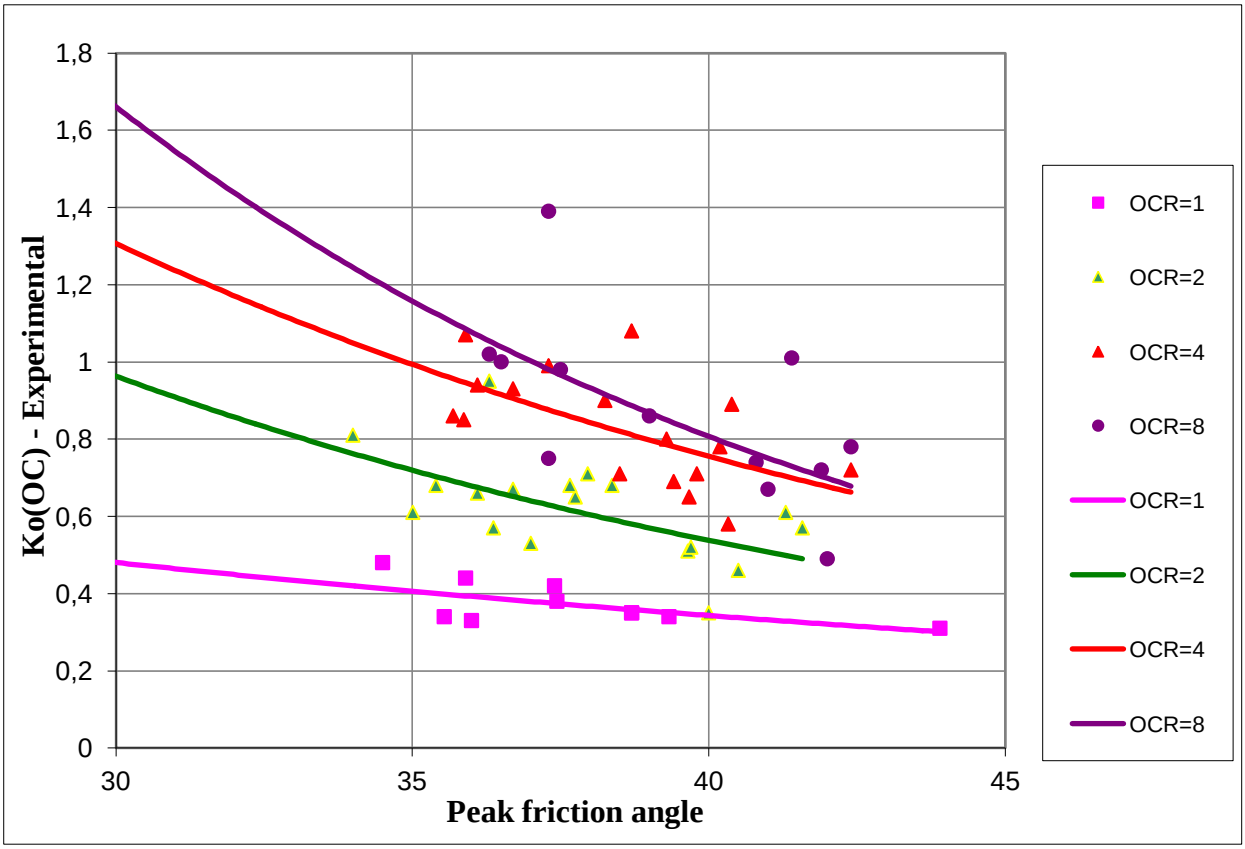


Figure 4.39. Variation of at rest earth pressre coefficient with peak friction angle

Variation of at rest earth pressure coefficient of overconsolidated sands with overconsolidation ratio for a single test has been monitored. Results show that $K_0$ for overconsolidated sands tends to increase with overconsolidation ratio in a logarithmic trend as shown in Figure 4.40 Therefore a logarithmic equation relating the at rest earth pressure coefficient of overconsolidated soil with overconsolidation ratio and at rest earth pressure coefficient of normally consolidated sands was proposed:

$$K_{0(OC)} = a_k \ln(OCR) + b_k \tag{4.41}$$

where $K_{0(OC)}$ is at rest earth pressure coefficient of overconsolidated soil, $\alpha_k$ is a coefficient which depends on soil relative density and $b_k$ is equal to at rest earth pressure coefficient of normally consolidated soil.

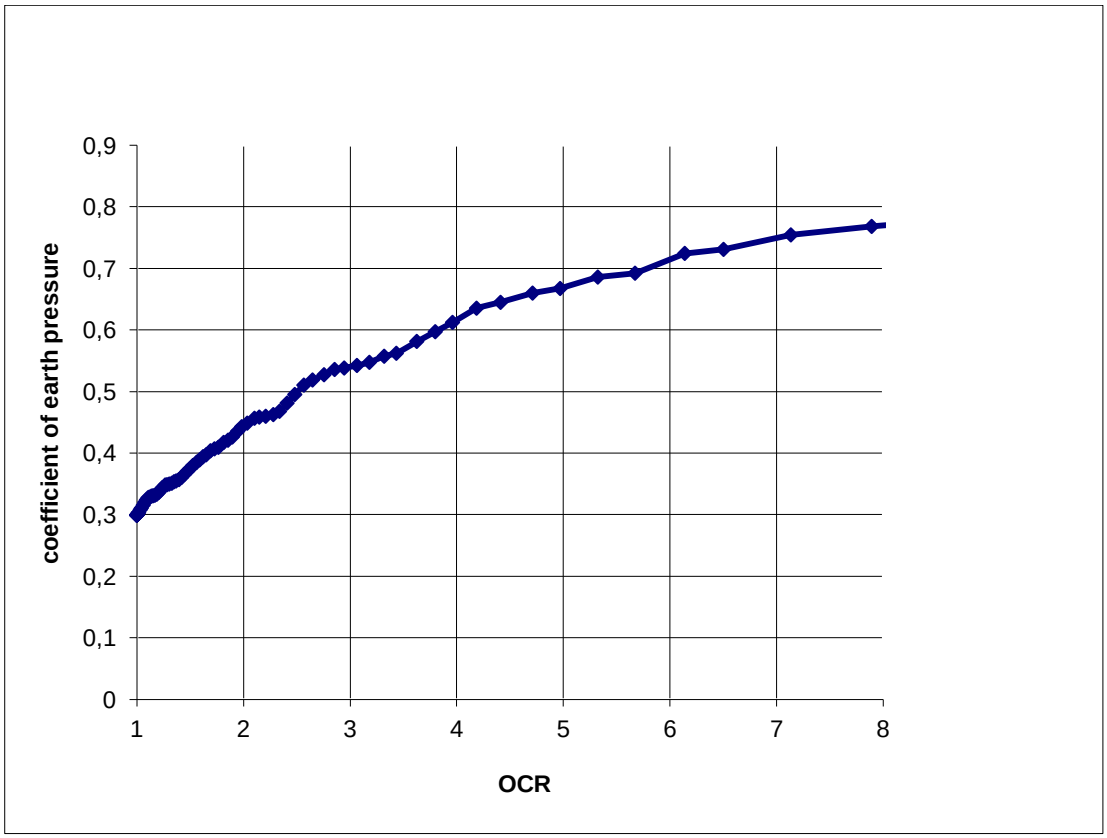


Figure 4.40. Variation of $K_{0(OC)}$ with overconsolidation ratio

In order to decrease the number of variables in Equation 4.42 both sides of the equation have been devided by $b_k$. Therefore Equation 4.42 can be written as the following equation:

$$\frac{K_{0(OC)}}{K_{0(NC)}} = \alpha_k \ln(OCR) + 1 \tag{4.42}$$

Results showed that $\alpha_k$ is a function of relative density as loose samples tend to owe greater at rest earth pressure coefficient rather than dense samples because of less degree of particle interlocking. Following equation defines the value for $\alpha_k$ :

$$\alpha_k = -1.3 D_R + 1.6 \tag{4.43}$$

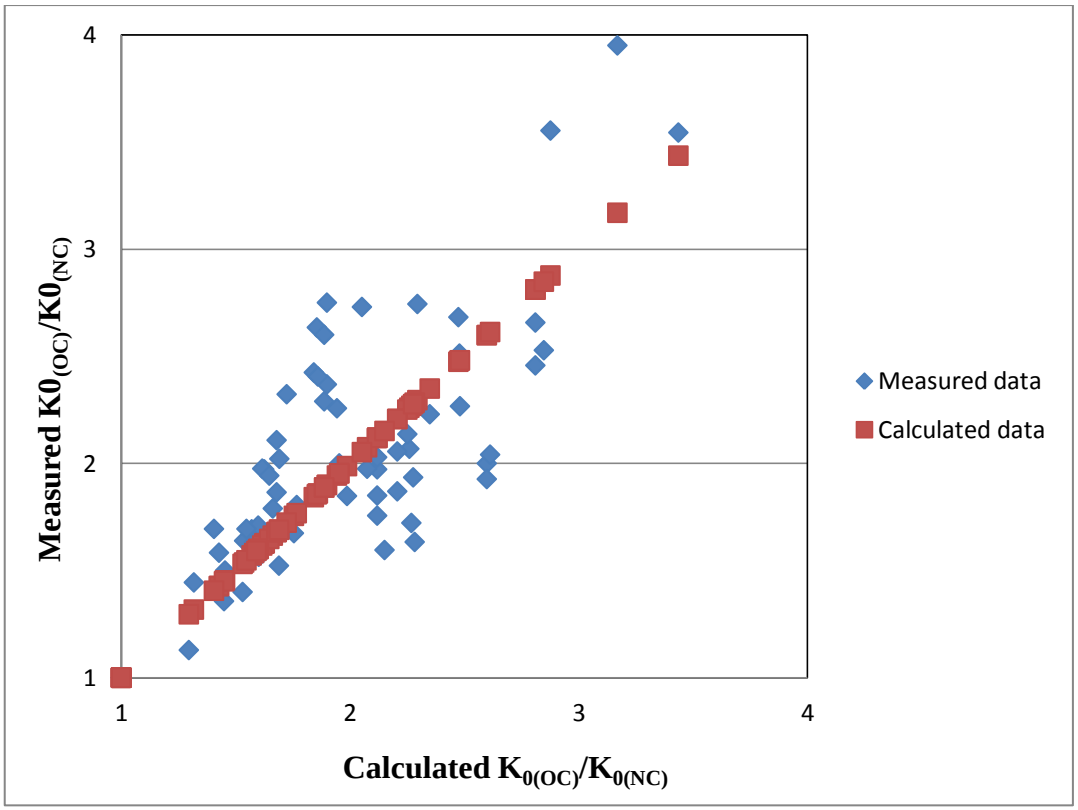


Figure 4.41. Comparisson of experimental results with proposed empirical equation

As observed in Figure 4.41 measured values are in good accordance with the proposed empirical equations.

In addition, values obtained from proposed empirical equation was compared with empirical equations suggested by Wroth (1973), Meyerhof (1976) and Mayne-Kulhawy (1982). It is observed that proposed equation is in good accordance with the experimental results rather than the other empirical equations.

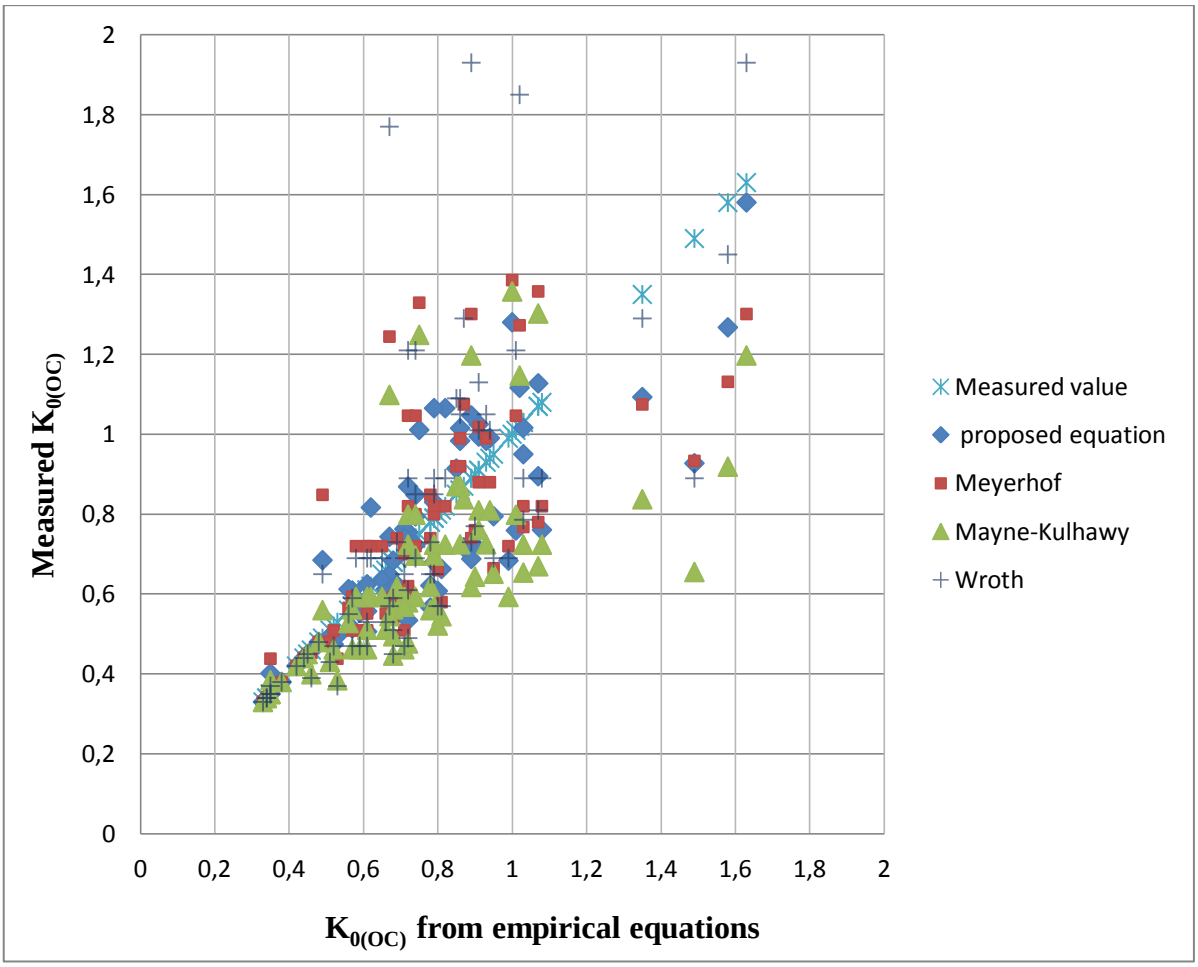


Figure 4.42. Comparisson of proposed equation with proposed empirical equations

# 5. DISCUSSION

Using similar triaxial test data obtained from the literature, proposed equations and theories are evaluated. The data that provides all the necessary parameters are given by Vaid and Sasitharan (1991) who conducted an experimental research using triaxial tests on isotropically consolidated sand samples. Their experimental program included more than 50 triaxial tests with different stress paths in order to simulate various modes of loading such as compression and extension. Erksak sand was used as the testing material which had the minimum and maximum void ratios of 0.525 and 0.775 respectively. Relative density of the samples varied from loose to dense. 10 different stress paths were applied on the samples. Consolidation stresses ranging from 100 to 2400 kPa were used.

Based on the results regarding the volumetric changes of the samples during shearing, Vaid and Sasitharan (1991) proposed empirical equations for determining the dilatancy angle for triaxial compression and extension tests. Later based on the obtained values of peak friction angle they adopted the empirical relationship suggested by Bolton (1986) to Erksak sand which is given below:

$$\phi'_p = \phi'_{cv} + 0.33\psi \tag{2.42}$$

The experimental research of Vaid and Sasitharan (1991) yielded useful information for checking the applicability of the proposed equations of this research as it included relative density and mean effective stress values in addition to the peak friction angle and dilatancy angle. As it is explained in the previous sections, the mentioned parameters were the main input of the empirical relationships in this research. Therefore the validity of the proposed equations and their trend were checked using the experimental data given in Vaid and Sasitharan (1991) study.

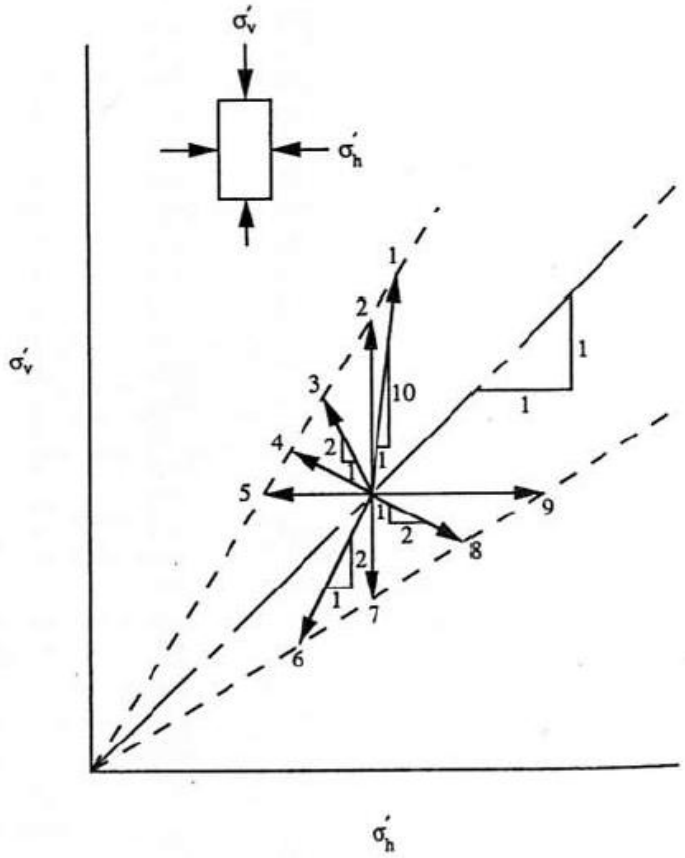


Figure 2.13. Schematic view of stress paths (Vaid and Sasitharan, 1991)

Although samples are isotropically consolidated in Vaid and Sasitharan study, stress path 2 corresponds to the shearing conditions the samples experience in this research program's tests. During the shearing phase, both the samples in this research and Vaid and Sasitharan (1991) research, cell pressure is kept constant and deviatoric stress is increased. Table below shows the experimental program conducted in Vaid and Sasitharan (1991) research. First column includes relative densities of the samples. Effective horizontal stresses and effective vertical stresses values at the end consolidation phase have been presented in the second and third columns. p′ stands for the mean effective stress before shearing and was calculated using the effective vertical and effective horizontal stress values. Peak friction angles are shown as $\phi'$ and last column represents the dilatancy angles.

Table 5.1. Summary of the tests performed by Vaid-Sasitharan (1991)

| $D_R$ | $\sigma'_{hc}$ at the end of consolidation (kPa) | $\sigma'_{vc}$ at the end of consolidation (kPa) | p' (kPa) | ϕ' (deg) | ψ (deg) |
|---|---|---|---|---|---|
| 0,26 | 250 | 250 | 250 | 34,5 | 8,9 |
| 0,26 | 100 | 100 | 100 | 34,9 | 9,5 |
| 0,26 | 400 | 400 | 400 | 34,1 | 8,7 |
| 0,26 | 600 | 600 | 600 | 34,9 | 8,4 |
| 0,26 | 1200 | 1200 | 1200 | 33,3 | 4,1 |
| 0,26 | 2400 | 2400 | 2400 | 32,2 | -0,4 |
| 0,26 | 100 | 234 | 145 | 34,6 | 9,6 |
| 0,26 | 250 | 585 | 362 | 34,7 | 10 |
| 0,26 | 400 | 936 | 579 | 34,1 | 6,3 |
| 0,56 | 250 | 250 | 250 | 37,7 | 16,3 |
| 0,56 | 250 | 250 | 250 | 38,6 | 20,1 |
| 0,56 | 200 | 2500 | 967 | 39,1 | 22,8 |
| 0,56 | 200 | 200 | 200 | 38,6 | 22,7 |
| 0,56 | 450 | 450 | 450 | 37,3 | 16,7 |
| 0,56 | 550 | 550 | 550 | 37 | 15,9 |
| 0,56 | 1200 | 1200 | 1200 | 36,2 | 10 |
| 0,56 | 2400 | 2400 | 2400 | 33,7 | 3,1 |
| 0,56 | 100 | 234 | 145 | 38 | 17 |
| 0,56 | 250 | 585 | 362 | 37,2 | 14,4 |
| 0,7 | 250 | 250 | 250 | 40,7 | 25,4 |
| 0,7 | 1200 | 1200 | 1200 | 37,8 | 14,7 |
| 0,7 | 2000 | 2000 | 2000 | 36 | 9,3 |
| 0,7 | 250 | 560 | 353 | 40,3 | 22,4 |

Based on the results given in table 5.1 variation of the dilatancy angle with the mean effective stress was investigated for three relative density groups presented.

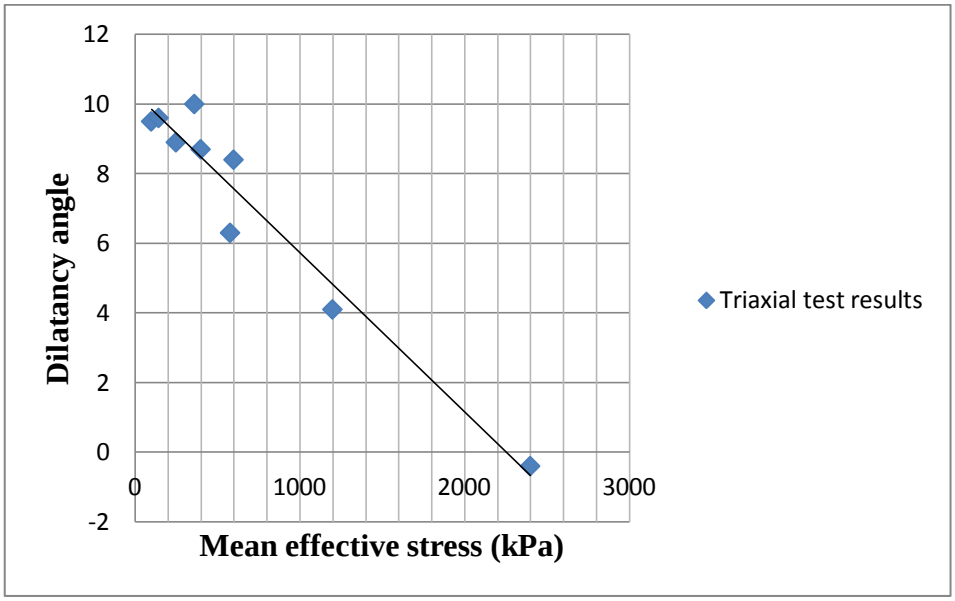


Figure 5.1. Variation of the dilatancy angle with mean effective stress for $D_R$=0.26

The following linear equation observed between the mean effective stress and dilatancy angle:

$$\psi = -0.0046\,p' + 10.299 \tag{5.1}$$

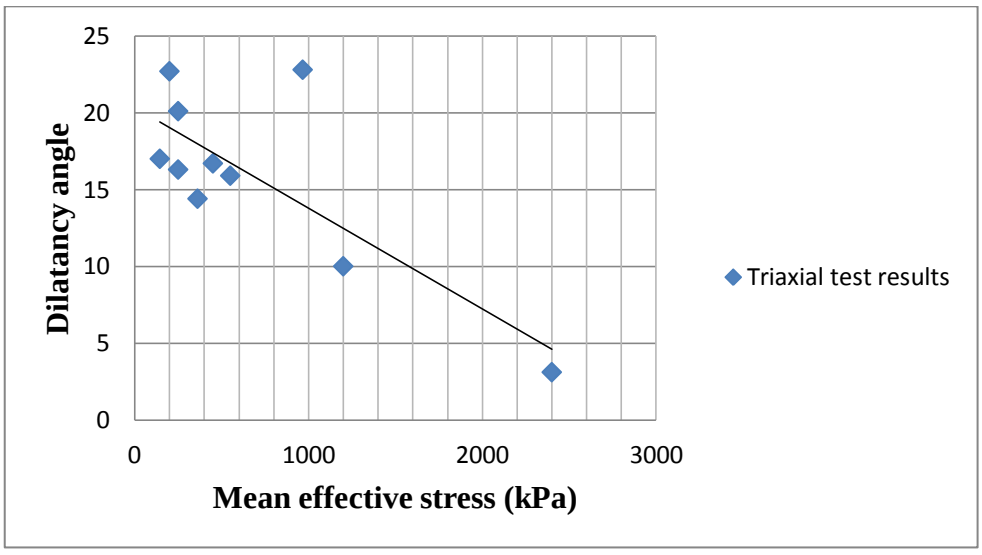


Figure 5.2. Variation of the dilatancy angle with mean effective stress for $D_R$=0.56

Equation 5.2 shows the variation of the mean effective stress with the dilatancy angle for the relative density value of 0.56.

$$\psi = -0.0066\,p' + 20.341 \tag{5.2}$$

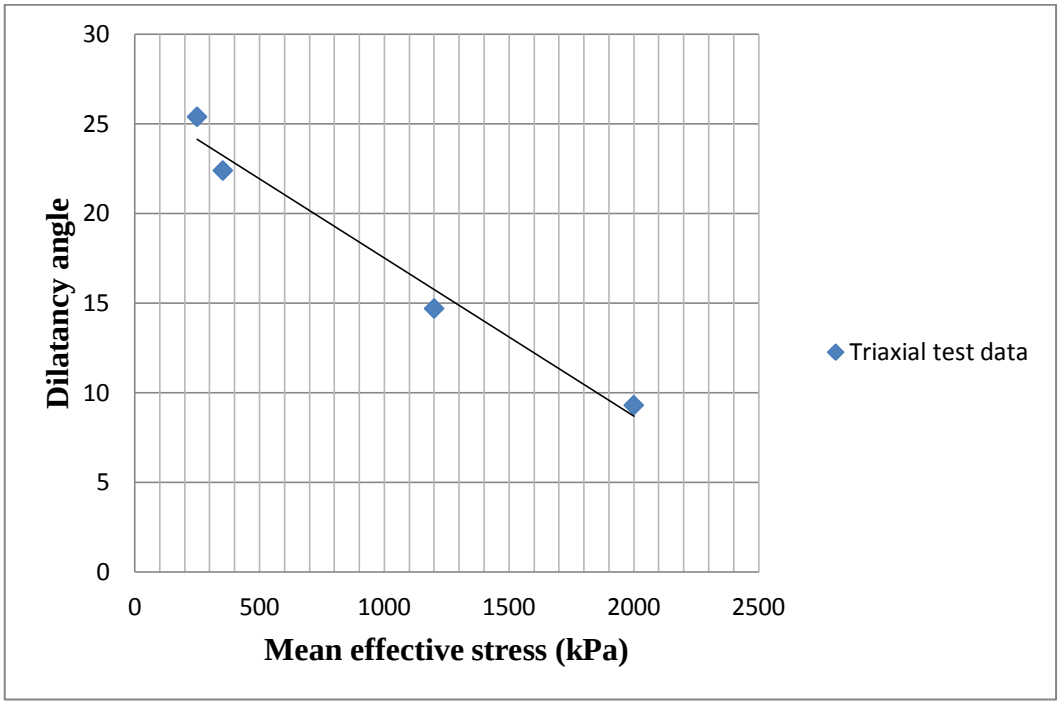


Figure 5.3. Variation of the dilatancy angle with mean effective stress for $D_R$=0.70

$$\psi = -0.0088p' + 26.35 \tag{5.3}$$

As observed in Figures 5.1, 5.2 and 5.3 a linear relationship exists between the mean effective stress and dilatancy angle which confirms to the trends observed in this research between mean effective stress and dilatancy angle. Dilatancy angle can be measured here also based on the mean effective stress and relative density values.

The proposed linear equation for determining dilatancy in Chapter 4:

$$\psi = \alpha_\psi p' + \beta_\psi \tag{4.14}$$

Variation of $\alpha_\psi$ and $\beta_\psi$ values with relative density was checked for Vaid and Sasitharan (1991) data.

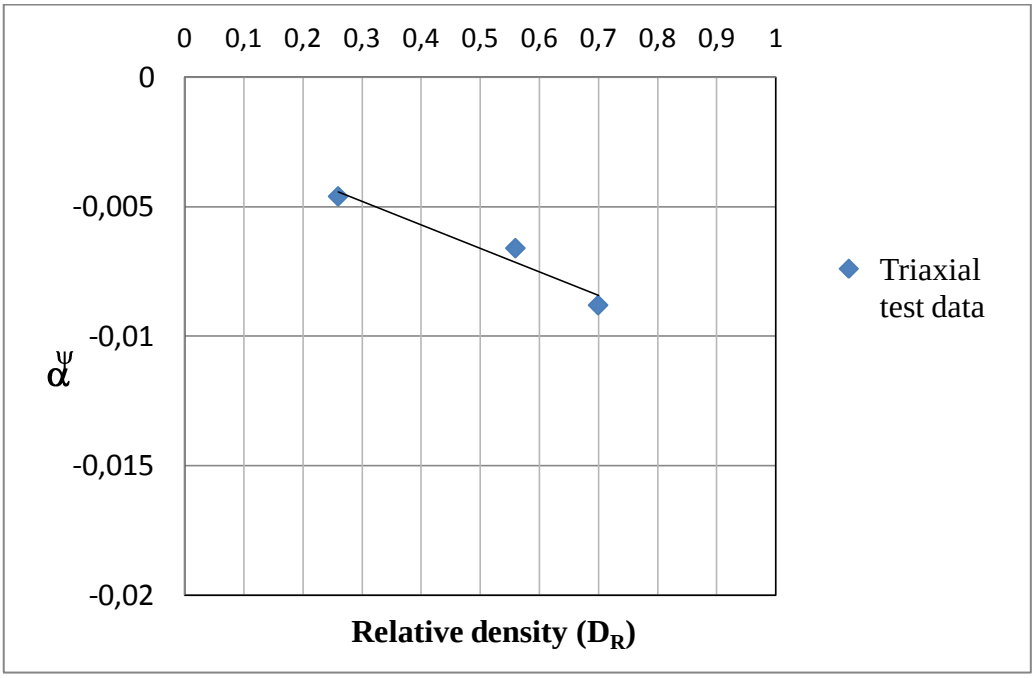


Figure 5.4. Variation of $\alpha_\psi$ parameter with relative density for Vaid-Sasitharan study

Based on equation 4.15 $\alpha_\psi$ can be written as:

$$\alpha_\psi = a_\psi D_R + b_\psi \tag{4.15}$$

According to Vaid-Sasitharan results:

$$\alpha_\psi = -0.0091 D_R - 0.0021 \tag{5.4}$$

Therefore: $a_\psi = -0.0091$ and $b_\psi = -0.0021$

According to equation 4.16, $m_\psi$ and $n_\psi$ values can be obtained for Vaid and Sasitharan data.

$$\beta_\psi = m_\psi D_R + n_\psi \tag{4.16}$$

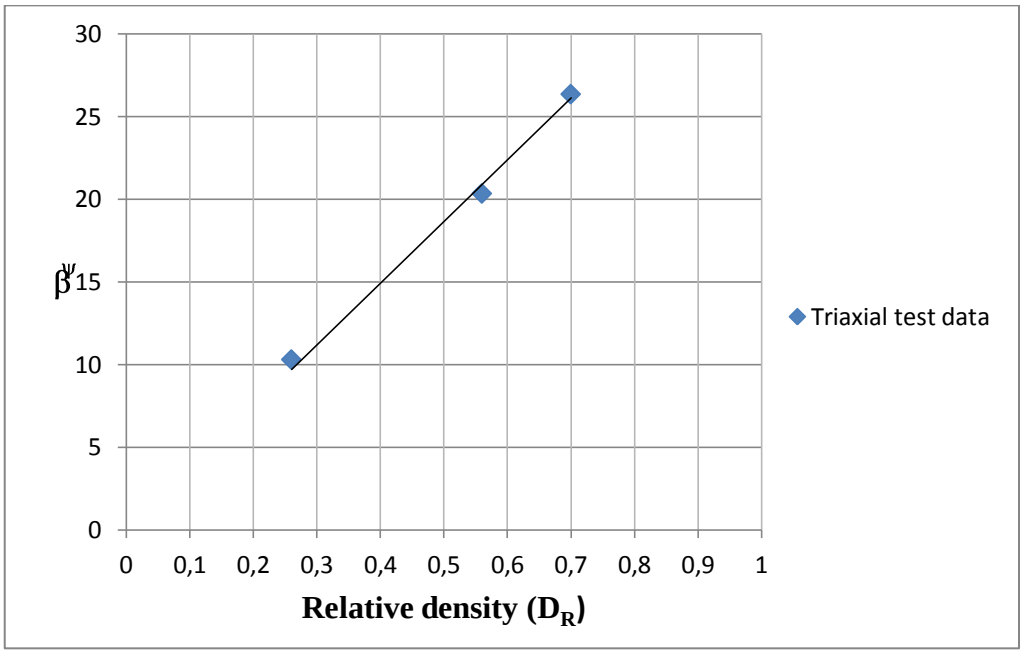


Figure 5.5. Variation of $\beta_\psi$ parameter with relative density for Vaid-Sasitharan study

$$\beta_\psi = 37.3 D_R \tag{5.5}$$

Therefore: $m_\psi = 37.3$ and $n_\psi = 0$

Based on equation 4.18 the following relationship can be defined for Vaid-Sasitharan values:

$$\psi = a_\psi D_R + b_\psi \quad p' + \quad m_\psi D_R + n_\psi \tag{5.6}$$

$$\psi = (-0.0091 D_R - 0.0021)\, p' + (37.3 D_R) \tag{5.7}$$

Based on equation 4.21 peak friction angle can be calculated by combining the critical state friction angle and a soil dependent proportion of the dilatancy angle.

$$\phi'_{\max} = \phi'_{cs} + r\psi \tag{4.21}$$

Therefore variation of r parameter with the mean effective stress and relative density is monitored to observe their effects on peak friction angle in Vaid-Sasitharan research.

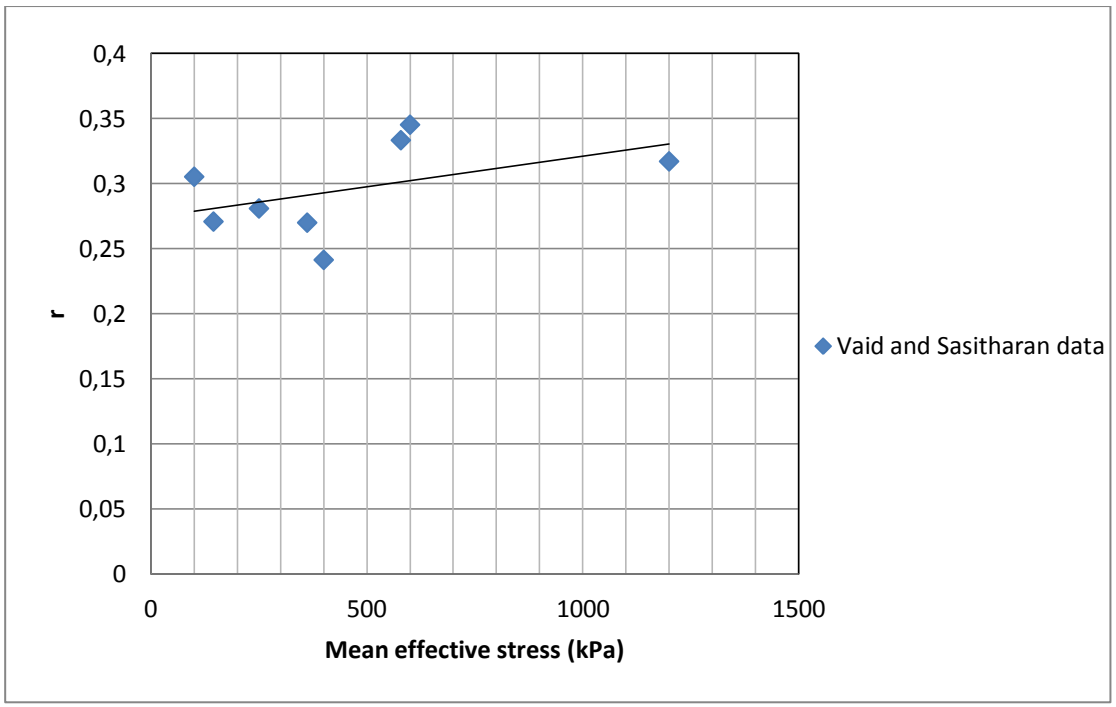


Figure 5.6. Variation of the r parameter with mean effective stress for $D_R$=0.26

For $D_R$=0.26 $$r = -0.0005 p' + 0.2743 \tag{5.8}$$

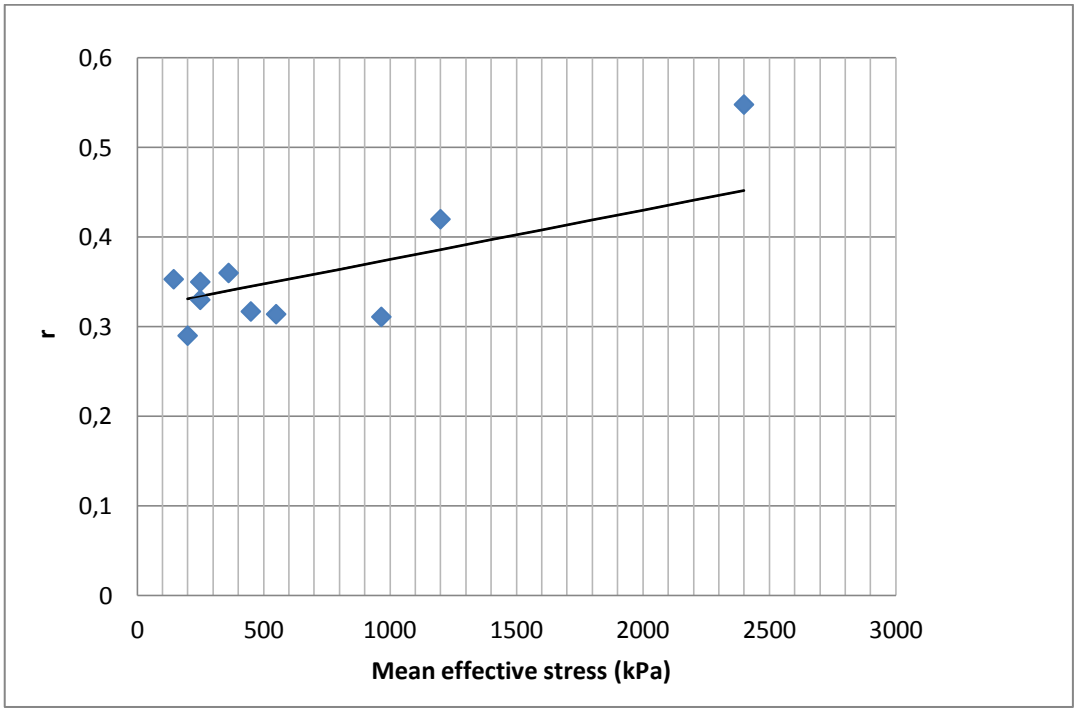


Figure 5.7. Variation of r parameter with mean effective stress for $D_R$=0.56

For $D_R$=0.56 $$r = 0.000055p' + 0.32 \quad (5.9)$$

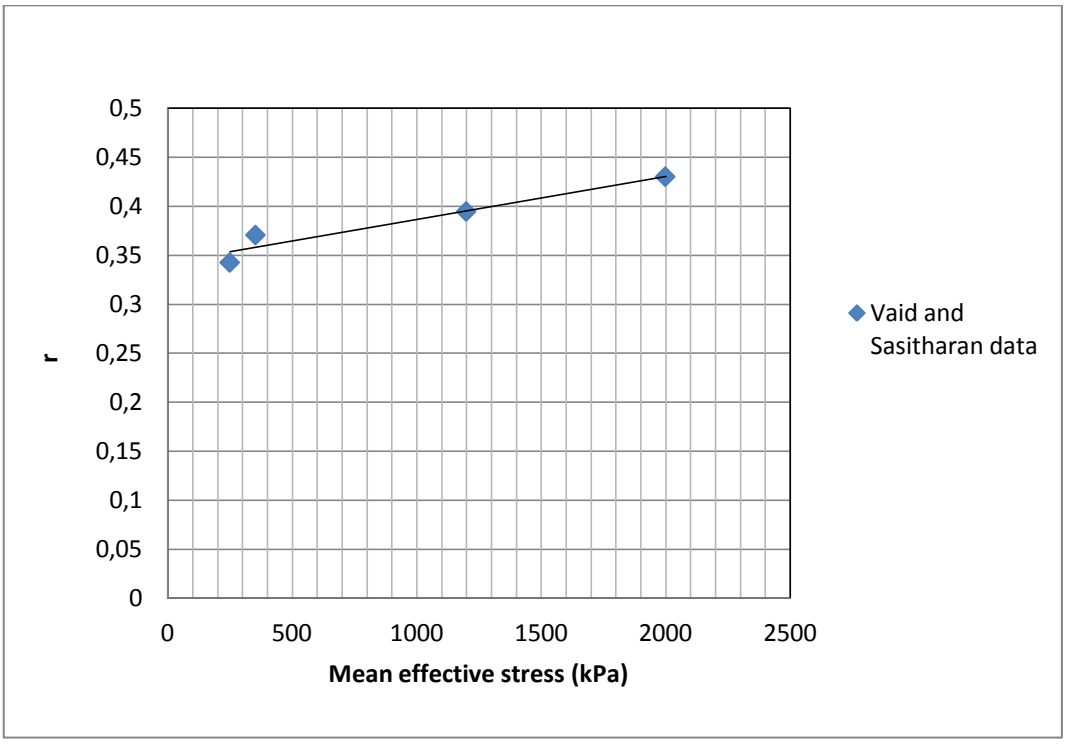


Figure 5.8. Variation of r parameter with mean effective stress for $D_R$=0.7

For $D_R$=0.70 $$r = 0.00004\,p' + 0.3428 \quad (5.10)$$

A linear equation has been observed between r parameter and mean effective stress for all relative density ranges in Vaid and Sasitharan experimental program. Therefore obtained linear relationships can be written as equation 4.33.

$$r = \alpha_r\, p' + \beta_r \quad (4.33)$$

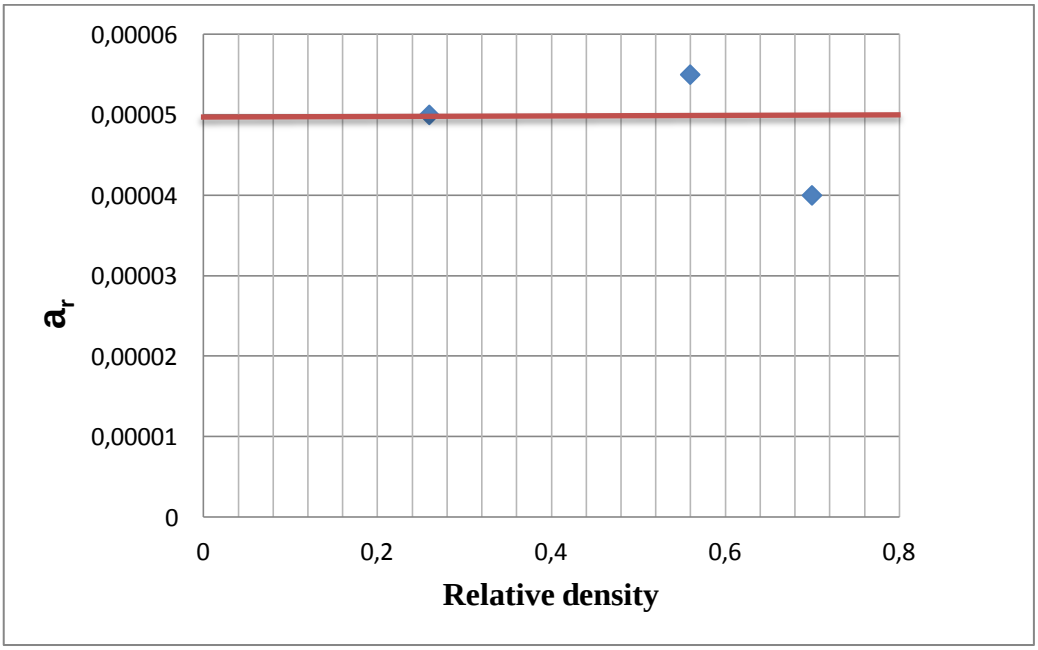


Figure 5.9. Variation of $\alpha_r$ parameter with relative density

$$\alpha_r = 0.00005 \quad (5.11)$$

According to equation 4.34:

$$\alpha_r = a_r D_R + b_r \quad (4.34)$$

Therefore: $a_r$ = 0 and $b_r$ = 0.00005

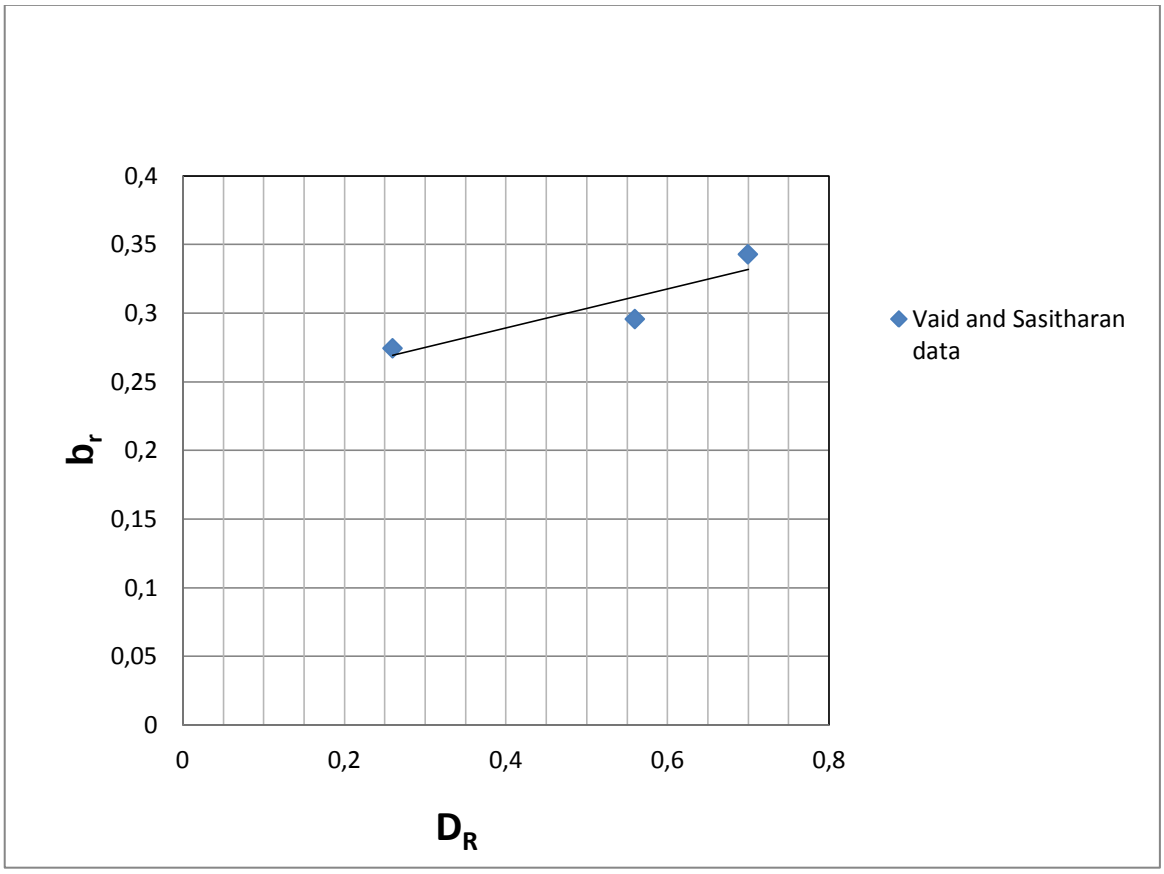


Figure 5.10. Variation of $\beta_r$ parameter with relative density

According to equation 4.35:

$$\beta_r = m_r D_R + n_r \tag{4.35}$$

From Vaid-Sasitharan results:

$$\beta_r = 0.1423 D_R + 0.2321 \tag{5.12}$$

Therefore: $m_r$ = 0.1423 and $n_r$ = 0.2321

r parameter can be written as equation 5.13:

$$r = \alpha_r p' + \beta_r = (a_r D_R + b_r) p' + m_r D_R + n_r \quad (5.13)$$

By substituting $a_r$, $b_r$, $m_r$ and $n_r$ into equation 4.36 r parameter can be determined as:

$$r = (0.00005) p' + 0.1423 D_R + 0.2321 \quad (5.14)$$

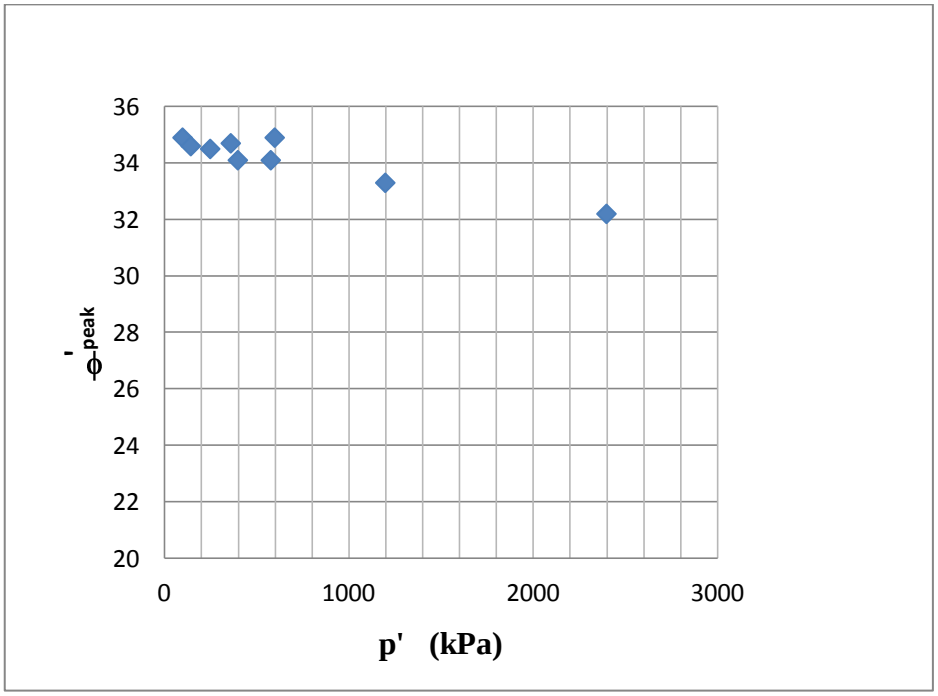


Figure 5.11. Variation of peak friction angle with mean effective stress for $D_R$=0.26

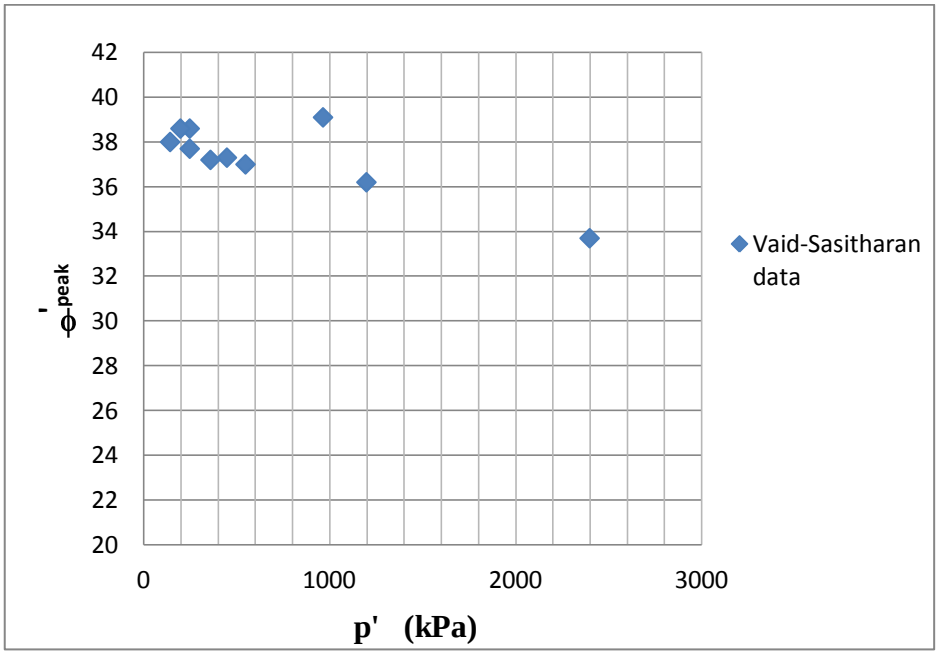


Figure 5.12. Variation of peak friction angle with mean effective stress for $D_R$=0.56

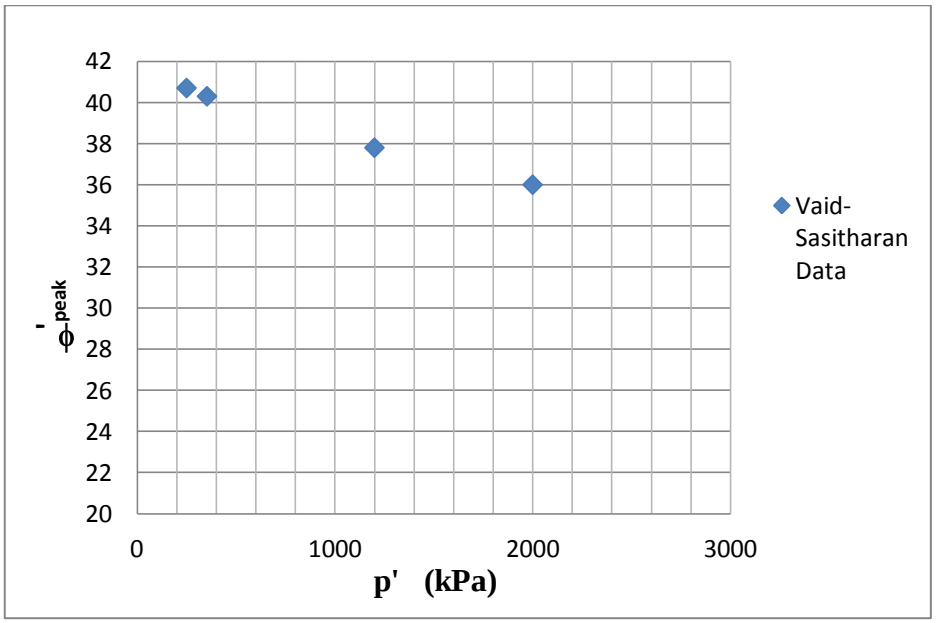


Figure 5.13. Variation of peak friction angle with mean effective stress for $D_R$=0.7

Equation 5.7 shows different values for $a_\psi$, $b_\psi$, $m_\psi$ and $n_\psi$. Therefore it can be argued that these parameters for Erksak sand are different from the values which were obtained for Ottawa sand it chapter 4. However in both sands the variation of dilatancy angle with mean effective stress and relative density has the same trend. It means that the coefficient $\alpha_\psi$ takes negative values for both sands which means the decreasing trend of dilatancy angle with mean effective stress while relative density coefficients are positive for both sands which approves the increase in dilatancy angle by the increase in the relative density of the soil although these coefficients varied in value but gained the same sign in both sands. Hence basic properties of each sand could be linked with the coefficients mentioned and using the same equation (Equation 5.7) dilatants properties of sands can be measured having the mean effective stress and relative density of the sand.

As mentioned in chapter 4.1.2 r parameter shows the contribution of dilatancy angle to shear strength of sands. Based on results obtained for $a_r$, $b_r$, $m_r$ and $n_r$ for Erksak sand it can be discussed that the effects of relative density and mean effective stress on the contribution to shears strength of soils vary from sand to sand. However results declare the positive effect of relative density to the increase in shear strength because of dilatants behaviour.

Based on the results shown in Figures 5.11-5.13 it can be argued that mean effective stress affects the peak friction angle of sands. This trend was also observed in Ottawa sand however it seems that the variation gains a steeper slope within higher pressures. It may be discussed that particle crushing affects the value of peak friction angle with mean effective stress.

# 6. CONCLUSION

An experimental investigation including more than 80 $K_0$ CD triaxial tests was conducted on cohesionless soils. The aim of the research was to observe the effect of several parameters such as overconsolidation ratio, mean effective stress and relative density on shear strength and at rest lateral earth pressure properties of cohesionless soils. Based on the result obtained from triaxial testing program following conclusions emerged from this study.

(i) Dilatancy angle is a function of both mean effective stress (p') and relative density ($D_R$). A linear equation can be defined for the relationship between dilatancy angle, mean effective stress and relative density.

(ii) A new empirical equation has been proposed for the evaluation of dilatancy angle using mean effective stress and relative density values as input. The advantage of this empirical equation is using measurable data while other relationships require volumetric changes of the sample which its measurement is difficult in most cases.

(iii) Coefficients of relative density and mean effective stress in the proposed equation may vary for different sands. Therefore these coefficients can be linked to the basic properties of sands such as coefficient of uniformity, coefficient of curvatures and etc.

(iv) Peak friction angle of sands is only affected by the relative density and mean effective stress of the sample despite it is a function of critical state friction angle and dilatancy angle. This means that a part of dilatancy angle has contribution to the peak friction angle of sand as dilatancy angle is a volumetric parameter itself. This part of the dilatancy angle has been named as strength dilatancy in this research.

(v) A new empirical relationship has been suggested for the at rest earth pressure of cohesionless soils. This relationship uses relative density and overconsolidation ratio for the calculation of the at rest earth pressure coefficient. The proposed relationship seems more reasonable for determining the at rest lateral earth pressure as it uses parameters regarding the consolidation phase of the sample rather than peak friction angle which is a shear strength parameter.

(vi) Proposed equation for determining at rest lateral earth pressure coefficient was compared with commonly used equations proposed by Wroth, Mayne-Kulhawy and Meyerhof. Results showed that the proposed equation in this reaserch suggest at rest lateral earth pressure coefficients for overconsolidated sand closer to the experimental measured data in this study rather than the other empirical equations.

# 7. REFERENCES

American Society for Testing and Materials, 2006, "Standard Test Methods for Maximum Index Density and Unit Weight of Soils Using a Vibratory Table", *ASTM Standards: D4253* .

American Society for Testing and Materials, 2006, "Standard Test Methods for Minimum Index Density and Unit Weight of Soils and Calculation of Relative Density", *ASTM Standards: D4254.*

American Society for Testing and Materials, 1995, "Standard Test Methods for Consolidated Undrained Triaxial Compression Test for Cohesive Soils", *ASTM Standards: D4767.*

American Society for Testing and Materials, 2011, "Standard Test Method for Consolidated Drained Triaxial Compression Test for Soils", *ASTM Standards D7181*.

American Society for Testing and Materials, 2006, "Standard Specification for Standard Sand" , *ASTM Standards C778*.

American Society for Testing and Materials, 2006, "Standard Test Method for Specific Gravity of Soil Solids by Water Pycnometer", *ASTM Standards: D854.*

American Society for Testing and Materials, 2009, "Standard Specification for Woven Wire Test Sieve Cloth and Test Sieves" *ASTM Standards*: E11.

Bolton, M. D., 1986, "Strength and Dilatancy of Sands", *Geotechnique*, Vol. 36, No. 1, pp. 65-78.

Chu, J. and C. L. Gan, 2004, "Effect of Void Ratio on $K_0$ of Loose Sand", *Geotechnique*, Vol. 54, No. 4, pp. 285-288.

Chakraborty, T. and R. Salgado, 2010, "Dilatancy and Shear Strength of Sand at Low Confining Pressures", *Journal of Geotechnical and Geoenvironmental Engineering*, Vol. 136, No. 3, pp. 527-532.

Cho, G. C., J. Dodds and C. Santamarina, 2006 , "Particle Shape Effects on Packing Density, Stiffness and Strength", *Journal of Geotechnical and Geoenvironmental Engineering*, Vol. 132, pp. 591-602.

Craig, R. F., *Soil Mechanics*, Spon Press, London and New York, 2004.

Daramola, O., 1980, "On Estimating $K_0$ for Overconsolidated Granular Soils", *Geotechnique*, Vol.92, pp. 310-313.

Feda, J., 1984, "$K_0$-Coefficient of Sand in Triaxial Apparatus", *Journal of Geotechnical Engineering*, Vol. 110, No. 4, pp. 519-524.

Fukushima, S. and F. Tatsuoka, 1984, "Strength and Deformation Characteristics of Saturated Sand at Extremely Low Pressures", *Soils and Foundations Journal*, Vol. 24, No. 4, pp. 30-48.

Hanna, A. and I. Romhein, 2008, "At-Rest Earth Pressure of Overconsolidated Cohesionless Backfill", *Journal of Geotechnical and Geoenviromental Engineering*, Vol. 134, No. 3, pp. 408-412.

Hanna, A. and N. Soliman-Saad, 2001, "Effect of Compaction Duration on the Induced Stress Levels in a Laboratory Prepared Sand Bed", *Geotechnical Testing Journal*, Vol. 24, No. 4, pp. 430-438.

Houlsby, G. T., 1991, "How the Dilatancy of Soils Affects Their Behavior", *The Written Version of an Invited Lecture Delivered at the Tenth European*

*Conference on Soil Mechanics and Foundation Engineering*, Florence, Italy.

Kolbuzewski, J., 1948, "An Experimental study of the Maximum and Minimum Porosities of sands", *Proc. Int. Conf. Soil Mech. And Found. Eng*., Vol. i, ii b, I.

Mayne, P. W. and F. H. Kulhawy, 1982, "$K_0$-OCR Relationships In Soil", *Journal of the Geotechnical Engineering*, Vol. 108, pp. 851-872.

McCarthy, D. F., 2002, "Essentials of Soil Mechanics and Foundations", *Prentice Hall*, Sixth Edition.

Meyerhof, G. G., 1976, "Bearing Capacity and Settlement of Pile Foundations", *Journal of Geotechnical Engineering*, Div. 102(3), pp. 195-228.

Meyerhof, G. G. and Hanna, A. M., "Ultimate Bearing Capacity of Foundations on Layered Soils under Inclined Loads", *Canadian Geotechnical Journal*, Vol.15, No.4, pp. 565-572.

Michalowski, R.L., 2005, "Coefficient of Earth Pressure at Rest", *Journal of Geotechnical and Geoenvironmental Engineering*, Vol. 131, No. 11, pp. 1429-1433.

Newland, P. L. and B. H. Alley, "Volume Changes In Drained Triaxial Tests On Granular Materials", *Geotechnique*, Vol. 24.

Rowe, P. W., 1969, "The Relation Between the Shear Strength of Sands in Triaxial Compression, Plane Strain and Direct Shear", *Geotechnique*, Vol. 19, No. 1, pp. 75-86.

Rowe, P. W., 1962, "The Stress-Dilatancy Relation for Static Equilibrium of an Assembly of Particles in Contact", *Proceeding of the Royal Society of*

*London. Series A, Mathematical and Physical Sciences,* Vol. 269, No. 1339, pp. 500-527.

Simpson, B., 1992, "Retaining Structures: Displacement and Design", *Geotechnique* Vol. 42, No. 4, pp. 541-576.

Sivakumar, V., I. G. Doran, J. Graham and T. Navaneethan, 2001, "Relationship between $K_0$ and Overconsolidation Ratio: A Theoretical Approach, *Geotechnique*, Vol.52, No. 3, pp. 225-230.

Schanz, T. and P. A. Vermeer, 1996, "Angle of Friction and Dilatancy of Sand", *Geotechnique*, Vol. 46, No. 1, pp.145-151.

Triaxial User's Manual, 2011, *Geocomp Corporation*

Vaid, Y. P. and S. Sasitharan, 1992, "The Strength and Dilatancy of Sand", *Canadian Geotechnical Journal*, Vol. 29, pp. 522-526.

Wroth, C. P., "General Theories of Earth Pressure and Deformation.", *Proceedings of 5th European Conference on Soil Mechanics and Foundation Engineering*, Vol. 2, pp. 33-52.

Wanatowski, D. and J. Chu, 2007, "$K_0$ of Sand Measured by a Plane-Strain Apparatus", *Canadian Geotechnical Journal*, Vol.44, pp. 1006-1012.

Yang, C. P., 2000, "Observation of Earth Pressure Coefficient by Using Deformation Mechanism", *Taiwan Geotechnical Journal*.